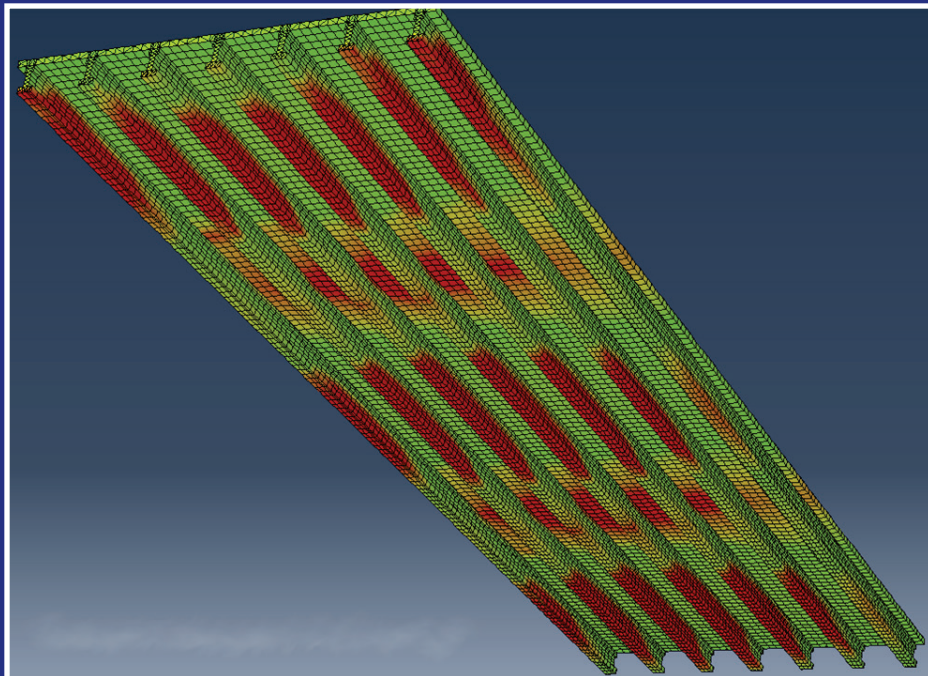


JOINT TRANSPORTATION RESEARCH PROGRAM

INDIANA DEPARTMENT OF TRANSPORTATION
AND PURDUE UNIVERSITY



Efficient Load Rating and Quantification of Life-Cycle Damage of Indiana Bridges Due to Overweight Loads



**Hun Cha, Boyuan Liu,
Arun Prakash, Amit H. Varma**

RECOMMENDED CITATION

Cha, H., Liu, B., Prakash, A., & Varma, A. H. (2016). *Efficient load rating and quantification of life-cycle damage of Indiana bridges due to overweight loads* (Joint Transportation Research Program Publication No. FHWA/IN/JTRP-2016/06). West Lafayette, IN: Purdue University. <http://dx.doi.org/10.5703/1288284316329>

AUTHORS

Hun Cha

Boyuan Liu

Graduate Research Assistants
Lyles School of Civil Engineering
Purdue University

Arun Prakash

Assistant Professor of Civil Engineering
Lyles School of Civil Engineering
Purdue University
(765) 494-6696
arunprakash@purdue.edu
Corresponding Author

Amit H. Varma

Professor of Civil Engineering
Lyles School of Civil Engineering
Purdue University

ACKNOWLEDGMENTS

This work was supported by the Joint Transportation Research Program (JTRP) administered by the Indiana Department of Transportation (INDOT) and Purdue University. The authors would like to thank all individuals associated with both of these organizations for making this research possible. The authors would also like to express their gratitude to all of the members of the Study Advisory Committee: Merrill Dougherty, Timothy Wells, Anne Rearick, George Snyder, Bill Dittrich, Raju Iyer, Badar Khan, Samy Nouredin, Guy Boruff, Donna Anderson, Dick Hayworth, Keith Hoernschemeyer, and Karen Stippich, as well as former SAC members Victor Hong, Edward Pollack, Ronald McCaslin, Autumn Young, and senior personnel Samuel Labi and Robert Connor for their guidance and assisting with data collection.

JOINT TRANSPORTATION RESEARCH PROGRAM

The Joint Transportation Research Program serves as a vehicle for INDOT collaboration with higher education institutions and industry in Indiana to facilitate innovation that results in continuous improvement in the planning, design, construction, operation, management and economic efficiency of the Indiana transportation infrastructure. <https://engineering.purdue.edu/JTRP/index.html>

Published reports of the Joint Transportation Research Program are available at <http://docs.lib.purdue.edu/jtrp/>.

NOTICE

The contents of this report reflect the views of the authors, who are responsible for the facts and the accuracy of the data presented herein. The contents do not necessarily reflect the official views and policies of the Indiana Department of Transportation or the Federal Highway Administration. The report does not constitute a standard, specification, or regulation.

COPYRIGHT

Copyright 2016 by Purdue University. All rights reserved.
Print ISBN: 978-1-62260-386-2
ePUB ISBN: 978-1-62260-387-9

1. Report No. FHWA/IN/JTRP-2016/06	2. Government Accession No.	3. Recipient's Catalog No.	
4. Title and Subtitle Efficient Load Rating and Quantification of Life-Cycle Damage of Indiana Bridges due to Overweight Loads		5. Report Date February 2016	
7. Author(s) Hun Cha, Boyuan Liu, Arun Prakash, Amit H. Varma		6. Performing Organization Code	
9. Performing Organization Name and Address Joint Transportation Research Program Purdue University 550 Stadium Mall Drive West Lafayette, IN 47907-2051		8. Performing Organization Report No. FHWA/IN/JTRP-2016/06	
12. Sponsoring Agency Name and Address Indiana Department of Transportation State Office Building 100 North Senate Avenue Indianapolis, IN 46204		10. Work Unit No.	
		11. Contract or Grant No. SPR-3630	
15. Supplementary Notes Prepared in cooperation with the Indiana Department of Transportation and Federal Highway Administration.		13. Type of Report and Period Covered Final Report	
		14. Sponsoring Agency Code	
16. Abstract <p>In this study, a computational approach for conducting durability analysis of bridges using detailed finite element models is developed. The underlying approach adopted is based on the hypothesis that the two main factors affecting the life of a bridge structure are the level of repetitive loading it sustains and the natural condition of the bridge that may be thought of as a combined effect of both, physical processes in the environment that cause deterioration and any maintenance activity undertaken to thwart such processes. Detailed finite element models of representative bridges are developed and subjected to a set of representative traffic loads repeatedly. Finite element model updation is used to characterize the evolution of damage over the lifetime of a bridge and real-life data from inspection reports of bridges is used to calibrate the durability models developed. The results of this approach may be used to evaluate the permit fee structure for overweight trucks and make informed decisions for asset management of the bridges in INDOT's inventory.</p>			
17. Key Words durability, bridges, damage, deterioration, overweight trucks, load rating		18. Distribution Statement No restrictions. This document is available to the public through the National Technical Information Service, Springfield, VA 22161.	
19. Security Classif. (of this report) Unclassified	20. Security Classif. (of this page) Unclassified	21. No. of Pages 94	22. Price

EXECUTIVE SUMMARY

EFFICIENT LOAD RATING AND QUANTIFICATION OF LIFE-CYCLE DAMAGE OF INDIANA BRIDGES DUE TO OVERWEIGHT LOADS

Introduction

Over the lifetime of a bridge, traffic loads cause numerous stress-strain cycles within bridge components, which in turn lead to the slow accumulation of damage. The rate of progression of this damage is affected by several human-induced and natural factors, such as volume and type of traffic loads, environmental conditions, and maintenance practices. Traffic volume and truck weights have been steadily increasing with the growth and technical development of the freight industry. Because further increased truck weight limits are anticipated in the future, this research focused on the potential detrimental effects of such increases on the durability of bridges, especially due to overweight trucks.

A computational approach to assess the effect of different load-related and environmental factors on the durability of bridge components is presented in this report. Detailed finite element models calibrated using data from inspection reports of real bridges were used for this study. The basic idea behind the durability model developed here is that repetitive loading and natural conditions cause damage to the bridge structure. Damage is represented as a degradation of the material properties of each and every point in a structure based on the level of stresses at that point resulting from repetitive traffic loading. In addition, an empirical relationship was used to represent degradation due to natural processes. Thus the finite element model of a representative bridge was subjected to a set of different vehicle loads to quantify the stresses (and hence the damage) at all the material points in the bridge. This damage was scaled by the annual daily traffic for each vehicle class to account for damage occurring over a year, and the finite element model updated to reflect this damage within its elements. The process was repeated successively to characterize the evolution of damage in the bridge over its lifetime.

Findings

It is shown that this computational approach, with certain assumptions, is capable of quantifying damage resulting from loading and environmental factors. The approach was also used to study different hypothetical scenarios of how this damage could potentially affect the life of bridge components as loading and environmental conditions were varied.

A challenging aspect of this research was the calibration of the durability models developed. A detailed study of all INDOT-owned bridges (approximately 6,000) and all Indiana bridges (approximately 18,000) using data from the NBI database was conducted. Three types of bridges were considered in this study:

reinforced concrete (RC), pre-stressed concrete (PSC), and steel. The bridges were first classified into 25 different classes according to 5 different levels of loading conditions and 5 different levels of natural conditions. Then, using historical condition rating data from 1994 to 2014 for each of these bridges, a rate of deterioration corresponding to the 25 different classes of bridges was determined. An empirical equation to characterize the variation of these deterioration rates with loading and natural factors was postulated and calibrated with actual data. The relative importance of load-related and natural factors in terms of their effect on the durability of bridge structures was also determined for different bridge types.

A limitation of the current approach for calibration of durability models is that annual daily traffic is taken to represent the level of loading on a bridge. This is usually insufficient since the loading experienced by a bridge is characterized not only the total number of vehicles, but also by the axle configurations and axle loads of each of those vehicles. Unless historical traffic data with vehicle weights and axle configurations is available for all bridges being investigated, a precise calibration of the load-related damage in durability model may not be possible. Another limitation of the calibration approach adopted is that location (latitude) of a bridge is taken to reflect its natural condition. This does not account for local environmental conditions and maintenance practices that may affect the durability of bridges significantly.

Implementation

Action items from this research include implementing measures to collect more detailed vehicular data, possibly with the use of weigh-in-motion stations, across all major highways to allow a better characterization of the loads incurred by bridge structures. Further, it is recommended that during bridge inspections the environmental conditions affecting durability be characterized on a scale similar to that presented in Chapter 6 of this study. It is also recommended that a more detailed component-wise record of condition ratings be undertaken during bridge inspections. Not only will this reduce the subjectivity in the determination of these ratings, but it is also essential for effectively calibrating the durability models constructed in this study. In addition, a database of maintenance activities performed on bridges should be maintained.

Despite some limitations, trends in the real data show that deterioration rate increases with increased loading and/or with worsening natural conditions. However, challenges remain with precisely calibrating the relative importance of load-related and natural factors on the durability of bridges with real data from inspection reports. Results from the durability analyses of different scenarios using the finite element models of representative bridges show that the effect of increasing trucks weight limits on these bridges can indeed be quantified and used to generate deterioration curves for the various bridge components. This information can also be used by INDOT to streamline permitting of overweight trucks and for bridge maintenance and operations.

CONTENTS

1. INTRODUCTION	1
1.1 Objectives	1
1.2 Research Approach	2
2. SELECTION OF REPRESENTATIVE BRIDGES AND LOADS	2
2.1 Representative Bridges	2
2.2 Statistical Analysis for Identifying Representative Bridges	4
2.3 Representative Loads	9
3. FINITE ELEMENT MODELING OF STEEL BRIDGES	10
3.1 Existing Approaches for Finite Element Modeling of Bridges	10
3.2 Finite Element Modeling of Concrete-Deck-on-Steel Girder Bridges	10
4. FINITE-ELEMENT MODELING OF REINFORCED AND PRE-STRESSED CONCRETE BRIDGES	19
4.1 Modeling of RC Components	19
4.2 Modeling of Pre-Stressed Concrete	20
4.3 Description of the FE Model of the Representative Concrete Bridge	22
5. COMPUTATIONAL FRAMEWORK FOR MODELING DURABILITY	24
5.1 Existing Models for Durability of Structures	24
5.2 Finite Element Framework for Durability Analysis Using Model Updation	26
5.3 Approach for Durability Analysis of Bridges	28
5.4 Numerical Case Studies Using the Framework for Durability Analysis	31
6. DURABILITY OF DECK JOINTS SUBJECT TO REPETITIVE SINGLE AXLE LOADS	35
6.1 Objective	35
6.2 Background	35
6.3 Research Approach and Scope	36
6.4 Description of Finite Element Model	39
6.5 Summary	46
7. CALIBRATION OF DURABILITY MODELS	46
7.1 Bridge Classification	46
8. SUMMARY AND CONCLUSIONS	60
8.1 Implementation and Recommendations	60
REFERENCES	61
APPENDICES	
Appendix A. Statistical Sampling of Representative Bridges	63
Appendix B. ABAQUS Subroutine for Durability Model	67

LIST OF TABLES

Table	Page
Table 2.1 Representative loads chosen (including superloads)	7
Table 2.2 Oversize/overweight limitation in Indiana	8
Table 2.3 Five representative vehicles (including superloads) chosen for durability analysis	10
Table 3.1 Comparison with two bridges for validation	11
Table 3.2 Key parameters for US 52 NBI-19027 bridge	11
Table 3.3 Description of 3D FE modeling parameters for the US 52 bridge	12
Table 3.4 Comparison of results from current FE model and prior research	15
Table 3.5 Information of NBI-38750 bridge on I-65	18
Table 3.6 Description of 3D modeling for I-65 bridge	19
Table 3.7 Comparison of ABAQUS modeling results with prior research	21
Table 3.8 Comparison of results for I-65 bridge with superload	22
Table 4.1 Comparison of FE results for the I-164 bridge with prior research	28
Table 6.1 Applied single axle loads considering overweight (OW) trucks	43
Table 6.2 Maximum pressure value for six groups	46
Table 6.3 Applied traffic volumes of five loading classes using AADT of NBI-19027 bridge	49
Table 6.4 Applied traffic volumes considered 200% increased overweight trucks	52
Table 7.1 Classification for INDOT owned RC bridges	54
Table 7.2 Classification for all Indiana RC bridges	54
Table 7.3 INDOT RC decks	55
Table 7.4 All Indiana RC bridge decks	55
Table 7.5 INDOT RC girders	56
Table 7.6 All Indiana RC girders	56
Table 7.7 Classification for INDOT owned PSC bridges	58
Table 7.8 Classification for all Indiana PSC bridges	58
Table 7.9 INDOT PSC concrete decks	59
Table 7.10 All Indiana PSC bridge decks	59
Table 7.11 INDOT PSC bridge girders	60
Table 7.12 All Indiana PSC bridge girders	60
Table 7.13 Classification for INDOT owned steel bridges	62
Table 7.14 Classification for all Indiana steel bridges	62
Table 7.15 INDOT steel bridge decks	63
Table 7.16 All Indiana steel bridge decks	63
Table 7.17 INDOT steel girders	64
Table 7.18 All Indiana steel bridge girders	64
Table 7.19 Summary of deterioration rates: average standard deviation	66
Table A.1 Bridges based on different materials and length	70
Table A.2 Bridges on routes with high AADT	70
Table A.3 Bridges on highways in the corridor with WIM stations	71
Table A.4 Bridges in the extra heavy duty highway corridor	71

Table A.5 Structurally deficient bridges	71
Table A.6 Bridges-based sufficiency rating	72
Table A.7 Bridges on Interstate routes	72
Table A.8 Bridges on state routes	72
Table A.9 Bridges on US routes	73

LIST OF FIGURES

Figure	Page
Figure 1.1 Project overview	2
Figure 2.1 Classification of bridges by material type	2
Figure 2.2 Distribution of pre-stressed concrete, reinforced concrete and steel bridges based on bridge length	3
Figure 2.3 AADT map of Indiana	4
Figure 2.4 WIM site location and choice of representative bridges	4
Figure 2.5 Extra heavy duty highways – northwest Indiana	5
Figure 2.6 Representative steel bridge chosen: US 52 bridge (NBI-19027) in Lafayette, Indiana	5
Figure 2.7 Representative concrete bridge: I-164 bridge in Evansville, Indiana	6
Figure 2.8 (a) 12-ton school bus, (b) HS-20 load, (c) toll road truck, and (d) 120 kip pre-approved truck	7
Figure 2.9 Compilation of permit request data for overweight and superload groups	8
Figure 2.10 Representative superload configurations	9
Figure 2.11 Transverse position of the representative loads on the representative bridges	10
Figure 3.1 Plan view of US 52 bridge	12
Figure 3.2 Finite element model of representative steel bridge	12
Figure 3.3 Applied truck loads	13
Figure 3.4 Applied maximum truck load on US 52 bridge	13
Figure 3.5 Results from FE modeling of the US 52 bridge	14
Figure 3.6 Location of maximum stresses on US 52 bridge	14
Figure 3.7 Response of structural elements to representative loads	15
Figure 3.8 Results of mesh convergence study	17
Figure 3.9 Model of simply supported beam used for calibrating damping	17
Figure 3.10 Displacement time history at center span	17
Figure 3.11 Estimation of damping	18
Figure 3.12 I-65 bridge in Lake County, Indiana	18
Figure 3.13 Side view of I-65 bridge	19
Figure 3.14 Beam element with L cross-sectional profile used for cross-beams	20
Figure 3.15 Applied test truck load on I-65 bridge	20
Figure 3.16 Results from FE modeling of the I-65 bridge	21
Figure 3.17 Applied superload configurations on the I-65 bridge	22
Figure 4.1 Geometry layout and static scheme of the numerical modeling	23
Figure 4.2 Comparison of deflection obtained from the FE model with theory	23
Figure 4.3 Comparison of stresses: <i>left</i> , concrete; <i>right</i> , rebar	24
Figure 4.4 Force applied to the sample beam	24
Figure 4.5 Explicit and implicit simulations: deflection	25
Figure 4.6 Explicit and implicit simulations: stress	25
Figure 4.7 FE modeling of a pre-stressed concrete beam	25
Figure 4.8 Test setup for the PSC beam	26
Figure 4.9 Load vs. deflection plot	26
Figure 4.10 Finite element of the representative concrete bridge showing the approximate cross-section used for the model	27

Figure 4.11	Placement of the test truck for validation of the finite element model	27
Figure 4.12	Displacement response of the bridge for the 80 kip truck on the bridge	27
Figure 4.13	Deflections at all girder locations of the representative concrete bridge	27
Figure 5.1	Corrosion region in steel girders obtained from field survey	29
Figure 5.2	Computational framework for modeling durability of bridges	31
Figure 5.3	Assumed damage profile due to corrosion in steel girders	33
Figure 5.4	Natural damage in concrete decks	34
Figure 5.5	Depiction of scenarios used in different case studies	35
Figure 5.6	Damage propagation in steel superstructure obtained from durability model	36
Figure 5.7	Photographs of the steel bridge superstructure in 2012	36
Figure 5.8	Evolution of condition rating of the representative steel bridge for case 0	37
Figure 5.9	Comparison of computational increment year	37
Figure 5.10	Comparison of deck condition rating for different cases	37
Figure 5.11	Comparison of condition rating of the steel superstructure under different cases	38
Figure 5.12	Detailed comparison of condition rating from cases 0 and 1	38
Figure 5.13	Detailed comparison of condition rating from cases 0 and 2	38
Figure 5.14	Typical damage profiles of the representative concrete bridge	39
Figure 5.15	Depiction of typical damage evolution obtained from the durability model	40
Figure 5.16	Comparison of condition rating for cases 0 and 1	40
Figure 5.17	Comparison of condition ratings for cases 0 and 2	40
Figure 6.1	Deck joints in Indiana	41
Figure 6.2	Possible intrusion path of chloride ion	42
Figure 6.3	Procedure of deck joint FE model analysis	44
Figure 6.4	Condition rating for bridge ages and spalling on deck joint	45
Figure 6.5	View of 3D deck joint model	45
Figure 6.6	View of FE model for moving plate	47
Figure 6.7	Reaction forces (RF) at BC1 in PART 1 for validation of deck joint model	47
Figure 6.8	Reaction forces (RF) at bearing in PART 1 for validation of deck joint model	47
Figure 6.9	Pressure-time history for six groups of elements on the deck joint	48
Figure 6.10	View of 3D FE modeling subject to different dynamic amplification factors (DAF) and potential cases	48
Figure 6.11	Von-Mises stress against lifetime due to 5 single axle load classes in concrete blockout obtained using DLOAD in ABAQUS 6.12	50
Figure 6.12	Comparison of averaged cumulative damage due to different dynamic amplification factors for four cases	50
Figure 6.13	Average cumulative damage for case 1 with replacement stage	51
Figure 6.14	Average cumulative damage with repair stage by four cases	51
Figure 6.15	Condition rating based on cumulative damage for four cases	51
Figure 6.16	Comparison of condition rating based on FE results to Inspection report data	51
Figure 6.17	Comparison of accumulated damage by case 3 considering 200% increased AADT of overweight truck	51
Figure 7.1	Classification of ADT and latitude for RC bridges	54
Figure 7.2	Deck condition rating for RC bridges	55
Figure 7.3	Girder condition rating for RC bridges	56

Figure 7.4 Distribution of deterioration rate for RC bridge decks	57
Figure 7.5 Distribution of deterioration rate for RC bridge girders	57
Figure 7.6 Classification of ADT and latitude for PSC bridges	58
Figure 7.7 Deck condition rating deterioration	59
Figure 7.8 Girder condition rating deterioration	60
Figure 7.9 Distribution of deterioration rate for PSC bridge decks	61
Figure 7.10 Distribution of deterioration rate for PSC bridge girders	61
Figure 7.11 Classification of ADT and latitude for steel bridges	62
Figure 7.12 Deck condition rating deterioration rate	63
Figure 7.13 Girder condition rating deterioration rate	64
Figure 7.14 Distribution of deterioration rate for steel bridge decks	65
Figure 7.15 Distribution of deterioration rate for steel bridge girders	65
Figure 7.16 Modeling the variation of deterioration rate with loading and natural condition	66
Figure 7.17 Variation of deterioration rates for RC bridge decks and girders	66
Figure 7.18 Variation of deterioration rates for PSC bridge decks and girders	66
Figure 7.19 Variation of deterioration rates for steel bridge decks and girders	67

1. INTRODUCTION

The deterioration of bridges and their components due to natural and human-induced factors is a major cause of concern for highway agencies responsible for transportation infrastructure. There are about 18,600 roadway bridges in the state of Indiana, which are the focus of this study. It has been reported that approximately 1,970 of these bridges are structurally deficient (see Transportation for America, <http://t4america.org/maps-tools/bridges/>). Although structurally deficient bridges are usually not in danger of immediate collapse, if left unchecked, they do pose a risk. The Indiana Department of Transportation (INDOT) continuously monitors and evaluates the condition these bridges based on National Bridge Inspection Standards (NBIS) and its own Indiana Bridge Inspection Manual (INDOT, 2010) to determine the need for repair and maintenance for ensuring public safety.

A study on bridge failures conducted by Wardhana and Hadipriono (2003) investigated 503 bridges that failed during 1989 to 2000 in the United States (486 of these had suffered collapse, and 17 had become un-serviceable). Approximately 53% of the 503 failures resulted due to natural events with flood being the primary cause. Failures caused by human-induced external factors such as overloading and deterioration (e.g., due to corrosion) accounted for approximately 18% of the 503 failures. Thus, understanding the processes behind damage and deterioration of bridge components and the factors affecting the rate of damage progression is of immense practical importance.

In 1971, Congress created the National Bridge Inspection Standards (NBIS), which are a set of federal guidelines pertaining to bridge inspection frequency, inspector qualifications, report formats, inspection and rating procedures, and the maintenance of a state bridge inventory. These standards were developed for bridge inspections nationwide and are minimum standards. Many states (including Indiana; see INDOT, 2010) have additional guidelines to ensure high standards in inspection.

Sinha et al. (2009) investigated the life cycle of approximately 5,500 bridges on the State of Indiana highway system, the Interstate system, and the US system documented in the Indiana Bridge Management System (IBMS). They suggested that bridges should be managed during their life cycle as follows: (i) first deck rehabilitation or replacement around 20 years, (ii) superstructure replacement around 40 years, (iii) second deck rehabilitation or replacement around 55 years, and finally (iv) bridge replacement around 75 years. In addition to the time-based criteria, the study also developed condition-based criteria for the assessment of the need for rehabilitation and deck replacement, depending upon the condition rating reported by inspectors, INDOT priorities and availability of funds.

With the growth and technical development of the freight industry, overweight trucks have become an important issue for state highway agencies (see Transportation

Research Board, 1990). Currently, INDOT and other state DOTs employ various empirical formulas to determine and allocate costs of the damage incurred by bridges due to natural- and human-induced causes and use them to collect permit fees from regular and overweight trucks. A TxDOT study by McIlrath et al. (2000) proposed ways to improve bridge rating and truck permitting procedures using finite element analysis rather than using empirical equations from AASHTO. They conducted more detailed analyses of bridges using SAP 2000 and BRUFEM to calculate the lateral load distribution factors more accurately and enable the bridge engineer to determine which trucks will likely cause damage to bridges. The model enables one to simulate the response and stress levels within bridge structures more accurately. When designed appropriately for these stresses and loads, longer bridge service lives are achieved in most cases.

The formulas that are used for highway cost allocation studies (both for initial construction and for regular maintenance) are usually highly empirical and are usually derived by allocating costs to different vehicle classes based on *static* measures of structural response such as bending moments or shear forces, etc. They do not account for the *temporal* variability in how damage of structural elements progresses with time and how the different vehicle classes affect this progression of damage differently (see Sinha et al., 2000). Recently, Ahmed et al. (2013) have accounted for bridge damage rates that are different for bridges at different ages. The current study provides a further, finer characterization of this relationship between vehicle load and bridge damage for bridges of different ages.

In this study, we investigate how the rate of deterioration is affected by different loading and environmental causes, largely focusing on the detrimental effect of overweight trucks (that are over 356 kN or 80 kip) on different bridge components. We use detailed finite-element models of *representative* bridges in the State of Indiana to study the progression of damage over the lifetime of a bridge. Finally, we quantify the effect of load-related causes vs. environmental factors on the resulting reduction in service-life of the bridge.

1.1 Objectives

The main objectives of this study are to:

- Develop a computational approach to model the effect of different natural- and human-induced factors on the cumulative damage sustained by bridges during their lifetime,
- Study the effects of changes in traffic patterns (such as changes in traffic volume or increased limits for overweight trucks) and changes in environmental conditions and maintenance strategies on the progression of damage in bridges,
- Validate the computational durability model against data from real inspection reports of Indiana's bridge inventory using the National Bridge Inventory Database.

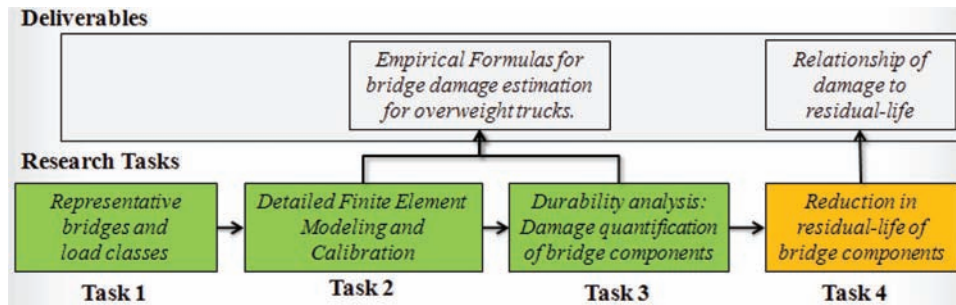


Figure 1.1 Project overview.

1.2 Research Approach

The research approach is based on Tasks 1–4 mentioned below and depicted in Figure 1.1:

1. Identification of a representative set of bridges and representative vehicular loads,
2. Finite element modeling of representative bridges for accurate estimation of localized stresses and strains
3. Quantification of damage due to localized stresses caused by all load classes, especially overweight trucks
4. Effect of damage caused by overweight trucks on residual life

This study enhances our understanding of how damage progresses in bridges and what factors affect its rate of progression. This study also provides an approach for evaluating how changes in traffic patterns and/or changes in current maintenance practices can affect the life of a bridge. Examples of how to use the results of this research to evaluate overweight permitting policies are also provided.

2. SELECTION OF REPRESENTATIVE BRIDGES AND LOADS

In order to study the life-cycle behavior of Indiana bridges, a set of representative bridges and representative vehicular loadings needs to be established. The following two tasks are the focus of this chapter:

1. Identify a set of representative bridges in Indiana; obtain detailed drawings for the same to facilitate detailed finite element modeling, and
2. Establish realistic load profiles/classes using AASHTO vehicle classes, WIM data, and overweight truck data.

The methodology used in this study to identify representative bridges and representative loads is discussed next.

2.1 Representative Bridges

Indiana has approximately 18,600 bridges, of which steel, reinforced concrete and pre-stressed concrete bridges account for almost 95% of the inventory (see National Bridge Inventory Database, 2011). The bridges can be classified based on different factors such as material type, span-length, skew, condition rating, AADT volume, proximity to WIM sites, and their location on

State, US, or Interstate highways. Identification of a set of bridges that is representative of a large percentage of Indiana’s bridge inventory was carried out by first generating a statistical sampling of bridges based on each of these classification criteria. Then specific bridges were identified for detailed finite element modeling as discussed in the following section. A detailed list of the representative bridges compiled after statistical sampling is given in Appendix A.

The statistical sampling of bridges in INDOT’s inventory was generated based on the following criteria noted in the following subsections. All bridges chosen are owned by the Indiana Department of Transportation.

2.1.1. Material Type and Length of Bridges

The evolution of damage in a bridge is primarily dependent on its material-type and geometrical characteristics such as length, breadth, number of spans, etc. Figure 2.1 shows the percentage distribution of all the bridges in Indiana classified by their material type.

Pre-stressed concrete, reinforced concrete and steel bridges are the three most common types of bridges accounting for nearly 95% of all the bridges in Indiana. The present study will be confined to these three material classes.

Figure 2.2 shows the distribution of bridges with respect to their total length, for each of material-type considered. Based on the distribution of lengths, it is clear that the most common lengths for prestressed concrete and reinforced concrete bridges are between 10 and 25 meters while steel bridges of length 50 to 100 meters are the most common. Steel bridges of length between 10 and 25 meters are the second most common bracket.

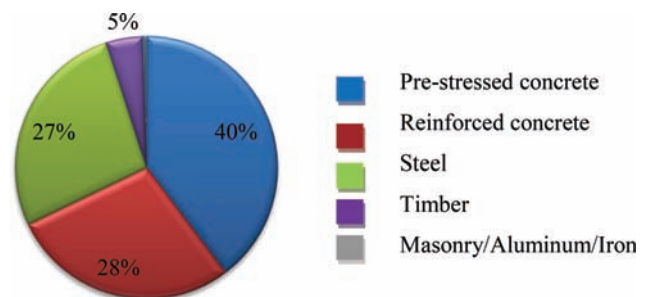


Figure 2.1 Classification of bridges by material type.

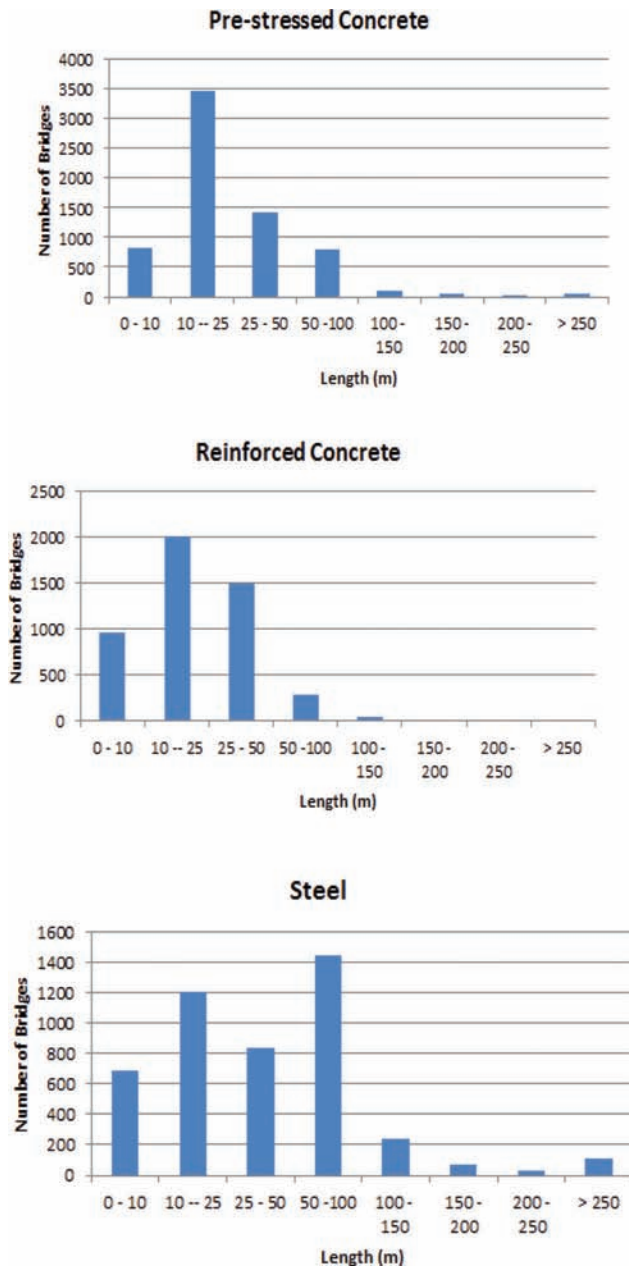


Figure 2.2 Distribution of pre-stressed concrete, reinforced concrete and steel bridges based on bridge length.

A sample of bridges from these length-brackets were chosen to be representative for each material type.

2.1.2. Bridges on Routes with High Annual Average Daily Traffic (AADT) Volume

High AADT values over a bridge are indicative of heavy usage and represent bridges likely to have greater load-related damage and deterioration. The AADT map of Indiana for the year 2007 is shown in Figure 2.3. It can be seen that corridors with high AADT volumes (over 15,000) and include I-65, I-69, I-70 and

I-74 highways. Representative bridges on each of these corridors were included in the statistical sampling.

2.1.3. Bridges on Corridors with Weigh-in-Motion (WIM) Stations

The Indiana Department of Transportation (INDOT), through its Traffic Statistics Section, collects information on traffic traveling on the state's highway system, primarily through two traffic-monitoring systems. A Statewide Traffic Monitoring System consisting of 106 permanent continuous count stations collects volume, speed, and vehicle classification data every hour and every day of the year. Nearly 50 of these sites also utilize weigh-in-motion (WIM) technology to collect continuous truck weight data. A second system is the Statewide Coverage Count Program, which utilizes portable traffic counters to collect 48-hour traffic counts.

Weigh-in-motion data helps in building a realistic load profile for the bridge and is important for the analysis of performance of a bridge. Hence, bridges close to WIM sites and on the corridors with the WIM stations were identified. The locations of the WIM sites and the selected bridges are shown in Figure 2.4.

2.1.4. Bridges on Extra Heavy Duty Highways

Another criterion that was considered was bridges on the extra heavy duty highways. These bridges that carry a significant portion of the heavy truck traffic and data from these bridges will help in studying the impact of overweight trucks on damage progression. For this, sample bridges on the extra heavy duty highway corridor (Figure 2.5) were included in the set of representative bridges considered.

2.1.5. Structurally Deficient Bridges

About 1845 bridges in Indiana are structurally deficient. Analysis of these bridges is important because it provides insight into the behavior of deficient structures under the influence of heavy loads and helps characterize the effect of damage on residual life of the structure.

2.1.6. Sufficiency Rating

Bridges of varying sufficiency ratings were selected to observe the behavior of a structure at different stages of its life cycle. While sufficiency rating does not directly reflect the structural condition of a bridge, a higher sufficiency rating generally indicates a relatively better or usable condition of a bridge. Bridges with sufficiency ratings varying between 40% and 80% were selected for the study.

2.1.7 Bridges on Different Interstate, State and US Routes

The state of Indiana has 14 Interstate routes passing through its region. It also has over 100 state routes and



Figure 2.3 AADT map of Indiana.



Figure 2.4 WIM site location and choice of representative bridges.

20 US routes passing through its domain. A sample of bridges were chosen from each of these types of highways including interstate, state and US routes.

2.2 Statistical Analysis for Identifying Representative Bridges

In order to restrict the number of bridges for detailed finite element modeling, a ranking of all the bridges in the sample pool of bridges identified in the previous section was generated. The ranking was based on a factor that measures how representative a particular bridge is of the entire set. This factor was calculated in the following manner. Data such as span length, AADT, age and sufficiency rating were assembled for each bridge. For each bridge, its representative factor (Z) for each of the criteria mentioned in the previous subsection was computed as follows:

$$Z = \left| \frac{X - \mu}{\sigma} \right| \quad (2.1)$$

where X is the observed value of that bridge for a particular criterion, μ is the mean for each criterion and σ is the standard deviation of each criterion.

The mean representative factor was then computed for each bridge for all the criteria and bridges were ranked based on this value. This process ensured that the bridges were ranked based on their proximity to the mean value across all criteria and therefore were ranked in order of being representative of INDOT's bridge inventory.

2.2.1 Representative Steel Bridge

Through statistical analysis, the westbound US 52 bridge (NBI-19027) in Lafayette IN, shown in Figure 2.6,



Figure 2.5 Extra heavy duty highways – northwest Indiana.

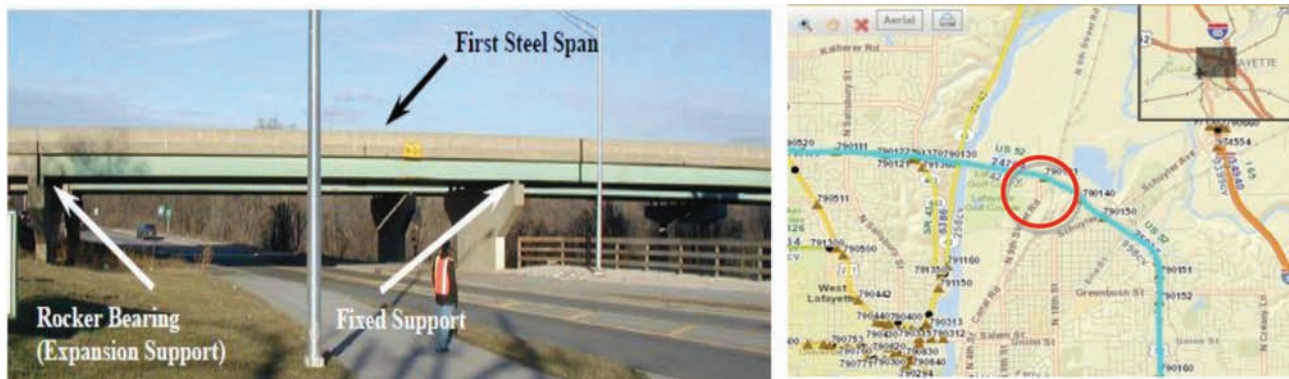


Figure 2.6 Representative steel bridge chosen: US 52 bridge (NBI-19027) in Lafayette, Indiana.

was identified as one of the bridges that was closest to the mean values of all the parameters and it was chosen as the representative steel bridge for this study. The US 52 bridge (NBI number: 19027) crosses over North 9th Street Road in Lafayette, Indiana. This bridge was built in 1970 and is a 5-span continuous steel bridge with no skew. Only the two steel spans were chosen for FE modeling due to computational limitations.

The roadway consists of two 3.66-meter-wide (12 ft.) traffic lanes and a 3.05-meter-wide (10 ft.) and a 1.83-meter-wide (6 ft.) shoulder. The deck is supported by 8 rolled shape steel girders that behave in full composite

action with the concrete deck. In addition, there are 1.83-meter-long (6 ft.) rolled shape steel diaphragms welded to the girders every 9.15 meters (23 ft.). According to the inspection report for this bridge (written before the superstructure of the bridge was reconstructed in late 2012), condition rating of deck was 4 (poor) due to many full depth patches and torn strip seal joints. Other deterioration in the 40-year-old bridge included small cracks in welded connections and many areas of light rust, which resulted in a condition rating of 5 (fair) for the steel superstructure. There was no other obvious evidence of fatigue damage reported.



Figure 2.7 Representative concrete bridge: I-164 bridge in Evansville, Indiana.

2.2.2 Representative Concrete Bridge

The I-164 bridge over Weinbach Avenue in Evansville, Indiana, shown in Figure 2.7, was identified as a representative pre-stressed concrete bridge. To simplify the finite element modeling of concrete bridge, both pre-stressed and reinforced concrete bridges were modeled in the same way (based on assumptions that will be discussed in detail in the next chapter). Dimensions of the concrete deck for this bridge are 12.70 m (41.67 ft.) in width and 41.15 m (135 ft.) in length. The bridge has three spans of lengths 12.65 m (41.5 ft.), 16.15 m (53 ft.), 12.65 m (41.5 ft.) with no skew. The thickness of the deck is 203.2 mm (8 in.) and the compressive strength of concrete (f'_c) as 28 N/mm² (4 ksi). The girders are 914 mm (36 in.) deep American Association of State Highway and Transportation Officials (AASHTO) Type-II pre-stressed concrete girders spaced at 2.03m (80 in.).

The two bridges identified here have also been previously studied using FE models by Wood et al. (2007) and the steel bridge was also instrumented by Canna and Bowman (2002). Data from these prior studies helped in calibrating the finite element models developed in this study.

2.3 Representative Loads

A set of representative vehicular loadings covering a wide range of truck weights, number of axles, spacing, etc., were developed based on conventional AASHTO load profiles and observed WIM data. Availability of WIM data enables the calculation of more realistic structural response envelopes. It also aids in predicting overweight load profiles in the event of increased truck weight limits in the future.

The representative loads chosen for this study are shown in Table 2.1 and depicted in Figure 2.8 and Figure 2.9. A 66-passenger 12-ton school bus load was

considered to encompass all non-truck traffic. The legal truck, overweight trucks and superload trucks were chosen using data on approximately 28,000 permit requests. The methodology used for selection of overweight and superload trucks is discussed next.

According to Oversize/Overweight vehicle permitting handbook in Indiana Department of Revenue (2010), an oversize/overweight load is one that exceeds the legal dimensions but does not exceed the limits shown in Table 2.2. Special permit vehicles include those that are over 120,000 lbs but less than 200,000 lbs. and finally superloads are vehicles with gross weight in excess of 200,000 lbs.

Representative overweight and superload truck profiles were developed using load configuration data from existing sources (such as previous INDOT studies and AASHTO profiles), and from sources such as WIM data and INDOT permit requests as shown in Figure 2.10. Superloads were selected with gross vehicle weights (GVW) 200 kips, 250 kips, 350 kips and 500 kips and these are considered as special route vehicles in the Bridge Inspection Manual (2010) as well as in INDOT studies. In order to determine the axle loads and spacings for each of the representative superloads, a normal distribution curve of the axle loads and spacings was generated from all the associated permit requests, as shown in Figure 2.9. The average value of the axle load and spacing was chosen for the representative superloads Group A, Group B, Group C and Group D. Axle spacing for tandems was chosen as 4.5 ft. based on INDOT studies (4 ft. to 7 ft.), the average value in the permit requests, as well as considering the minimum spacing manual.

To further reduce the computational burden of simulating the effect of different load classes, while still maintaining fidelity with the above load profiles, a set of 5 representative vehicles listed in Table 2.3 were chosen to represent the spectrum of traffic loading for this study.

TABLE 2.1
 Representative loads chosen (including superloads).

Loading	GVW (kips)	Total Number of Axles	Total Vehicle Length
School bus	24	2	21 ft.
HS-20	72	3	28 ft.
Toll road truck	90	28 ft.	
Trucks able to get preapproved	120	7	44 ft.
Group A	200	9	78 ft.
Group B	250	13	133.5 ft.
Group C	350	18	161.5 ft.
Group D	500	16	95 ft.
Max. truck*	824	21	127.5 ft.

*Max. truck has 8 tires per axle and was introduced by Wood et al. (2007).

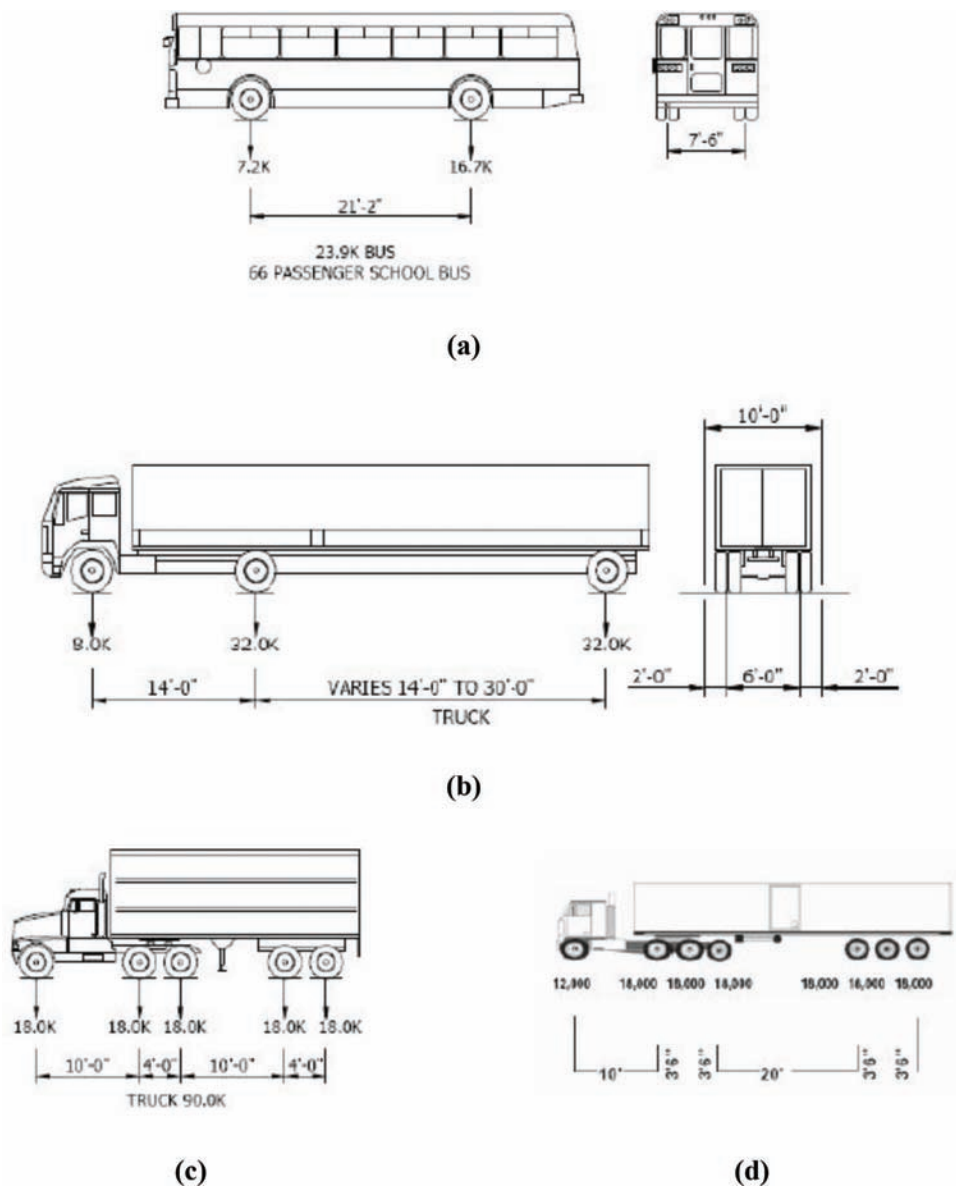


Figure 2.8 (a) 12-ton school bus, (b) HS-20 load, (c) toll road truck, and (d) 120 kip pre-approved truck.

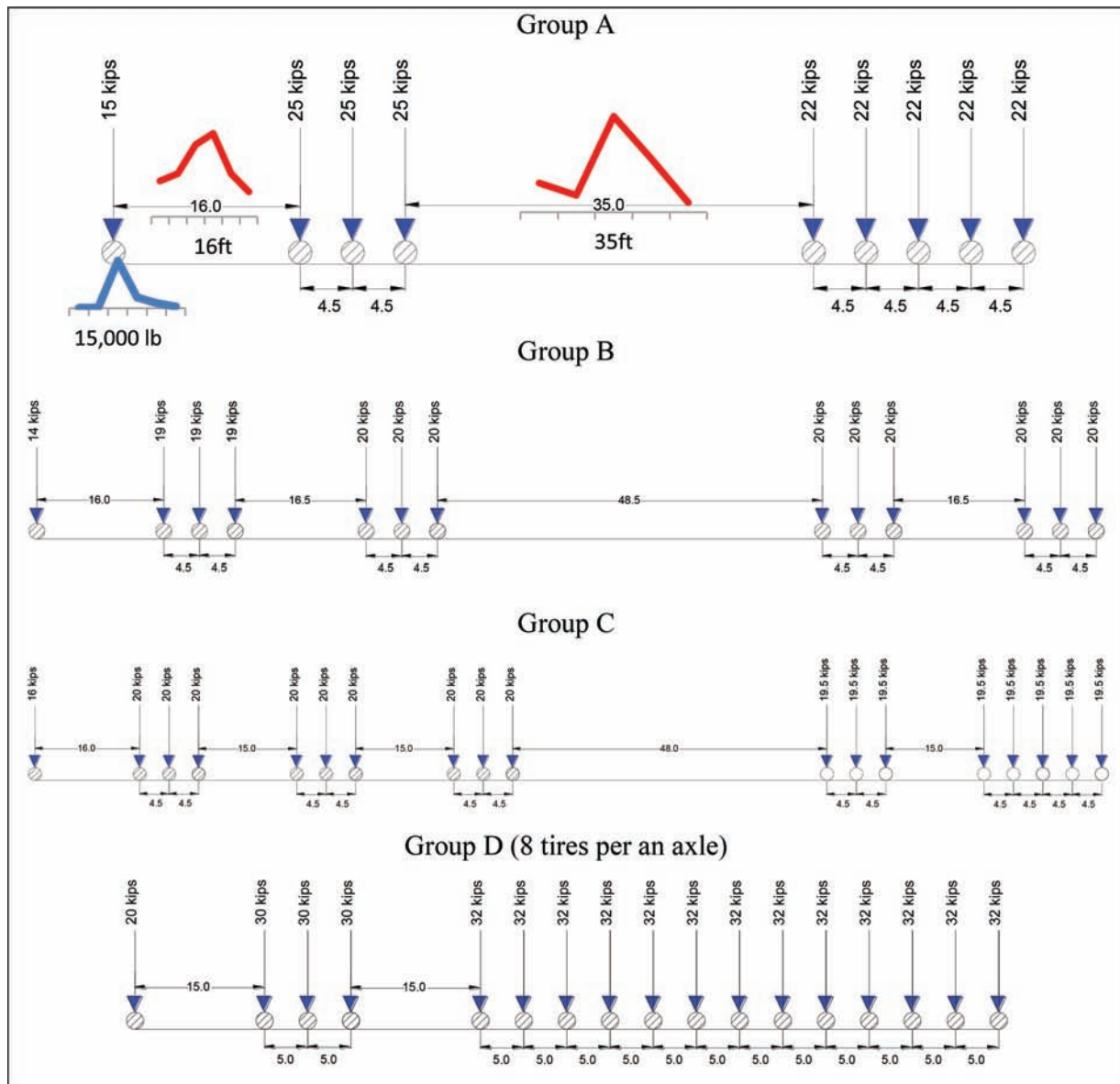
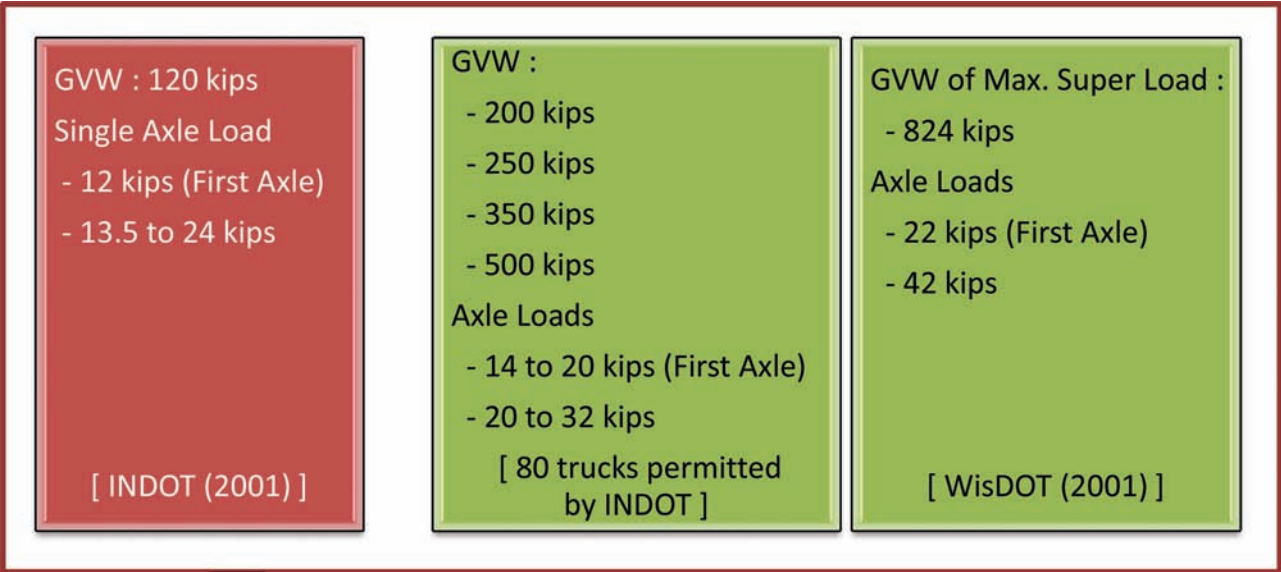


Figure 2.9 Representative superload configurations.

TABLE 2.2
Oversize/overweight limitation in Indiana.

Dimensions for Overloads	
Width	12 ft. 4 in. ~ 16 ft.
Length	95 ft. ~ 110 ft.
Height	13.5 ft. ~ 15 ft.
Weight	80,000 lb. ~ 120,000 lb.



27,818 Trucks including INDOT's Data (2009)

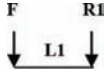
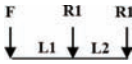
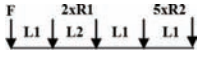
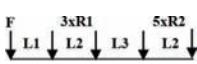
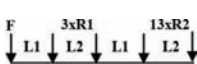
GVW (lb.)	Total	Single Axle Load (lb.)	Total
120,000 to 200,000	4,192	20,000 to 25,000	18,341
200,000 to 250,000	38	25,000 to 30,000	1,198
250,000 to 300,000	42	30,000 to 35,000	74
300,000 to 400,000	18	35,000 to 40,000	28
400,000 to 510,000	11	40,000 to 50,000	19
510,000 to 800,000	3	50,000 to 80,000	4
Over 800,000	0	Over 80,000	0
	Of 27,818		Of 163,258

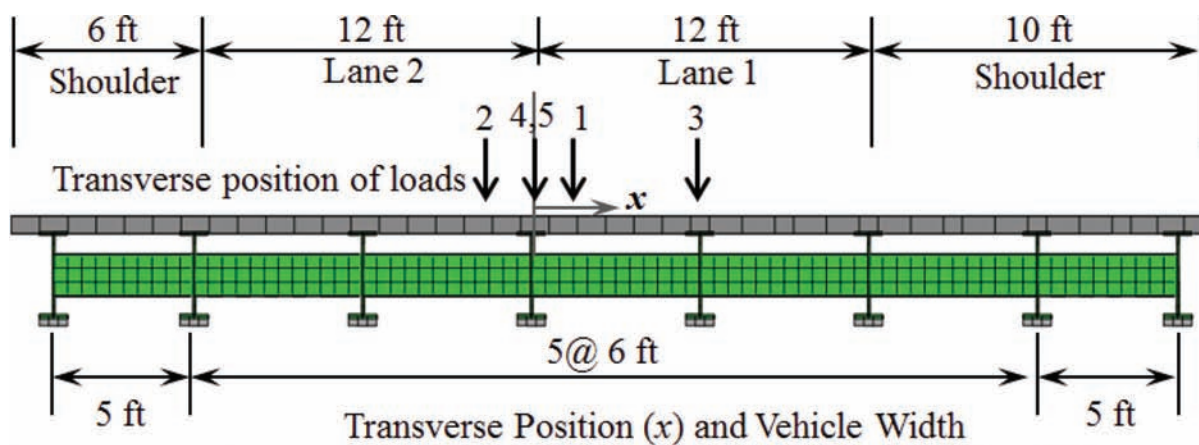
Re-arranged Superload Trucks in 4 groups

Representative Loads (lb.)	Variation (lb.)	Truck counts
120,000	120,000 to 125,000	2,125
150,000	125,000 to 150,000	2,558
200,000	150,000 to 200,000	1,485
250,000	200,000 to 300,000	55
350,000	300,000 to 400,000	18
500,000	400,000 to 600,000	14
824,000	Maximum load considered	

Figure 2.10 Compilation of permit request data for overweight and superload groups.

TABLE 2.3
Five representative vehicles (including superloads) chosen for durability analysis.

Loading Class (AADT)	GVW	Illustration	Axle Configuration					
			F	R1	R2	L1	L2	L3
School Bus (8,000)	107 kN (24 kip)		71 (16)	36 (8)		6.4 (21)		
Regular truck (600)	357 kN (80 kip)		45 (10)	156 (35)		3.05 (10)	4.27 (14)	
Michigan trailer truck (3,400)	596 kN (134 kip)		54 (12)	71 (16)	80 (18)	2.74 (9)	1.37 (4.5)	
Group A (200)	890 kN (200 kip)		67 (15)	111 (25)	98 (22)	4.88 (16)	1.37 (4.5)	7.62 (25)
Group D (80)	2,224 kN (500 kip)		70 (20)	120 (30)	138 (32)	4.57 (15)	1.52 (5)	



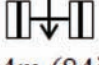
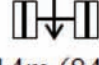
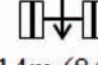

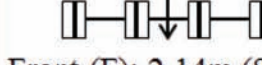
Load #1	Load #2	Load #3	Load #4	Load #5
School bus	HS20	Michigan Truck	Superload Group A	Superload Group D
12 in.	-18 in.	72 in.	0 in.	0 in.
				
2.14m (84in.)	2.14m (84in.)	2.14m (84in.)	3.05m (120in.)	Front (F): 2.14m (84in.) Rear (R): 4.88 m (192in.)

Figure 2.11 Transverse position of the representative loads on the representative bridges.

For simulating the effect of the 5 representative loadings depicted in Table 2.3, the transverse position of each of these vehicles on the bridge, shown in Figure 2.11, was decided based on the lane-wise traffic data recorded from a traffic station close to the US 52 bridge.

As evident, the superload classes 4 and 5 (Group A and Group D) are placed in the center of the bridge according to INDOT practices for superloads crossing a bridge.

Having identified the representative steel and concrete bridges and a representative set of loads, detailed

finite element modeling of these bridges was conducted as explained in the following chapter.

3. FINITE ELEMENT MODELING OF STEEL BRIDGES

In this chapter we describe details of how the finite element (FE) models for the two representative bridges were developed and calibrated with existing data.

3.1 Existing Approaches for Finite Element Modeling of Bridges

Structural analysis programs used by INDOT to process special weight permits utilize simplified analysis with lateral load distribution factors specified by AASHTO (2012) to determine instantaneous girder stresses. This process of analysis usually gives conservative results for girder stresses (see Wood et al., 2007). Guo et al., (2012) constructed a 3-dimensional FE model in the ANSYS (<http://www.ansys.com/>) software program to investigate the fatigue performance of specific details on the bridge and recommended that the optimal size of the element be determined by weighing the required level of accuracy against the need for computational efficiency. Saydam and Frangopol (2011) also built FE models using the ABAQUS (2011) software program and suggested that 8-node shell elements with reduced integration (S8R) be used to model the bridge deck and the plates of steel girders. They also modeled the connections between concrete deck and steel girders using tie connections and rigid links.

3.2 Finite Element Modeling of Concrete-Deck-on-Steel Girder Bridges

In order to analyze the representative steel bridge using FE modeling, two steel bridges were investigated and modeled. One was the representative US 52 bridge under consideration and another similar bridge chosen was the I-65 bridge over Ridge road in Lake County, Indiana. The US 52 bridge has rolled shape girders with diaphragms while I-65 bridge has steel plate girders with stiffeners and L-shape cross beams. Table 3.1 compares some key features of these two bridges. Results validated through FE modeling can be applied to other

TABLE 3.1
Comparison with two bridges for validation.

Parameter	NBI-19027 (US 52)	NBI-38750 (I-65)
1. Span	2 Continuous span 2 @ 92 ft.	1 span (simply supported) 118 ft.
2. Girder	W36 Rolled Shape	Plate Girder
3. Secondary Elements	Diaphragm: W18 Rolled Shape	Stiffener and L-crossbeam
4. Measurement	Canna & Bowman (2002)	Wood et al., (2007)
5. FE analysis	SAP2000 and ANSYS (Wood et al., 2007)	SAP2000 and ANSYS (Wood et al., 2007)

bridges with similar details. Both these bridges have been instrumented and analyzed by FE modeling in previous studies and therefore help in calibrating the FE models for this study.

The US 52 bridge chosen in this study had previously been instrumented by Canna and Bowman (2002) who had also developed a simple beam-type FE model for it. They suggested that the diaphragms need to be connected to girders as fully rigid or hinged connections to obtain more realistic results. Wood et al. (2007) developed a full 3-dimensional FE model using 4-node shell elements in the SAP2000 (<http://www.csiamerica.com/products/sap2000>) and ANSYS (<http://www.ansys.com/>) software programs and compared their results to the experimental study conducted by Canna and Bowman (2002).

3.2.1 Description of the FE Model for the US 52 Representative Steel Bridge

Basic properties of the US 52 bridge are described in Table 3.2 and depicted in Figure 3.1. For the FE modeling of the US 52 bridge, shell elements and solid elements were used for the superstructure such as deck, parapets, girders and diaphragm. The bearing was not considered in this study. Table 3.3 shows FE modeling of US 52 bridge using ABAQUS version 6.11.

In this study, a full-scale FE model of the US 52 bridge (NBI-19027) was constructed as shown in Figure 3.2. The steel superstructure was modeled using 4-node shell elements (S4R) and 8-node solid elements (C3D8I) were used for the concrete deck. The dimensions of concrete deck were 12.2 meters (40 ft.) width and 28.0

TABLE 3.2
Key parameters for US 52 NBI-19027 bridge.

Parameter	NBI-19027 (US 52)
1. Main Girder	W36X150 (Positive moment area), ASTM A572 steel W36X230 (Negative moment area), ASTM A572 steel
2. Slab	7.5 in thickness, $E_c = 3,605$ ksi, $\sigma_{ck} = 4$ ksi
3. Frames	8 main girders with welded diaphragms of W18X45
4. Others	No skew; Built in 1970; Parapet height: 33 in. Interior girder spacing: 6 ft. (see the plan view)

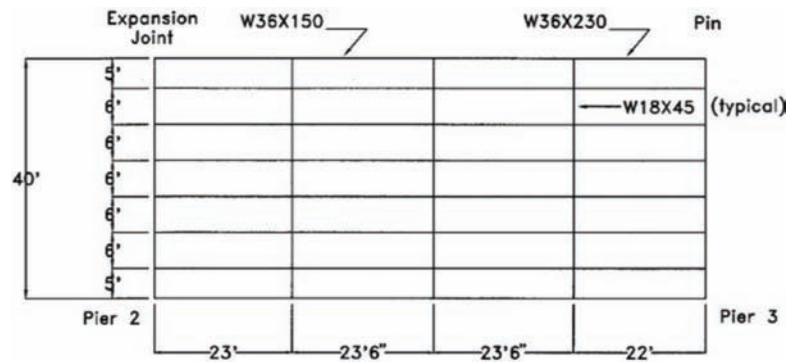


Figure 3.1 Plan view of US 52 bridge. (Source Wood et al., 2007.)

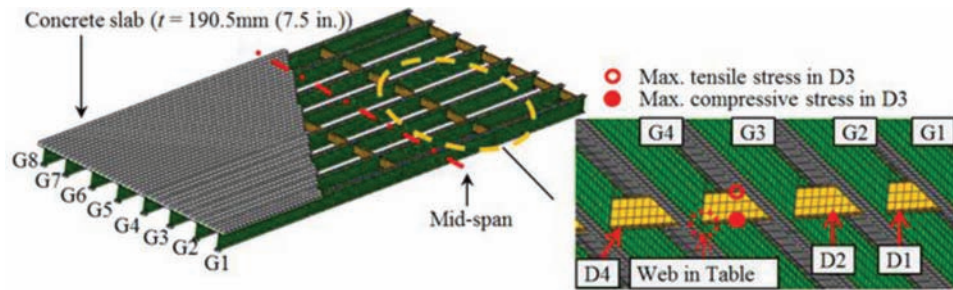
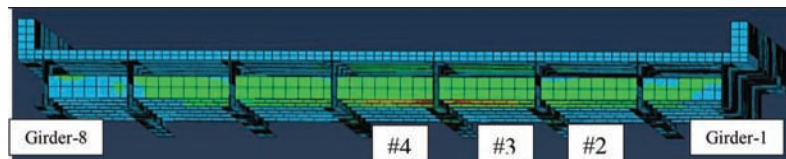


Figure 3.2 Finite element model of representative steel bridge.

TABLE 3.3
Description of 3D FE modeling parameters for the US 52 bridge.

Parameters	3D Modeling Using ABAQUS
Slab	Solid modeling (C3D8R, C3D20R)
Parapets	Solid modeling (C3D8R)
Girders	Solid modeling (C3D8R, C3D20R) Shell modeling (S4R)
Diaphragms	Solid modeling (C3D8R, C3D20R) Shell modeling (S4R)
Connection conditions	Main girders to concrete slab (Tie-constraint) Diaphragms to main girders (Merge)
Boundary conditions	Both of the end supports: Roller Interior support: Fixed

Cross-section view



meters (92 ft.) length per span. The thickness of the deck was 190.5 mm (7.5 in.) and the compressive strength of concrete (f'_c) was taken as 28 N/mm² (4 ksi). The deck was connected to girders using the option for tie connection in ABAQUS (2011) to simulate full composite action. The girders were composed of W920 × 343 (W36 × 230) rolled-shape beams of ASTM A572 steel with Young's modulus of 200 GPa (29,000 ksi) and Poisson's ratio 0.27. For the steel diaphragms W460 × 68 (W18 × 45) rolled-shape beams of A36 steel

were used. All the steel diaphragms were connected to girders using the merge option in ABAQUS.

For validation of the 3D modeling, two load cases were applied as shown in Figure 3.3. The stress values were obtained at the location with respect to the corresponding measurements of Canna and Bowman (2002) and of the FE analysis by Wood et al. (2007). In both these studies, the bridge was subjected to static load using a truck weighing 232 kN (52 kip). In addition, Wood et al. (2007) also considered a "superload" truck weighing 3,665 kN

(824 kip). Sensors were installed on flanges and the web of the mid-span of Girder-4 (Canna & Bowman, 2002). Diaphragms in Row 2 (#2, #3 and #4) were also instrumented as shown in Table 3.3.

In order to validate ABAQUS modeling subjected to superload, comparison with Maximum truck load results was conducted using 824 kips truck superload shown in Figure 2.9. The maximum truck load was applied on US 52 bridge as shown on Figure 3.4. Sample results from these test cases of the bridge are shown in Figure 3.5 and Figure 3.6.

Table 3.4 compares the results obtained from the FE model in this study to previous studies for both these truck loads where the locations of the stresses mentioned in Table 3.3 are shown in Figure 3.2. The current study uses both shell and solid elements for steel components in the ABAQUS modeling program. However, solid elements (especially C3D20R) took much more time in

ABAQUS to calculate the solution than the shell element models. Nevertheless, results of detailed solid modeling with C3D20R elements were also very similar to the results from Wood et al. (2007). The potential reasons for some of the discrepancies observed in the stress values are discussed in the next subsection.

In addition to the analysis for the two test trucks and the maximum load described above, additional analysis was conducted for all the representative loads mentioned in Table 2.1. Figure 3.7 shows how the response of specific structural elements changes with increasing load classes. One may note that the localized structural response for increases load classes is similar to cost allocation curves which are typically used in determining permit costs. In these plots, zero applied load corresponds to dead load only. It is also noted that the web gap stress in the US 52 bridge model was close to ultimate tensile strength of ASTM A572 steel.

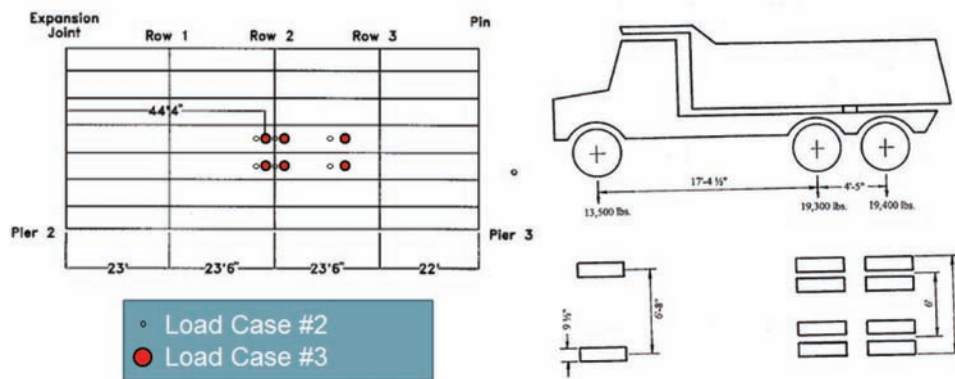


Figure 3.3 Applied truck loads. (Source: Wood et al., 2007.)

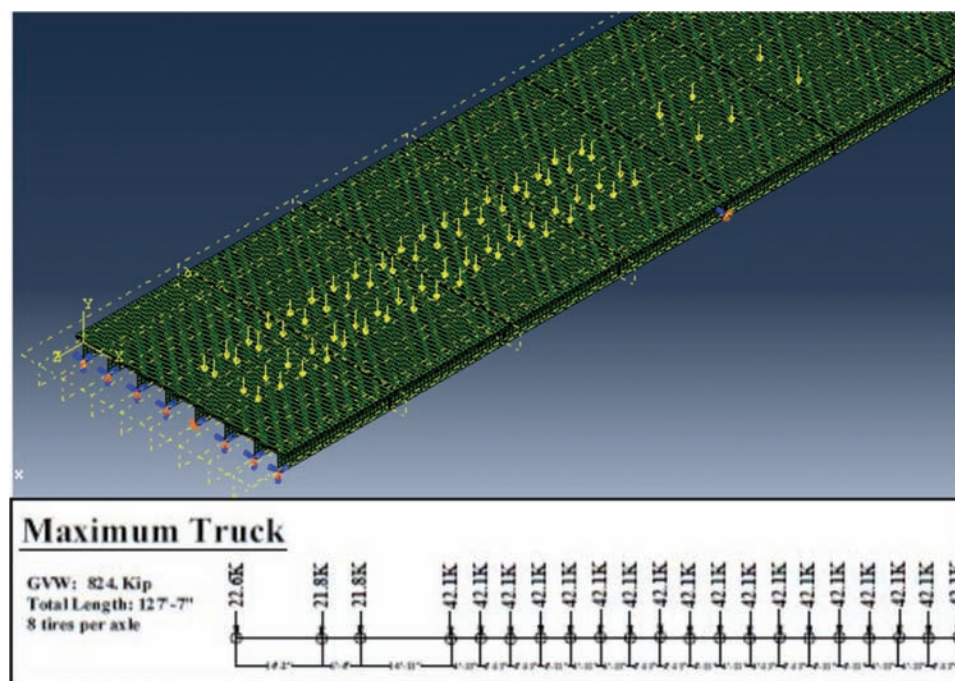
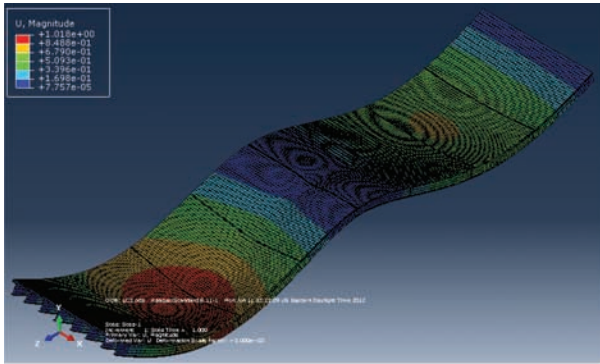
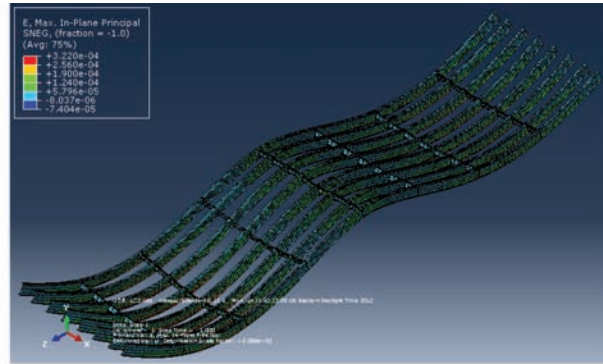


Figure 3.4 Applied maximum truck load on US 52 bridge.

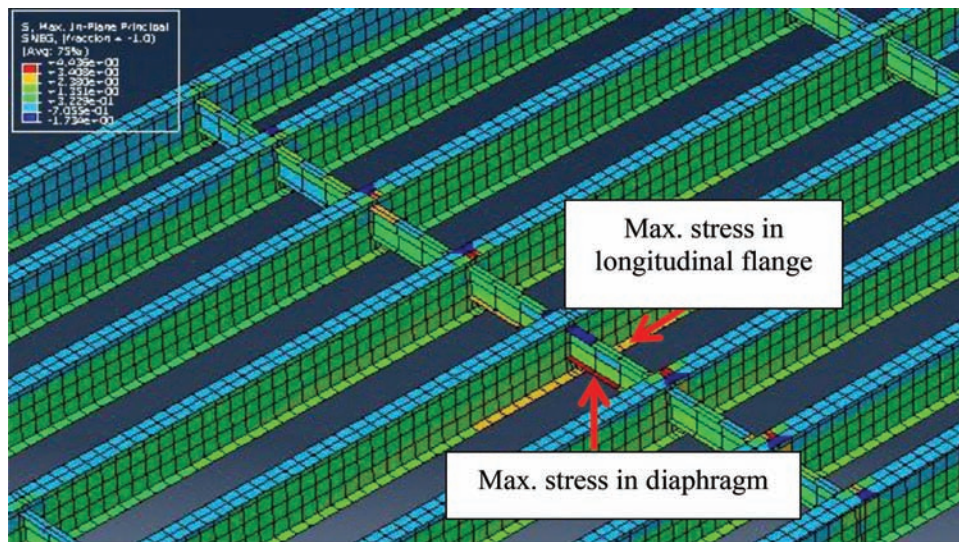


(a) Deflection shape of US 52 bridge

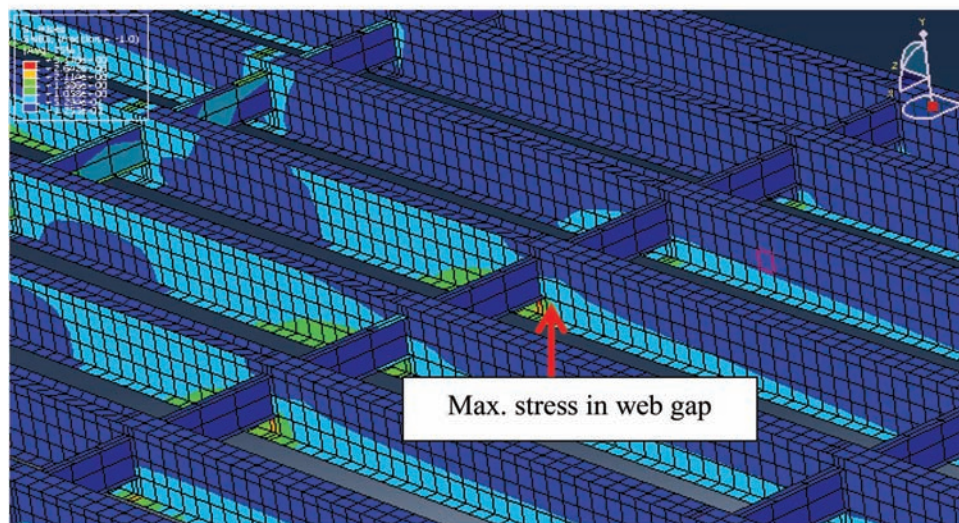


(b) Deflection shape of US 52 steel parts

Figure 3.5 Results from FE modeling of the US 52 bridge.



(a) Maximum stress in diaphragm and longitudinal flange



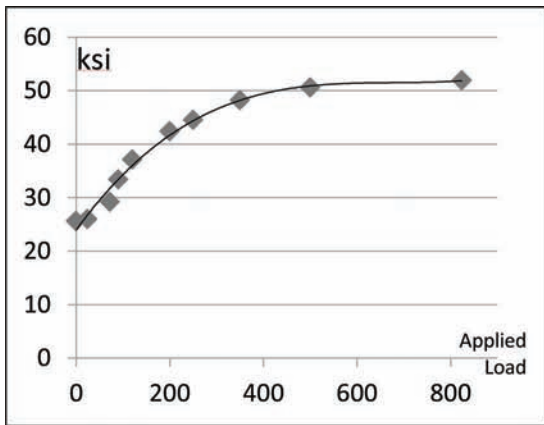
(b) Maximum stress in web gap region

Figure 3.6 Location of maximum stresses on US 52 bridge.

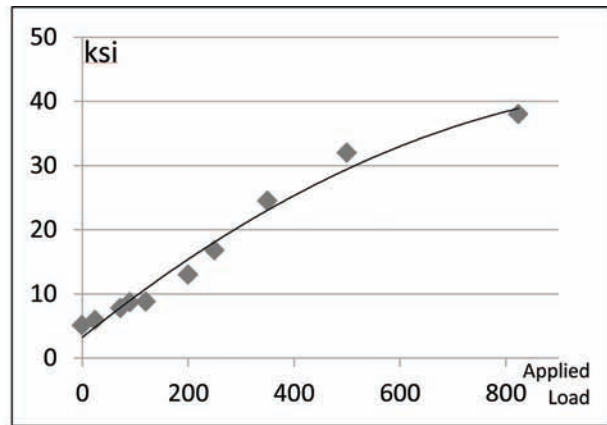
TABLE 3.4
Comparison of results from current FE model and prior research.

Stress Location	Results from This Study (S4R)	Modeling Results Wood et al. (2007)		Measurement Data Canna & Bowman (2002)			
		Value	S4R/Value	Value	S4R/Value		
Max. longitudinal Stress in bottom flange of girder #4	18.2 N/mm ² (2.64 ksi)	17.9 N/mm ² (2.59 ksi)	1.02	18.1 N/mm ² (2.63 ksi)	1.01		
Max. longitudinal stress in girder #4 bottom flange*	175.8 N/mm² (25.5 ksi)	193.1 N/mm² (28.0 ksi)	0.91	N/A	N/A		
Max. stress of Diaphragm	#2	Top	2.76 N/mm ² (0.40 ksi)	0.55 N/mm ² (0.08 ksi)	5.02	2.34 N/mm ² (0.34 ksi)	1.18
		Bottom	11.0 N/mm ² (1.60 ksi)	7.52 N/mm ² (1.09 ksi)	1.46	7.58 N/mm ² (1.10 ksi)	1.45
	#3	Top	-12.4 N/mm ² (-1.80 ksi)	-8.89 N/mm ² (-1.29 ksi)	1.39	-0.83 N/mm ² (-0.12 ksi)	14.94
		Bottom	21.7 N/mm ² (3.15 ksi)	19.8 N/mm ² (2.87 ksi)	1.10	19.9 N/mm ² (2.89 ksi)	1.09
	#4	Bottom*	237.9 N/mm² (34.5 ksi)	234.4 N/mm² (34.0 ksi)	1.01	N/A	N/A
		Top	10.3 N/mm ² (1.50 ksi)	5.86 N/mm ² (0.85 ksi)	1.76	2.69 N/mm ² (0.39 ksi)	3.83
	Bottom	21.0 N/mm ² (3.05 ksi)	16.3 N/mm ² (2.37 ksi)	1.29	20.1 N/mm ² (2.91 ksi)	1.04	
	Max. vertical stress in web gap of girder #4*	350.9 N/mm² (50.9 ksi)	434.4 N/mm² (63.0 ksi)	0.81	N/A	N/A	

*The bolded rows correspond to stresses due to a maximum truck load of 3,665 kN (824 kips). The rest of the rows correspond to stresses due to the test truck load of 232 kN.



(a) Web gap's response of US 52 bridge



(b) Stiffener's response of US 52 bridge

Figure 3.7 Response of structural elements to representative loads.

3.2.2 Discussion of Finite Element Modeling and Calibration

While most stress values matched well with existing studies, there were discrepancies also. In order to address the potential effect of these discrepancies, first, we note that the longitudinal stresses in the flanges of the girders (which are the main load bearing structural components) matched very well, and this shows that the FE model in this study was able to capture the overall response of the bridge very well. The large discrepancies in the stresses primarily occurred in the diaphragms, which are secondary structural elements that redistribute the load in the transverse direction between the main girders. Discrepancies in these stresses can be attributed to a variety of reasons ranging from imperfect composite action between the deck and girders due to bridge aging, imperfect weld connections between the girders and diaphragms, presence of cracks (which can cause redistribution of stresses away from the cracked locations) that were not modeled in this study, possible flaws in the measured data, differences in the FE models used in this study and that of Wood et al. (2007), and a range of other possibilities.

Secondly, we point out that the objective of the FE model in this study is not to accurately capture the behavior of this particular US 52 bridge in minute detail, rather it is to model a *representative* bridge to study the durability of similar bridges. Since the FE model in this study is based on the original design of the bridge, we expect that the durability of the subset of bridges that are similar to this representative bridge will be modeled well, on an average. Bridges in this subset that deviate significantly from the FE model of the representative bridge used in this study will indeed not be modeled well with this approach, in much the same way that two identical material test coupons don't fail at the same number of load cycles in a fatigue test because of minute differences in the microscopic defects within them. In this particular case, for the US 52 bridge chosen in this study, despite the large differences in stresses within some of the secondary structural elements of the bridge, the overall structural behavior of the bridge is modeled very well and these local discrepancies are expected to have minimal effect on the evolution of average damage (especially when averaged over all the elements) of the bridge.

3.2.3 Calibration of Mesh Size

In order to determine an appropriate element size for the steel superstructure, the bridge was modeled using three different levels of FE mesh refinement and was subjected to a controlled load of 4,450 N (1 kip) moving along the longitudinal direction. Figure 3.8 shows the stress-time history under this load at two locations near the middle of the first span, one at the bottom flange of a main girder and the other within a diaphragm. With considerations to aspect ratios of elements, the required accuracy and the need for computational speed, mesh 2 was chosen as an appropriate level of refinement as it

seemed to provide good results in a moderate amount of computational time (3 hours for each ΔT simulation period). Mesh 2 consisted of 76 mm \times 76 mm (3 in. \times 3 in.) elements for the diaphragm flange, 76 mm \times 114.3 mm (3 in. \times 4.5 in.) elements for the diaphragm web, 152.4 mm \times 114.3 mm (6 in. \times 4.5 in.) elements for the girder flange, and 114.3 mm \times 114.3 mm (6 in. \times 4.5 in.) elements for the girder web. Mesh 2 resulted in a total of 137,000 elements for the entire bridge model.

3.2.4 Calibration of Model Damping

In order to calibrate default damping ratio considering gravity, a simply supported beam 250 feet long with a cross section 30-inch-deep \times 20-inch-wide was modeled in ABAQUS IMPLICIT as shown in Figure 3.9. Free vibration response of the beam after an initial downward displacement of 0.5 inch at center of span was used to compute the appropriate damping. The displacement time history at the center of span was measured for 10 seconds as shown in Figure 3.10.

Using Figure 3.10 and the logarithmic decrement method, damping ratio was computed as:

$$\delta \cong \ln(x_n \div x_{n+1}) = \ln\left(\frac{0.403}{0.335}\right) = 0.184$$

where δ denotes the natural logarithm of the ratio of successive peak displacements. The damping can then be computed as:

$$\xi = \delta \div 2\pi = \frac{0.184}{2\pi} = 0.03 = \mathbf{3.0\%}$$

The damping ratio was also calculated using exponential curve with successive peak value yielding a value of 4% as shown in Figure 3.11. For steel bridges, a damping ratio of 3.0% to 4.0% is realistic and is used in current FE modeling with ABAQUS 6.12.

3.2.5 Description of the FE Model for the I-65 Bridge (NBI-38750)

The I-65 bridge over Ridge road is located in the Northwest corner of Indiana in Lake County between Gary and Hobart (see Figure 3.12). This bridge location was selected because it is on a known route for overweight trucks and superloads. More information of this bridge is described in Table 3.5.

For the FE modeling of the I-65 bridge, shell and solid elements were used for deck, parapets, girders and stiffeners. Modeling for the L-shape cross-beam was conducted using beam elements. Table 3.6 shows parameters used in the FE modeling of I-65 bridge using ABAQUS version 6.11.

For validation of the 3D modeling of the I-65 bridge, the load case causing maximum stress in bottom flange and stiffener was applied as shown in Figure 3.15. Stress values were obtained at the different locations corresponding to the measurements and FE analysis conducted

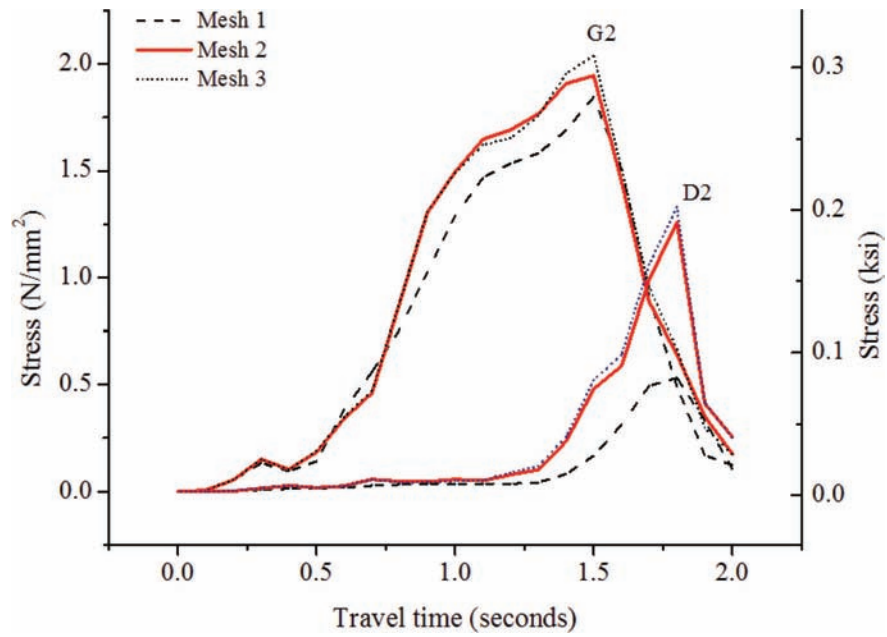


Figure 3.8 Results of mesh convergence study.

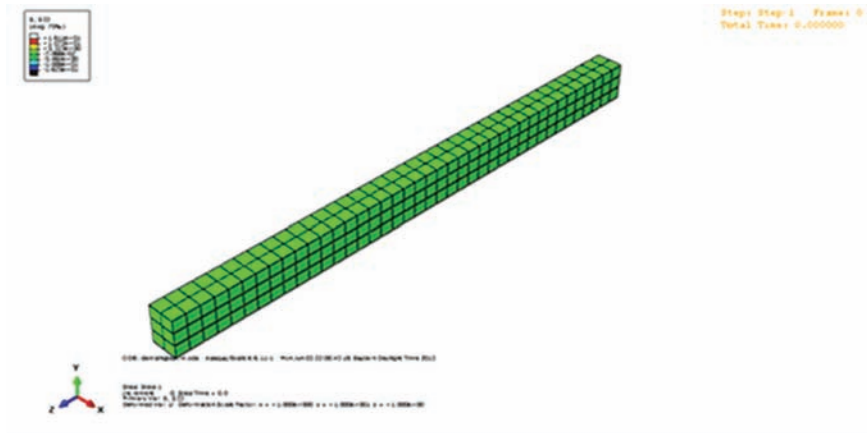


Figure 3.9 Model of simply supported beam used for calibrating damping.

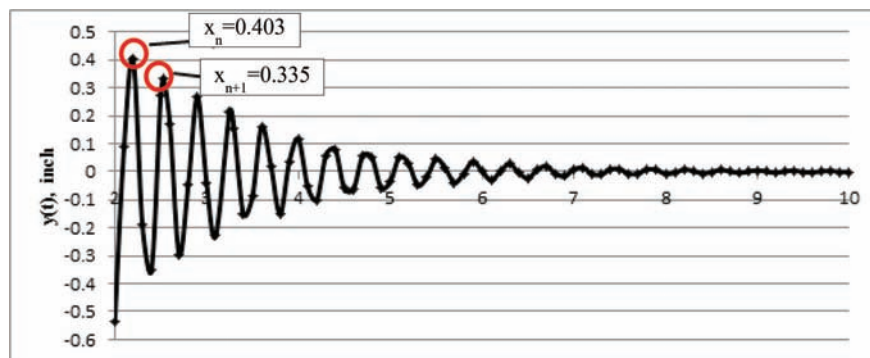


Figure 3.10 Displacement time history at center span.

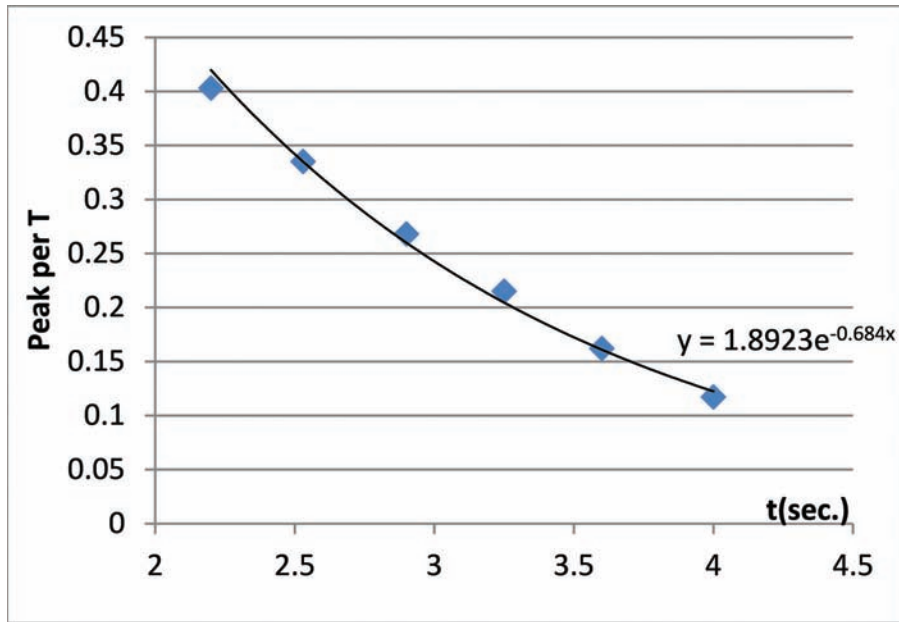


Figure 3.11 Estimation of damping.



Figure 3.12 I-65 bridge in Lake County, Indiana.

TABLE 3.5
Information of NBI-38750 bridge on I-65.

Parameter	NBI-38750 (I-65)
1. Main Girder	Plate girder (57 in deep), ASTM A572 steel
2. Slab	9.0 in thickness, $E_c = 3,605$ ksi, $\sigma_{ck} = 4$ ksi
3. Frames	10 main girders with welded L-shape cross beam of Grade 36
4. Others	No skew; Built in 2001 Interior girder spacing: 11.2 ft. Stiffeners (see Figure 3.13)

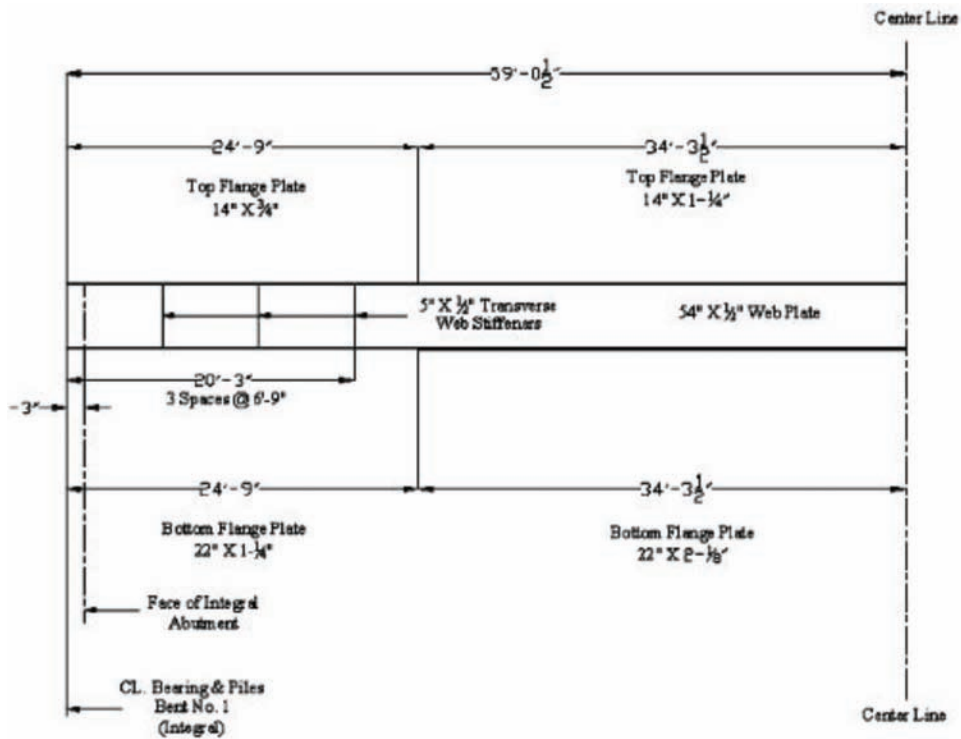
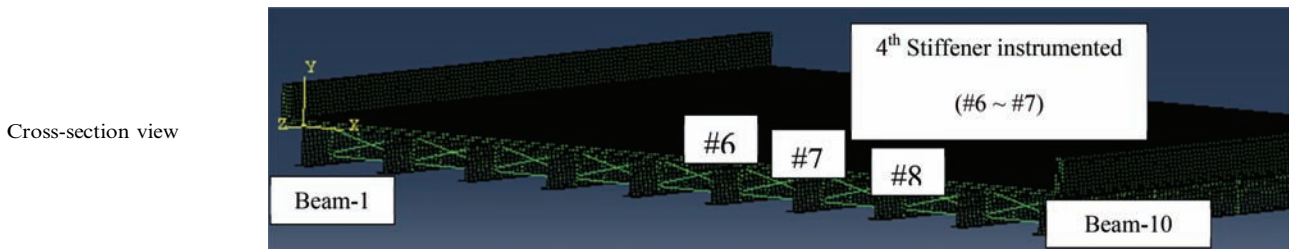


Figure 3.13 Side view of I-65 bridge.

TABLE 3.6
Description of 3D modeling for I-65 bridge.

Parameters	3D Modeling Using ABAQUS
Slab	Solid modeling (C3D8R)
Parapets	Solid modeling (C3D8R)
Girders	Solid modeling (C3D8R) Shell modeling (S8R), (2 different flange thicknesses as shown in Figure 3.13)
Stiffeners	Solid modeling (C3D8R) Shell modeling (S8R)
Crossbeam	Wire with L profile (see Figure 3.14)
Connection conditions	Main girders to concrete slab (Tie-constraint) Between flanges and web, Stiffeners to girder, Cross beam to Stiffener (Merge)
Boundary conditions	Both of the end supports: Integral Abutment (Fixed support)



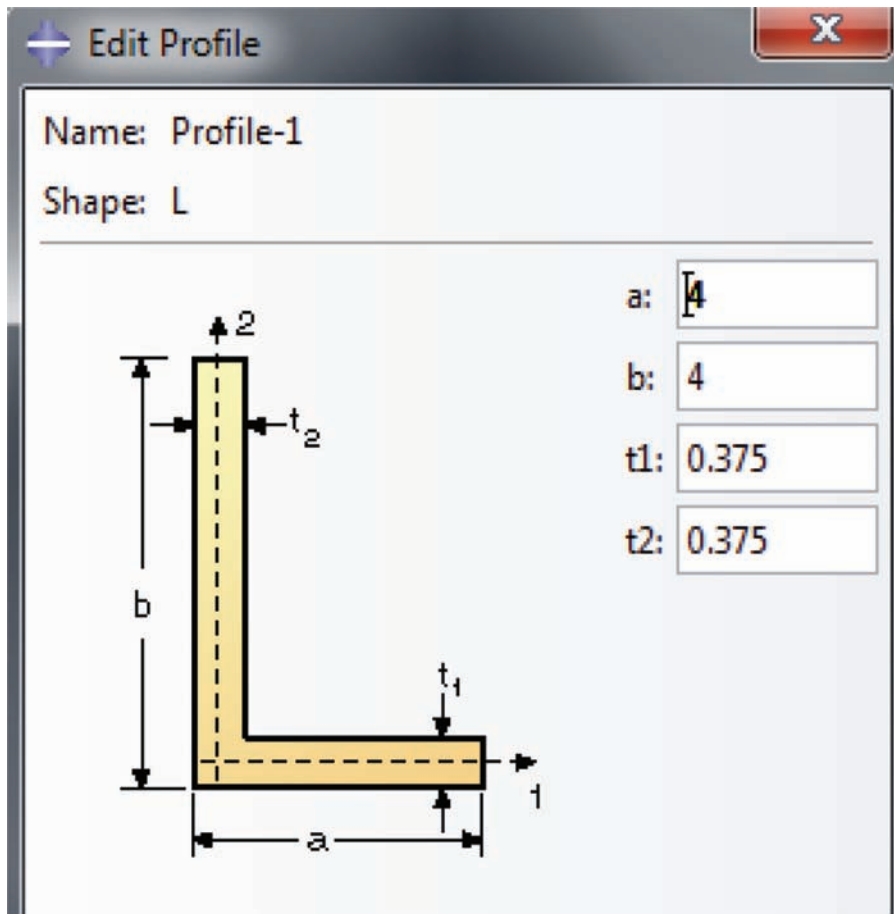


Figure 3.14 Beam element with L cross-sectional profile used for cross-beams.

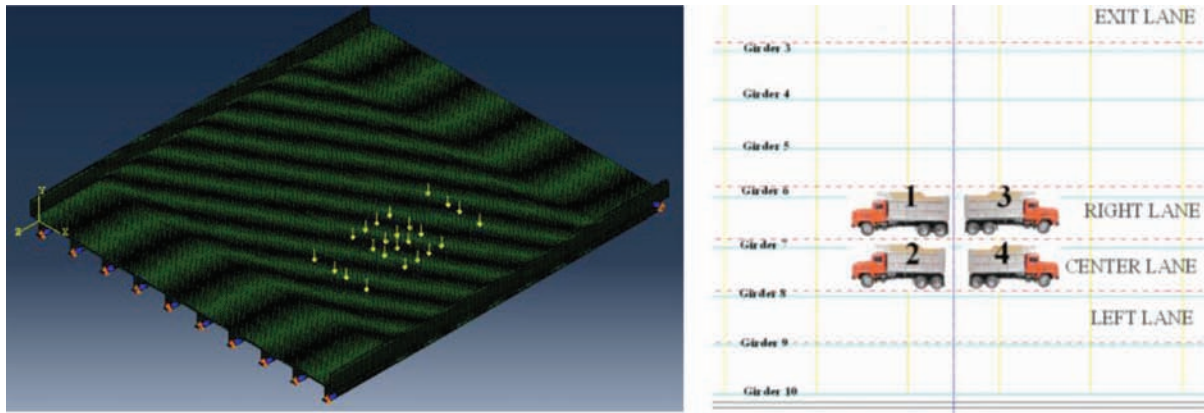


Figure 3.15 Applied test truck load on I-65 bridge.

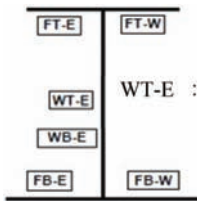
Wood et al. (2007). Especially, sensors were installed on flanges and the web of the mid-span of the girder 6, 7 and 8 as shown in Table 3.6. The 4th cross beams from the end support between girder 6 and 8, which are closest to the mid-span, were also instrumented.

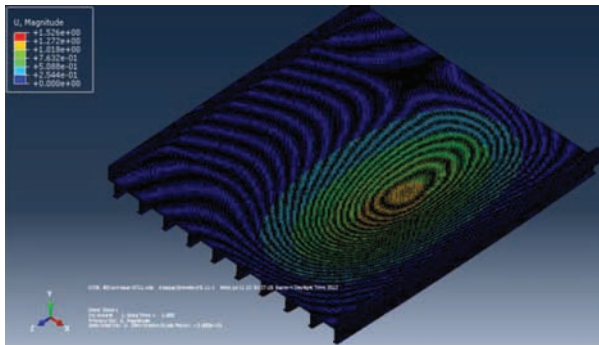
Compared to modeling results and instrumentation data from Wood et al. (2007) in Table 3.7, the current ABAQUS modeling results based on shell elements for

steel structures of I-65 bridge were very close. Solid modeling (C3D8R) was similar with the stresses in tension area such as top flanges. However, detailed solid modeling with C3D20R was not used for I-65 analysis due to having over 500,000 elements. Figure 3.16 shows the deflection shape of the I-65 bridge subjected to the test load.

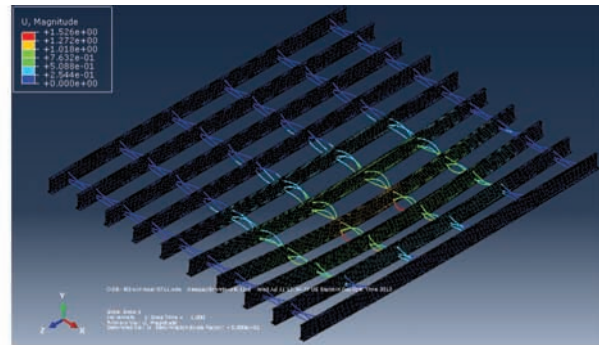
For NBI-38750 I-65 bridge, four superload groups including the maximum truck load were applied.

TABLE 3.7
Comparison of ABAQUS modeling results with prior research.

Stress Subjected to Test Load		Wood's Measurement	Wood's Model	Solid model (C3D8R)	Shell Model (S8R)
Flange of Girder #7 at mid-span 	FT-E	-0.3 ksi	-0.6 ksi	-0.6 ksi	-0.03 ksi
	FT-W	-0.4 ksi	-0.6 ksi	-0.6 ksi	-0.07 ksi
	WT-E	-0.7 ksi	1.5 ksi	2.1 ksi	1.7 ksi
	WB-E	2.0 ksi	2.8 ksi	3.0 ksi	3.4 ksi
	FB-E	2.5 ksi	3.8 ksi	7.9 ksi	5.5 ksi
	FB-W	2.4 ksi	4.0 ksi	7.9 ksi	5.5 ksi
	WT-E				
Flange of Girder #6 at mid-span	Top	-0.4 ksi	-0.6 ksi	-0.5 ksi	-0.15 ksi
	Bottom	2.2 ksi	3.2 ksi	5.39 ksi	3.54 ksi
Stiffener close to mid-span	Horizontal	–	0.02 ksi	0.56 ksi	0.14 ksi
	Vertical	2.4 ksi	2.2 ksi	2.0 ksi	1.81 ksi
Cross-beam at mid-span	Girder 6~7	2.16 ksi	2.47 ksi	8.4 ksi	2.97 ksi
	Girder 7~8	1.92 ksi	2.44 ksi	9.1 ksi	2.13 ksi



(a) Deflection shape of I-65 bridge



(b) Stress distribution in steel for I-65 bridge

Figure 3.16 Results from FE modeling of the I-65 bridge.

Prior research of Wood et al. (2007) does not include the exact location of applied superload on the bridge. So, the superload groups were applied by considered single axle loads multiplied by influence line values to find maximum stresses (see Figure 3.17). The maximum stresses in the longitudinal flange and

stiffeners through ABAQUS modeling are shown in Table 3.8.

Comparing with the modeling results from Wood et al. (2007), the current FE model of I-65 bridge based on shell elements for steel structures performs very closely to in terms of stresses of longitudinal flanges at the mid-span.

TABLE 3.8
 Comparison of results for I-65 bridge with superload.

Max. Stress	Longitudinal Girder #7 at Mid-Span		Stiffener of Girder #7 Closest to Mid-Span	
	Wood's Modeling	Shell Model of ABAQUS	Wood's Modeling	Shell Model of ABAQUS
Group A	2.0 ksi	1.89 ksi	8 ksi	7.9 ksi
Group B	2.0 ksi	1.60 ksi	9 ksi	11.7 ksi
Group C	2.5 ksi	2.43 ksi	12 ksi	19.4 ksi
Group D	5.0 ksi	4.58 ksi	22 ksi	26.9 ksi
Max. Truck	7.2 ksi	6.95 ksi	35 ksi	38 ksi

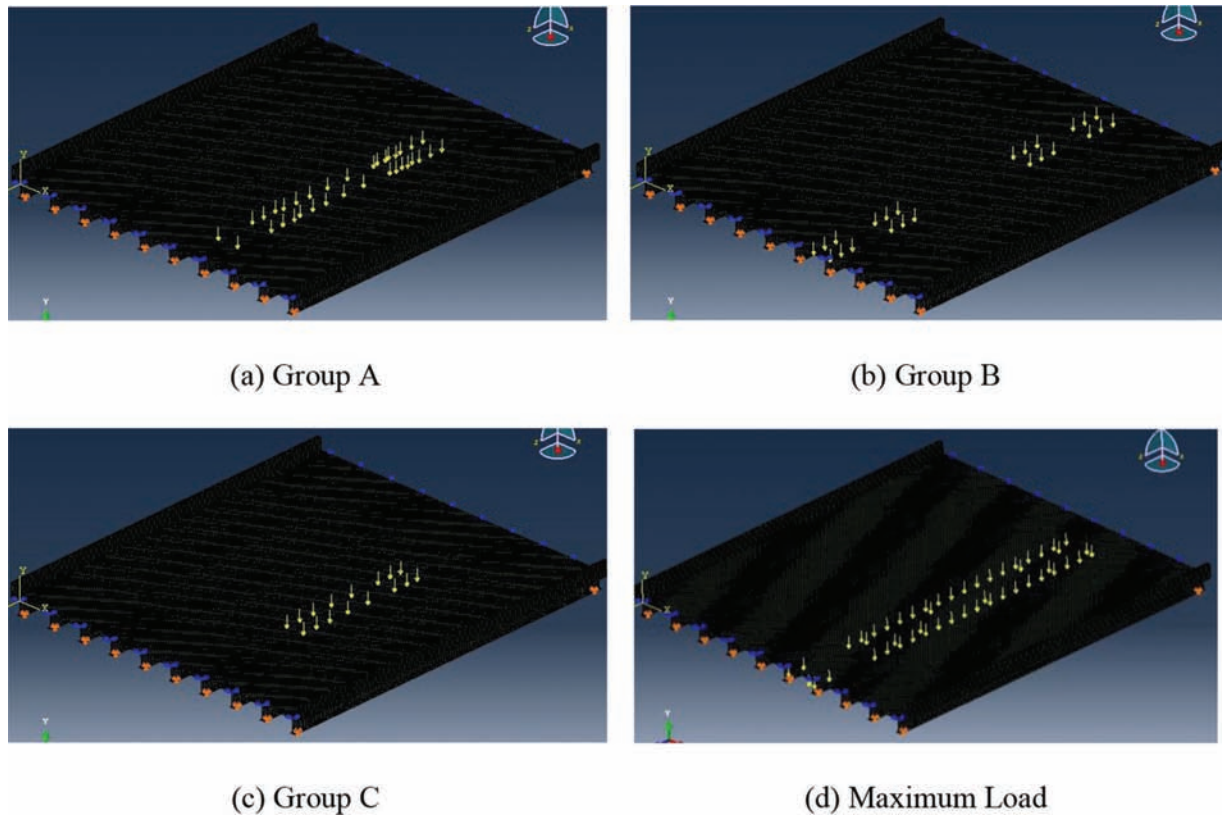


Figure 3.17 Applied superload configurations on the I-65 bridge.

3.2.6 Summary of FE Modeling of Representative Steel Bridges

Finite element modeling in 3D using ABAQUS for this study was validated through two representative bridges against tests and modeling conducted by Wood et al. (2007) and Canna and Bowman (2002). While there were some differences in secondary elements for the stresses obtained from the finite element models constructed in this study, the overall behavior of the two bridges was very similar to existing studies.

4. FINITE-ELEMENT MODELING OF REINFORCED AND PRE-STRESSED CONCRETE BRIDGES

In order to construct detailed finite element models of RC and PSC bridges, modeling the bond and interaction between the reinforcing bars and the surrounding concrete is essential. A simple reinforced concrete beam model was first tested to ensure the proper modeling of this aspect.

4.1 Modeling of RC Components

A simply supported RC beam of length 20 feet with cross-section shown in Figure 4.1 (12 inch \times 20 inch) was modeled in ABAQUS 6.11. The concrete strength, f'_c , was taken as 6,000 *psi* (41.4 *Mpa*) and the Young's modulus was taken to be 4,000 *ksi* (2.7 *Mpa*). The total area of the reinforcing steel was taken to be 3.14 in^2 with modulus 29,000 *ksi* (200 *Gpa*) and a yield stress of 60 *ksi* (414 *Mpa*). The reinforcing steel is bonded to the concrete material in ABAQUS using the merge option

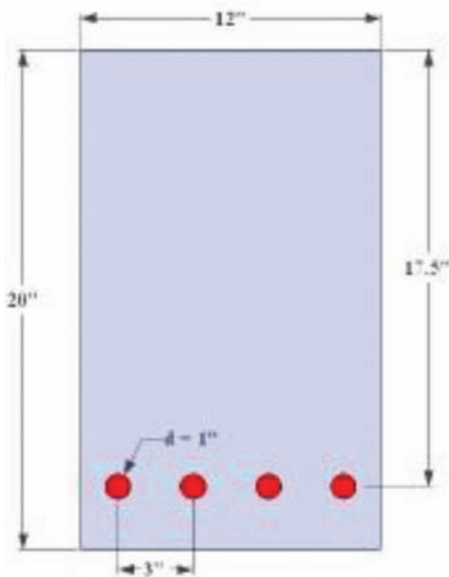


Figure 4.1 Geometry layout and static scheme of the numerical modeling.

while specifying two different material properties for the concrete and steel components.

4.1.1 Verification for Static Loads

The beam was first subjected to a uniformly distributed load of $w = 0.012 \text{ kips/in}$ (6.8 *kN/m*). As a reference solution, theoretical deflections can be computed as:

$$y = \frac{wx}{24EI} (I^3 - 2Ix^2 + x^3)$$

The maximum stress in the middle span is:

$$\sigma_{max} = \frac{5wI^4}{384EI}$$

The bending moment is given as well:

$$M_x = \frac{wLx}{2} - \frac{wx^2}{2}$$

where the stress could be written as:

$$\sigma_{bending} = \frac{M_x y}{I}$$

By choosing elements along the beam in the finite element model, one can compare the calculated and simulated deflections as shown in Figure 4.2 and stresses in Figure 4.3. There is a strong correlation with the theoretical predictions and the results in the finite element model. The finite element techniques could be used to model the concrete bridges under static loadings.

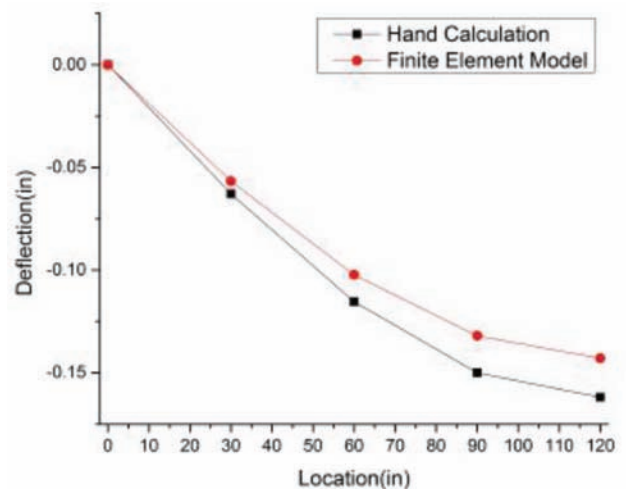


Figure 4.2 Comparison of deflection obtained from the FE model with theory.

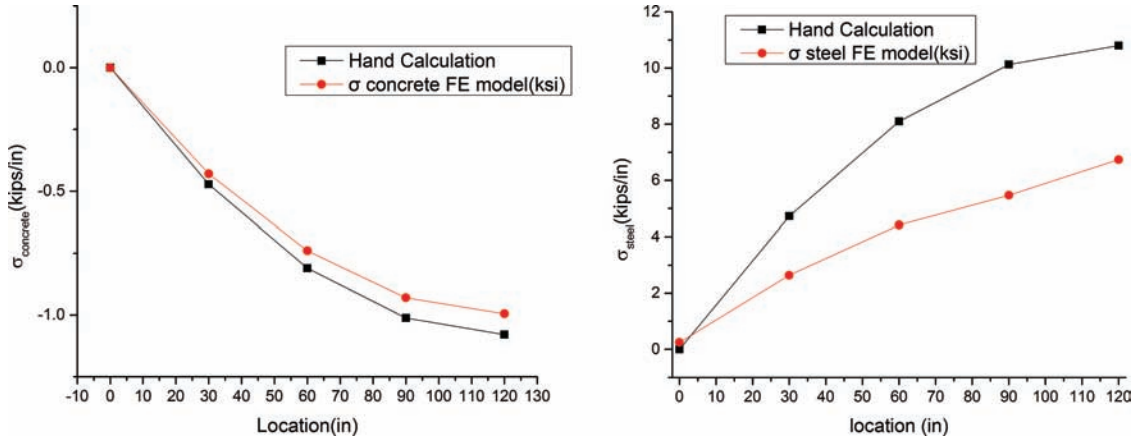


Figure 4.3 Comparison of stresses: *left*: concrete, *right*: rebar.

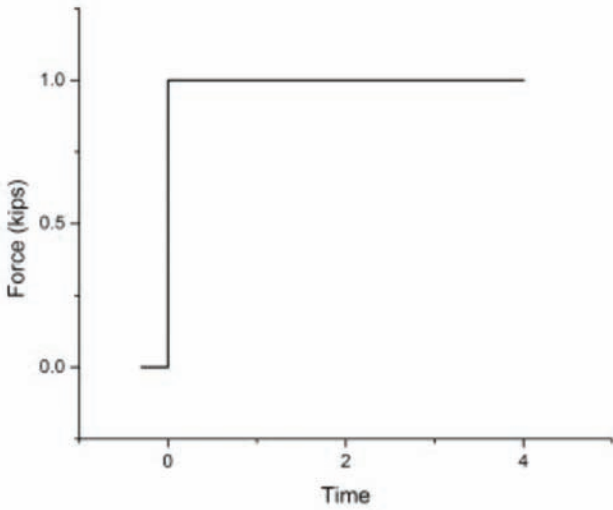


Figure 4.4 Force applied to the sample beam.

4.1.2 Dynamic Loadings on the Composite Beam

To check the dynamic response of the beam, a transient unit force shown in Figure 4.4 is applied at the center of the beam ($x=L/2$).

The natural vibration frequencies are given by:

$$\omega_n = \frac{\pi^2 n^2}{L^2} \sqrt{\frac{EI}{m}}$$

and the modes is given by:

$$\Phi_n(x) = \sin\left(\frac{n\pi x}{L}\right)$$

where m the mass per length of the bridge, E is the modulus of the concrete, 4,000 *ksi*. I is the moment of inertia, and L is the total length of the beam.

Theoretical displacement at $x = L/2$ as a function of time is given by:

$$u\left(\frac{L}{2}, t\right) = \frac{2p_0 L^3}{\pi^4 EI} (1 - \cos\omega_1 t)$$

The theoretical bending moments at mid-span:

$$M\left(\frac{L}{2}, t\right) = -\frac{2p_0 L}{\pi^2} \left[1 - \cos\omega_1 t + \frac{1 - \cos\omega_3 t}{9} + \dots \right]$$

In Figure 4.5 and Figure 4.6 the deflection and stress at the center span of the finite element model are compared to hand calculations with both implicit and explicit simulations. The time period for deflection is observed to be 0.048 seconds, which is close to the theoretical value of 0.046 seconds. Thus the results show a good match of the FE model with theoretical predictions.

4.2 Modeling of Pre-Stressed Concrete

To simulate the effect of pre-stress we developed a two-part model containing concrete and reinforcing strand components, and applied a negative temperature field to the beam to simulate contraction of the steel after cutting of the pre-stressing strands. This provided the concrete portions of the beam with an initial compressive stress as shown in Figure 4.7a. A subsequent application of load then results in the beam reacting in a manner shown in Figure 4.7b. The advantages of this model are that the initial stresses in both the materials: concrete and steel (used in the rebars), can be accounted for, by providing two different temperature coefficients to both these materials and the magnitude of compressive force can be varied by changing the temperature field and/or the temperature coefficients. The procedure is also relatively simple and convenient to implement in the ABAQUS software as it only requires calibrating material properties of the model to obtain the right amount of pre-stress.

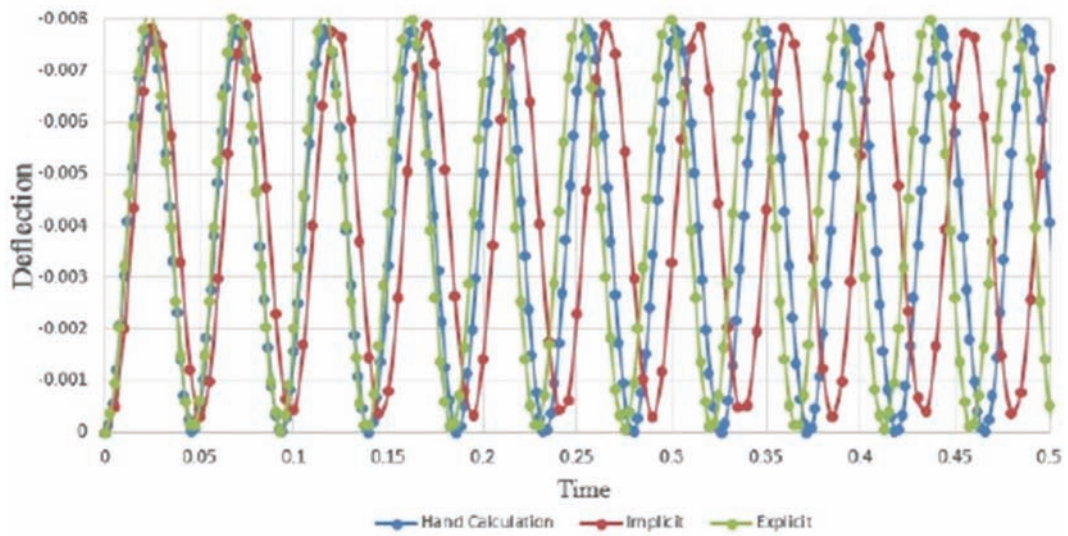


Figure 4.5 Explicit and implicit simulations: deflection.

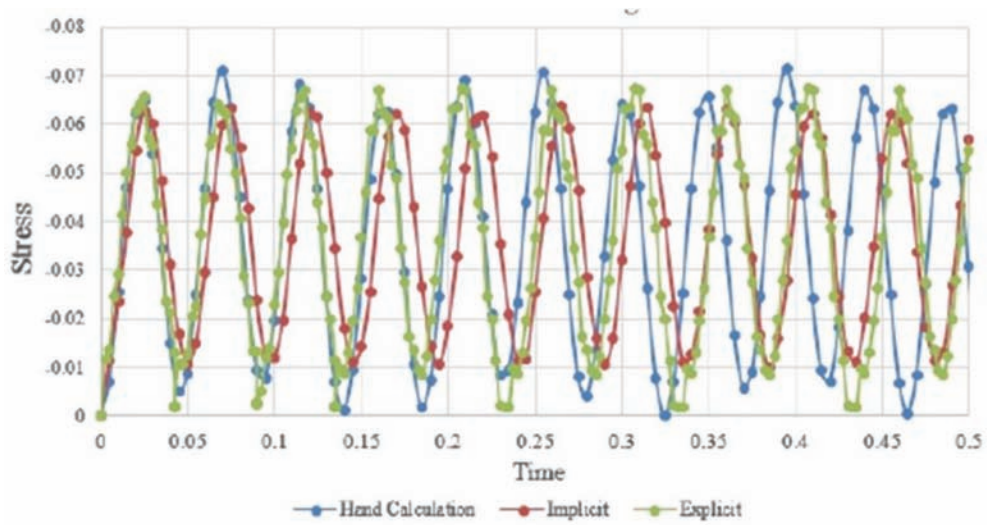


Figure 4.6 Explicit and implicit simulations: stress.

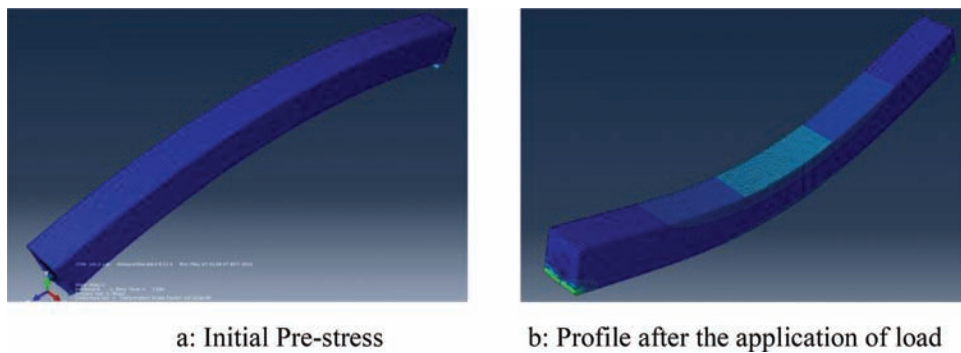


Figure 4.7 FE modeling of a pre-stressed concrete beam.

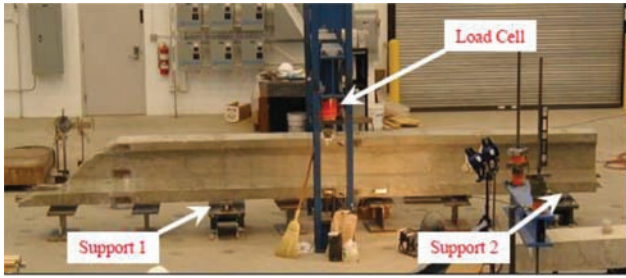


Figure 4.8 Test setup for the PSC beam. (Source: Wood et al., 2007.)

The temperature field to be applied to the model can be computed as:

$$\Delta T = \sigma_c \frac{[A_c + m \cdot A_s]}{\alpha \cdot E_s \cdot A_s}$$

where “ σ_c ” is the desired compressive stress in the concrete after pre-stressing, “ A_c ” is the area of concrete section, “ A_s ” is the area of pre-stressing steel, “ m ” is the ratio of the moduli (E_p/E_c), E_s and E_c are the elastic modulus of steel and concrete respectively and “ α ” is the coefficient of thermal expansion of steel.

4.2.1 Validation of PSC Modeling

In order to test the performance of this approach for modeling PSC beams against available experimental data, the results of a load test performed on a full size pre-stressed concrete beam from Wood et al. (2007) were compared. This beam was cast in the Bowen Lab of Purdue University’s School of Civil Engineering. It was reported that because of some problems with the formwork, the cross-sectional properties, such as flange widths, were varying up to 25% along the span. The original span length of this AASHTO Type-I beam was 30 ft. and its depth was 28 in. The beam had already been tested before for a different research project on shear resistance of beams made of high strength concrete.

Compressive strength of the concrete used for this beam was 10 ksi. The beam was loaded at its mid-span. There was no shear reinforcement along the beam except at the supports. Therefore shear failure and major cracks occurred around the load point at mid-span. The beam was fractured into two pieces at the end of the test. A remaining 18 ft. piece of that beam was used for testing strain gages and transducers (Figure 4.8). For the strain gage and transducer test, the remaining segment of the beam was positioned such that the shear cracks were not included in the 13 ft. span between the supports (Figure 4.8). However, there were two visible cracks at the top of the beam close to the loading point.

The loading ram used for the test was capable of applying 150 kips. The load point was located at 4 ft. from Support 1 and 9 ft. from Support 2. The beam was loaded up to 100 kips for testing the gages and

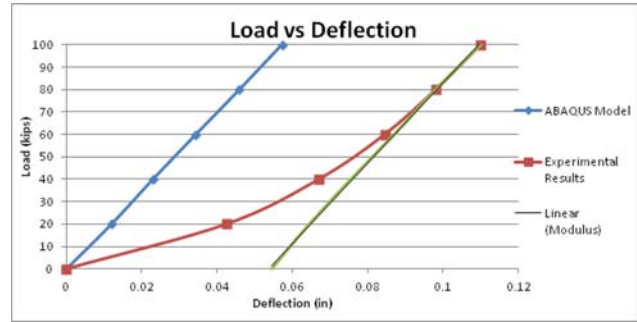


Figure 4.9 Load vs. deflection plot.

transducers several times without causing any additional cracks. A linear voltage displacement transducer was also attached to the bottom of the girder at the load point for measuring the deflections. The load deflection curve of the beam is presented in Figure 4.9.

The load vs displacement plots for this test compared with the FE modeling results are presented in Figure 4.9. The results show that the stiffness of the beam as obtained from the ABAQUS model, matches with the stiffness of the beam for higher load values. This is attributed to the fact that the initial cracks in the beam, as well as non-uniform cross sectional properties of the beam, cause a reduction in the stiffness of the beam for initial cases of loading whereas closing of cracks in the compression region of the beam, on application of higher magnitudes of loads causes an increase in the stiffness of the beam.

It may be noted that Type-II PSC girders are designed to ensure that concrete does not come into tension for normal loading scenarios. Further, both RC and PSC beams are expected to remain in the linear response regime for all permissible truck loads. Thus to simply the modeling procedure for PSC and RC bridges, it was decided that the same process would be used where the concrete would be treated as an elastic material and no temperature field would be applied to create an initial pre-stress. Even with this assumption, models were found to give very close results compared to the detailed modeling of pre-stressed and reinforced concrete as described in the previous sections.

4.3 Description of the FE Model of the Representative Concrete Bridge

A full-scale three-dimensional finite element model of the representative I-164 bridge (NBI-70100) was constructed using 8-node solid elements (C3D8I) for both concrete deck and girders, as shown in Figure 4.10. The dimensions of concrete deck were 12.70 m (41.67 ft.) in width and 41.15 m (135 ft.) in length. There were three spans in the bridge in the length of 12.65 m (41.5 ft.), 16.15 m (53 ft.), 12.65 m (41.5 ft.) with no skew. The thickness of the deck is 203.2 mm (8 in.) and the compressive strength of concrete (f'_c) was taken as 28 N/mm² (4 ksi). The girders were 914 mm (36 in.) deep American Association of State

TABLE 4.1
Comparison of FE results for the I-164 bridge with prior research.

Stress Location	Results of This Study		Results of Wood et al. (2007)		
	N/mm ²	ksi	N/mm ²	ksi	
Longitudinal Stress	Top of Girder 1	-0.199	0.003	0.013	0.002
	Top of Girder 2	-0.262	-0.011	-0.069	-0.010
	Top of Girder 3	-0.399	-0.030	-0.206	-0.030
	Top of Girder 4	-0.655	-0.065	-0.483	-0.070
	Top of Girder 5	-0.668	-0.072	-0.538	-0.078
	Top of Girder 6	-0.414	-0.037	-0.276	-0.040
	Top of Girder 7	-0.255	-0.010	-0.083	-0.012

to the fact that the FE model in this study is based on the assumption of linear behavior while the FE model in Wood et al. (2007) is non-linear. In addition the current model does not consider the influence of pre-stress. Nevertheless, the structural behavior of the bridge is very similar to the reference numerical model from Wood et al. (2007).

In order to choose an appropriate mesh size, a convergence study was also conducted. As we decrease the mesh size the difference of change diminishes thus the results become convergent. Even though the finest mesh can provide more accurate results, the computational time and memory required for such simulations make it infeasible. In this study, we decide to use mesh size shown in Figure 4.10.

With finite elements of steel and concrete bridges calibrated and checked against existing studies, the next focus will be on studying the durability of the representative bridge against natural deterioration and damage caused by traffic loads.

5. COMPUTATIONAL FRAMEWORK FOR MODELING DURABILITY

Assessing the durability of structures is a very challenging problem. Even individual structural components display an immense variation in their life-spans. As is well known, this variation results from the presence of different microscopic defects in otherwise identical virgin specimens of the same component. Nevertheless, when considering a large number of samples, statistical relationships describing how various parameters affect the life of a component are well established in the literature. Fatigue curves (Stress — Number of cycle relationships) are an example of how the magnitude of stress under cyclic loading affects the number of loading cycles that a specimen of material can sustain.

In this research, we restrict our attention to modeling the durability of bridges with steel, reinforced concrete or pre-stressed girder systems and reinforced concrete decks. Some existing models for assessing the durability of structures are presented first and then a detailed description of the

computational framework for durability analysis developed in this research is provided.

5.1 Existing Models for Durability of Structures

Most existing studies suggest that durability of structures is primarily affected by environmental factors and load-related factors.

5.1.1 Deterioration of Steel Components due to Corrosion

For steel superstructures, corrosion is the primary cause of environmental damage, especially due to deicing salts that leach into the structure. Van de Lindt and Ahlborn (2005) conducted analytical work with corrosion of steel bridge beams due to deicing media. The deterioration of steel beam ends due to deck joint leakage and occasional spray from passing vehicles usually consists of irregularly shaped holes, termed section losses, which typically occur in the web near or directly above the bearing area. This may result in decreased shear capacity, web crippling, or web buckling. This study provided the structural analysis with simplified methods for computing the reduced capacity of the steel sections. Kayser and Nowak (1989) performed a field survey to study the corrosion profiles of steel beams and indicated that corrosion is likely to occur over the entire height of the web of steel girders near the supports, and only up to $\frac{1}{4}$ the height of the web at mid-span, as shown in Figure 5.1. This damage profile was also used in a study conducted by Komp (1987) to reduce the area of cross section of the steel girders to simulate structural response. In this study, we adopt a similar approach to adapt the finite element model with age and progression of corrosion.

5.1.2 Models for Deterioration of Concrete

Concrete deterioration is caused by a diverse set of physical and chemical processes which occur in tandem with each other. Chemical processes include corrosion of reinforcing steel, Alkali-Silica Reaction (ASR),

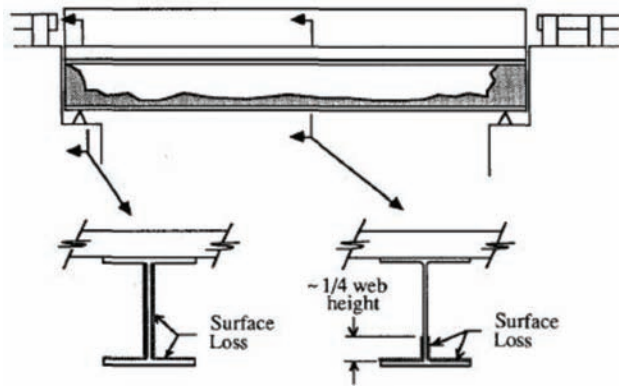


Figure 5.1 Corrosion region in steel girders obtained from field survey. (Source: Kayser & Nowak, 1989.)

external sulfate attack due to contact with Sulfate ions in water, Delayed Ettringite formation (DEF), and other acid attacks. Physical processes include freeze-thaw scaling and physical salt attacks. All these processes — physical or chemical — are affected by permeability and cracking of concrete in a complicated inter-connected way.

The factor that causes that most direct damage to the structure as a whole is the corrosion of steel reinforcement. Ahmad (2003) described the electrochemical processes of steel rebar corrosion as that in a flash battery. The surface of the corroding steel functions as a mixed electrode composed of anodes and cathodes electrically connected through the body of steel itself, upon which coupled anodic and cathodic reactions take place. Concrete pore water functions as an aqueous medium, i.e., a complex electrolyte, thus forming a reinforcement corrosion cell. These processes are influenced by factors both external and internal to the concrete. External factors affecting corrosion pertain mostly to various pollutants and environmental conditions that contain or transport the chemicals that cause/help in accelerating the corrosion process of the reinforcement. These include availability of oxygen and moisture at rebar level, relative humidity and temperature, carbonation and entry of acidic gaseous pollutants to rebar level, aggressive anions (mostly chlorides) reaching the rebar level either through the concrete ingredients or from the external environment, stray currents, bacterial action, etc. Internal factors affecting corrosion are related to substances that are the constituents of the concrete mix used for the construction of the structure or the physical or chemical properties of the mix itself. Various design and construction practices also fall under this category due to their indirect contribution to the strength and stability of the structure. Internal factors affecting corrosion include cement composition, impurities in aggregates, impurities in mixing and curing water, admixtures, water/cement ratio, cement content, aggregate size and grading, construction practices, cover over reinforcing steel, chemical composition and structure of the reinforcing steel, etc. (Krykowski &

Zybura, 2009), the electrochemical description of rebar corrosion and a method of numerical analysis of concrete over degradation resulting from corrosion based on the plasticity theory with distortion. Other works of note on this topic include Morinaga (1990), Beddoe et al. (2009), Boulfiza et al. (2003), Francois and Arliguie (1999), Marchand et al. (1996), and Menéndez et al. (2013).

5.1.3 Modeling the Effect of Natural (Non-Load) Related Factors on Service Life of Structures

There is a rich literature on the various aspects of the damage and deterioration processes and how they affect the life of the structure. Bridge life models try to integrate several deterioration mechanisms and complicated long-term evolution of the damage. For natural deterioration procedures, a general framework of modeling the durability of structures was given by Hjelmstad et al. (1998). They designed a numerical model to simulate the effect of environmental stimuli, including material degradation, structural performance criteria and maintenance strategies over the life of a structure.

Most commonly, service life predictions are based on the time it takes for environmental elements to reach and corrode critical structural components such as girders in steel structures and the steel rebars in reinforced concrete structures. This time to corrosion usually consists of two parts, a depassivation time and a propagation time. Depassivation is the time it takes for chloride ions to penetrate the passive protective layers surrounding structural steel, be it some sort of coating or surrounding concrete cover. Cracking, even micro-cracking, in concrete increases its permeability and leads to acceleration of this stage. Propagation is time it takes for the chemical reaction of rust formation to occur and advance the corrosion within the element.

One of the first attempts to provide a mathematical model of the corrosion process to predict service life was made by Bazant (1979). This model considers the volume expansion due to the formation of red rust ($\text{Fe}(\text{OH})_3$) around the rebar core. The volume of this rust is approximately four times the volume of parent steel and therefore this expansion causes a radial pressure to be exerted onto the surrounding concrete ultimately leading to the spalling of concrete. Another model for corrosion of reinforcing steel was given by Morinaga (1990). This is an empirical model that computes the amount of corrosion when the concrete cover cracks due to expansion caused by rust formation at the rebar surface and relates that to rate of corrosion at steady state. Cusson et al. (2011) developed a service life prediction model based on the transportation of chlorides in concrete. They used the Crank's solution of Fick's second law of diffusion (see Crank, 1979) to determine the chloride ingress in uncracked concrete. In cracked concrete, chloride ingress through cracks can also lead to premature reinforcement corrosion and therefore the chloride diffusion coefficient needs to be

modified to represent the cracked medium (see Boulfiza et al., 2003; De Schutter, 1999; Francois & Arliguie, 1999; Gérard & Marchand, 2000; Rodriguez & Hooton, 2003). This model relates the formation of the corrosion products to radial stress around the rebar at different stages of corrosion-induced damage (i.e., internal cracking, surface cracking, spalling or delamination) and to the time it takes for these stages to occur. Other studies of interest on this topic include Shi et al. (2012), Stark (2011) and Yang et al. (2004).

5.1.4 Modeling the Effect of Load-Related Factors on Service Life of Structures

Several studies have been conducted to investigate the effect of traffic loadings on the life-cycle of bridge structures. Fehlmann and Vogel (2009) performed large-scale tests with frames under cyclic loading showing how fatigue damage can be detected at an early age. Olsson and Pettersson (2010) compared available methods of fatigue assessment and showed that the number of load cycles is not a leading factor governing fatigue life, instead it is primarily affected by the number and range of high-stress causing events.

With the rapid development of computer-aid-engineering (CAE) techniques and the need to analyze more complicated problems, commercial software for predicting service life are also becoming available. One such software is STADIUM by SIMCO Corporation, which covers different types of reinforced concrete structures. A free software is Life-365 (<http://www.life-365.org/>), which can estimate the service life and life-cycle costs of alternative concrete mixtures taking into account corrosion protection systems, effects of chloride exposure, environmental temperature, high-performance concrete mixture proportions, surface barriers, and different steel types. A recent software from Dassault Systems is the FE-SAFE software, a durability analysis software that uses finite element methods. This software can accommodate different types of loading and incorporates a variety of fatigue models to conduct durability analysis.

5.2 Finite Element Framework for Durability Analysis Using Model Updation

In this study, we postulate that statistical arguments that are used to study the fatigue life of individual material coupons can also be extended to study the durability of a bridge inventory (comprising thousands of bridges) within a particular state or even across the nation. We argue that within a given inventory of bridges, one can identify multiple subsets of bridges that are *similar* to each other (based on some classification criteria), and that the behavior of each of these subsets of bridges can be studied using computational models of one or more bridges that are *representative* of that particular subset. Detailed finite element (FE) models of these representative bridges were developed and calibrated with real-life data for studying the effect

of various nature- and human-induced factors on their durability.

In general, FE models are great for analyzing a structure's behavior for short periods of time on the order of seconds or minutes, such as the response of a bridge to a vehicle crossing over it. However, they are not well-suited for directly simulating long-term damage progression of incremental damage resulting from repetitive vehicular loading and environmental factors. To overcome this limitation, we employ the technique of FE model updation as shown in Figure 5.2. Using this technique the durability analysis of a representative bridge can be conducted by dividing the life-span of a bridge into several simulation time-steps ΔT (which can be of the order of months or years), and the FE model is continuously updated at the end of every time step as the simulation progresses, to reflect the progression of damage in the bridge.

Within each simulation time step, the FE model was analyzed for its dynamic structural response when subjected to a few chosen vehicles crossing over it. These vehicles were chosen in a way so as to ensure that they were representative of the spectrum of traffic crossing the bridge during a given time step. In this study, five representative vehicles listed in Table 2.1 were chosen by carefully examining actual traffic data obtained from INDOT, truck permit requests, and weigh-in-motion (WIM) data from traffic stations located near the selected bridge. The transverse position of each of these vehicles on the bridge was also decided based on the lane-wise traffic data recorded from the traffic stations and is shown in Figure 2.11.

Note that the parameters of the FE model (such as material properties, damage, etc.) were assumed to remain stationary (not evolving) within the duration of each time step, so that the effect of all the vehicular crossings over the bridge during that time step can be approximated as a superposition of multiple crossings of the same representative vehicles. The FE analysis is used to obtain the short-term time-history of the variation stresses at all points in all the components of the bridge during the crossing of an individual representative vehicle. Then, using a Rain-flow load-cycle counting method (see Downing & Socie, 1982), we obtain the number of loading cycles that the various bridge components underwent during each vehicle crossing and multiply it with the average annual daily traffic (AADT) and the number of days in the time step to obtain the total number loading cycles for each vehicle class during that time step. In reality, of course, vehicles don't cross a bridge one at a time, but it is argued the effect of simultaneous crossing of multiple vehicles over the bridge at the same time can also be represented by superposing the effect of each vehicle individually. Finally, the number of loading cycles obtained from this process is used in conjunction with the Miner's cumulative damage model (see Miner, 1945) to estimate the incremental damage sustained at every material point in the bridge. In addition to damage due to loading, the damage due to environmental factors

5.3 Approach for Durability Analysis of Bridges

In this section we describe in detail each of the steps involved in the proposed approach for conducting durability analysis of a bridge as presented in Figure 5.2.

5.3.1 Damage Accumulation due to Vehicular Loads

Within each time step of simulation, first the FE model of the bridge was subjected to the chosen representative vehicles crossing over it to obtain its structural dynamic response to each of the vehicular loads. During this step, vehicle-bridge interaction was not explicitly considered, but a dynamic amplification factor of 1.3 was multiplied to the vehicle load to account for vehicle dynamics as per AASHTO (2012). The displacements and stress time histories obtained at each point in the FE model is usually oscillatory due to the cyclic nature of the vehicular loading as shown in the top-right subfigure in Figure 5.2. Each of the peaks shown in the stress time histories corresponds to the maximum stress caused by one of the representative vehicles crossing the bridge. The oscillatory nature of the structural response suggests the use of a fatigue model, such as the Miner's cumulative damage model (see Miner, 1945), that can be used to correlate the number of stress cycles to a cumulative damage index. This has also been suggested by AASHTO (2012) and Fisher et al. (1998). Thus we use a Rainflow cycle counting method (see Downing & Socie, 1982) to count the number of stress cycles that each point in the bridge has undergone for each of the representative vehicles. Assuming linearity of the damage model and making use of the superposition principle, we multiply this number of cycles with the estimated AADT of each vehicle class and the number of days in ΔT to obtain the total number of stress cycles experienced by each point in the bridge in a given ΔT period.

The use of S-N curves is well established to study the fatigue damage in metal structures, however, for concrete structures it is not so well established. Nevertheless, there have been studies where researchers have attempted to quantify the damage in concrete structures under cyclic loadings in a very similar fashion to fatigue damage models for metals. Gylltoft (1983) and Johansson (2004) suggested formulas to obtain S-N curve as:

$$\log N = \frac{1}{0.043} \left(0.93 - \frac{\sigma_{\max}}{\sigma_{ck}} \right) \quad (5.2)$$

where $\log N$ is the logarithm (to base 10) of the number of load cycles (N) to failure, at a specific maximum stress level (σ_{\max}). Concrete strength (σ_{ck}) for the FE model in this study was chosen as 28 N/mm² (4 ksi) in compression, and 3.3 N/mm² (0.47 ksi) in tension. The maximum recorded stress during the cyclic loading, σ_{\max} , was determined during the FE analysis and was found to be 14.7 N/mm² (2.1 ksi) in

compression and 2.7 N/mm² in tension, both for load class #5.

Finally, based on Miner's rule, the total fatigue damage accumulated ($d_{Loading}$) can be defined as:

$$d_{Loading} = \sum (1 + \alpha) \frac{n_i}{N_i} \quad (5.3)$$

where n_i is a number of stress cycles corresponding to the i -th stress range ($\sigma_{\min}^i - \sigma_{\max}^i$) and N_i is the fatigue resistance corresponding to this stress-range which is obtained from standard S-N curves (see Pascual & Meeker, 1999). In the present study, we used stress ranges of 3.5 kN (0.5 ksi) with a 0 threshold in the rainflow cycle counting method to count stress cycle at each point in the model. In addition, we have introduced a parameter α to account for the effect of different long-term stresses sustained at different points in the bridge due to self-weight. Thus we define α at each point in the bridge as the ratio of the average stress level at that point to the material's limiting stress. Limiting stress for the steel components was taken as the yield strength 250 N/mm² (36 ksi) and the compressive strength of concrete 28 N/mm² (4 ksi) was used for the concrete deck.

5.3.2 Damage Accumulation due to Environmental Factors

In addition to the damage due to vehicular loads, we also used different empirical relationships to model the damage that may be incurred by different components of a bridge purely due to environmental factors.

5.3.2.1 Environmental damage model for steel superstructure. The primary cause of environmental damage in steel components is corrosion. In cold environments, state DOTs use deicing salts on the roadways that further cause deterioration of steel components as chlorides leach into the structure. In this study, we focus on the damage caused by corrosion as the only cause of damage in steel due to environmental factors. Consistent with the findings of Kayser and Nowak (1989) who performed a field survey to study the corrosion profiles of steel beams, we modify the cross-sectional properties of the steel girders to model the effect of corrosion over the entire height of the web of steel girders near the supports and upto 1/4 the height of the web at mid-span, as shown in Figure 5.3. However, rather than reducing the cross-sectional properties (which is difficult to automate in a FE model), we chose to reduce the section modulus by reducing the Young's modulus of the damaged region by an appropriate amount. Thus as the simulation progressed from one ΔT period to the next, the region of the girder highlighted in red in Figure 5.3, became progressively more damaged due to corrosion. The amount of reduction in the section modulus was calculated based on a study conducted by Albrecht and Naeemi (1984) where the following empirical relationship was developed:

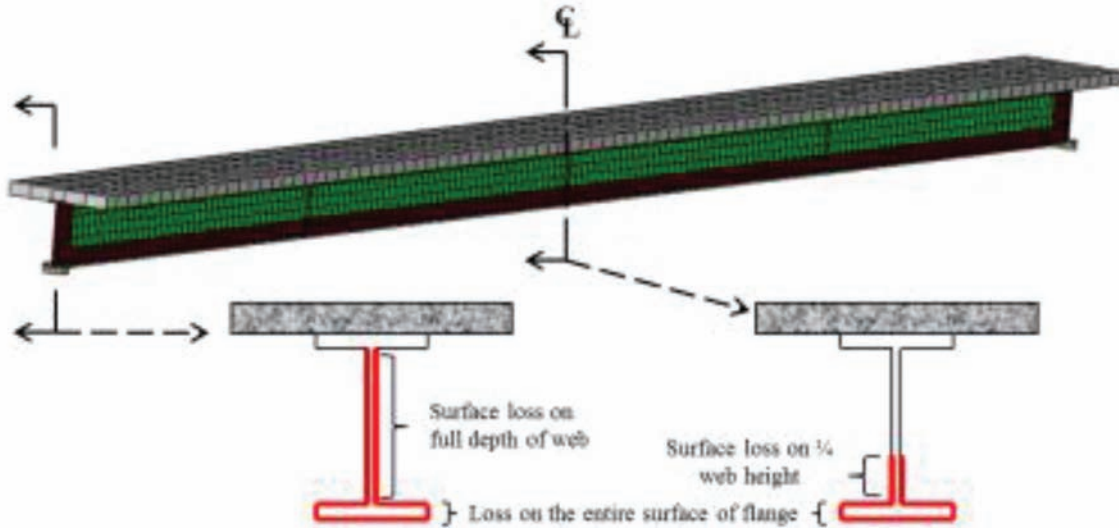


Figure 5.3 Assumed damage profile due to corrosion in steel girders.

$$C = A \cdot t^B \quad (5.4)$$

to determine the corrosion depth C (μm), in terms of the exposure time t (years), using constants A and B , which depend upon environmental conditions. The coefficients were defined for three sets of conditions: good ($A: 34.0, B: 0.65$), fair ($A: 80.2, B: 0.59$), and poor ($A: 70.6, B: 0.79$). In addition, we defined two more conditions: excellent ($A: 45.0, B: 0.45$) and critical ($A: 93.0, B: 0.86$) by extrapolation for use in this study. It is important to note that the coefficients A and B above encapsulate the effects of both the actual environmental conditions, and regular maintenance practices. Thus it is possible for a bridge to be located in a “critical” environment and for it to be maintained in an “excellent” fashion, so that the combined effect would be to have a “fair” or even “good” natural condition for the bridge.

The corrosion depth C obtained from Equation 5.3 was used to determine the damaged section modulus due to corroded steel using the following equation:

$$d_{Natural} = (\Delta S / S_0) \times C_{st} \quad (5.5)$$

where, $d_{Natural}$ is the estimated damage due to corrosion, S_0 is undamaged section modulus, ΔS is the amount of reduction in section modulus due to corrosion, and C_{st} is a calibration factor that is obtained using data from inspection reports described as follows. According to the Indiana Bridge Inspection Manual (INDOT 2010), repair or replacement of superstructure is recommended when the condition of the steel girders becomes poor (a rating of 4), which is defined as 5% to 25% of section-loss, and under normal (fair) conditions it usually occurs around 40 years of life (see Sinha et al., 2009). In this paper, a mean value of 15% was selected

as the value corresponding to a condition rating of 4, at which replacement would be recommended. Furthermore, using Equation 5.4 to reduce the area of cross-section of the girder, it was found that at 40 years, the ratio of the change in section modulus (ΔS) to original modulus (S_0) was 0.03 for normal (fair) environmental conditions. Using this as a guideline we calibrated the value of C_{st} to 5, so that at 40 years under normal (fair) environmental conditions we would obtain a section loss of 15%.

5.3.2.2 Environmental damage model for concrete deck. An empirical natural damage model was used to model deterioration in the concrete deck, including corrosion of rebar as:

$$d_{Natural} = (1 - \exp(-(\text{year})^{7.5} \times n \times 10^{-11})) \quad (5.6)$$

where, n is a parameter representing different environmental conditions as shown in Figure 5.4. Equation 5.5 was derived based on a study conducted by Hu et al. (2013) that used experimental and simulated data to consider environmental effects of atmospheric CO_2 concentration and Chloride diffusion process on concrete decks. By correlation the values of n corresponding to excellent, good, fair, poor, and critical environmental conditions were found to be 0.0128, 0.0235, 0.8, 1.78, and 3.33 respectively.

5.3.3 Total Damage due to Vehicular Loads and Environmental Conditions

Cumulative damage for both the steel superstructure and concrete deck, considering effects of both vehicular loads and environmental damage, can be expressed as:

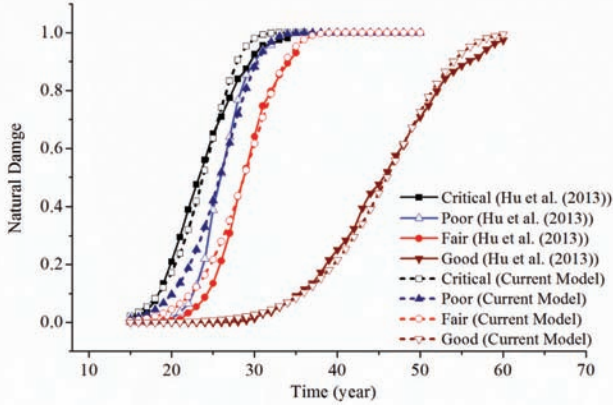


Figure 5.4 Natural damage in concrete decks.

$$D_{Total} = \alpha_L \times d_{Loading} + \alpha_N \times d_{Natural} \quad (5.7)$$

where, “ $d_{Loading}$ ” is obtained from Equation 5.2 and “ $d_{Natural}$ ” is obtained from Equations 5.4 and 5.5. Coefficients α_L and α_N were used to represent the relative impact of loading damage and environmental damage on the total cumulative damage. Several simulations with different combinations of (α_L , α_N) ranging between (0.3, 0.7) and (0.7, 0.3) respectively were conducted to assess the effect of these parameters. It was found that the higher values of α_L led to a predominantly linear increase in D_{Total} (and a correspondingly linear decrease in the condition rating) as it was primarily governed by $d_{Loading}$, whereas larger values of α_N led to an exponentially increasing D_{Total} that was dominated by $d_{Natural}$. It was found that a value of 0.5 for both coefficients α_L and α_N resulted in the right mix of $d_{Loading}$ and $d_{Natural}$ and the correct shape of the deterioration curve as observed in inspection reports and existing deterioration formulas. Calibration of D_{Total} was conducted by reviewing bridge inspection reports from INDOT as explained in the next section.

5.3.4 Simulation of Major Repairs and Replacement of the Bridge in the Durability Analysis

Life cycle of all bridges includes maintenance, repair and replacement. Assessment of the need for rehabilitation and deck replacement depends on the condition rating reported by inspectors, DOT priorities and availability of funds. To correlate the condition rating reported in inspection reports to the total cumulative damage index in this study, we use the following linear relationship between total cumulative damage index ($\bar{D}_{Average}$) averaged over all the elements in the FE model and condition rating (CR):

$$\bar{D}_{Average} = \frac{1}{N_{el}} \sum_{i=1}^{N_{el}} D_{Total_i} = \kappa \left(\frac{9 - CR}{9 - 2} \right) \quad (5.8)$$

where N_{el} is the total number of elements in the FE model. This relationship simply maps the CR scale (9 for excellent down to 2 for extremely critical) to the scale for damage index (0 for no damage to 1 for complete damage) with an appropriate factor of proportionality. During the FE analysis it was found that the spread of individual values of D_{Total} around the value of $\bar{D}_{Average}$ was quite high, such that some elements in the critical regions of the bridge had significantly more damage compared to $\bar{D}_{Average}$. After a careful study, it was found that a value of 0.7 for the proportionality factor κ led to a realistic match between the observed damage in the FE model and that reported in the inspection reports. Thus in accordance with established INDOT practices, we assumed that the CR of a component at the time of replacement would be “poor” (4) and found the corresponding damage index $\bar{D}_{Average}$ to be 0.5.

We assume that, under normal (fair) conditions, the concrete deck is replaced at 20, 40 and 55 years, the steel superstructure is replaced at 40 years, and the bridge is replaced at 70 years (see Sinha et al., 2009). In this study, first replacement of any component was conducted when the average cumulative damage in all elements of that component reached 0.5. Upon replacement, the initial damage index was reset not to zero but to 10% of the damage at the time of replacement (i.e., $0.1 \times 0.5 = 0.05$), which is also in accordance with the data observed from CR plots obtained by examining several inspection reports. In addition, it was found that the CR corresponding to replacement had progressively lower values as the bridge aged overall. To account for these changes we adopted the following equation to determine the damage index corresponding to a replacement level of damage (RD):

$$RD(t) = RD + FID \times \frac{t - t_R}{t_R} \quad (5.9)$$

where, t is the current life of the bridge (years) and t_R is the year of the last replacement, and FID denotes increases in RD for the next replacement. For the first life cycle, RD is taken as 0.5 as noted above.

One drawback of this approach is that the FE model may predict that different components of the bridge need to be replaced at different times without taking any practical considerations into account. For instance, even though the concrete deck can be replaced by itself if needed (usually around 20 years), replacement of the steel superstructure (usually around 40 years) is accompanied by replacement of the deck as well. To account for such considerations in the replacement process, additional empirical criteria were imposed. It was assumed that when considering replacement of the concrete deck, the replacement criteria for the steel superstructure would also be examined. If the steel superstructure is within 80% of its replacement criterion (i.e., $\bar{D}_{Average} > 0.8 \times 0.5$) then the replacement of the deck would be delayed until replacement criterion for the steel superstructure is met. However, during this waiting period, if the damage $\bar{D}_{Average}$ for

the concrete deck exceeds 0.7 (corresponding to a critical condition rating), then both, the steel structure and the concrete deck would be replaced immediately, even though there may still be some life left in the steel superstructure.

5.4 Numerical Case Studies Using the Framework for Durability Analysis

The chosen representative US 52 bridge (NBI-19027) in Lafayette, Indiana, was used to conduct several case studies to investigate the effect of different problem parameters on the durability of the bridge as described next. See Figure 5.5 for a depiction of scenarios used in different case studies.

5.4.1 Simulation of Durability of the Representative Steel Bridge

Case 0 (default). Realistic AADT values listed in Table 2.1 were applied and a 10% increase in traffic every 10 years was considered. Bridge components were replaced when cumulative damage reached 0.5 ($RD = 0.5$). Normal (Fair) conditions were adopted for the natural damage (encapsulating the actual effect of the environment and regular maintenance practices, as mentioned before). The simulation time step ΔT was chosen as 5 years. Since using a smaller ΔT would result in a more accurate model, simulations were also conducted with $\Delta T = 1$ year, 2 years, and 10 years. It was found that the differences between $\Delta T = 1$ year, 2 years, and 5 years were very minute, whereas $\Delta T = 10$ years led to an appreciable difference in the damage evolution of the model. Damage progression in girder #4 and the adjoining deck is shown in Figure 5.6 for different instants of time during its life. Figure 5.7 shows photographs of the steel bridge superstructure taken in 2012. Figure 5.8 shows the average cumulative damage $\bar{D}_{Average}$ and condition rating plots for the concrete deck and steel superstructure. Figure 5.9, a comparison of computational increment year, is discussed later in this section. Figure 5.10 and Figure 5.11

show a good agreement with data from inspection reports and the IBMS deterioration curve (for steel). Figure 5.10 and Figure 5.11 also show the distribution of damage in the various elements of the bridge in the form of horizontal bar charts at specific instants of time (the percentage shows the fraction of the total number of elements with that level of damage). In addition, the plots also show the contribution of $d_{Natural}$ to D_{Total} where the difference between these curves is accounted for by $d_{Loading}$. The durability model predicts the need for replacing the concrete deck at 25, 41 and 71 years and the steel superstructure at 41 and 71 years. Note that between 41 and 71 years, the replacement of concrete deck was delayed in the present scenario to allow for simultaneous replacement of the deck and superstructure (along with bridge replacement) at 71 years. Due to this delay, the deck damage had reached a critical level of 0.7 by 71 years and that prompted the immediate replacement of the steel superstructure and the deck, as per the repair and replacement policies implemented in the model. Note that by 41 years some elements in the steel superstructure had reached a damage index of close to 1 (“complete” damage). This artifact of the durability analysis should be interpreted with some caution. Most FE models have areas of high stress concentrations due to modeling assumptions, which can lead to large build-up of stresses (and damage) that is unrealistic. One should examine the damage contours as shown in Figure 5.6 to determine if this is the case or if there is really some area of high damage which may be a cause for concern.

The time step for the durability simulation Δt was defined as year increment of applied load group considering computation limitation and accuracy. For an example, if Δt is equal to 5 years, load classes are applied one time for 5 years with AADT.

For simulation of realistic bridge with AADT, it would be reasonable to use Δt of 1. But, it was required to find optimized Δt due to limitation of result size and analysis time. Figure 5.9 shows the damage in steel superstructure with $\Delta t = 5$ and $\Delta t = 2$ for 45 years. The superstructure was designed to be repaired when the

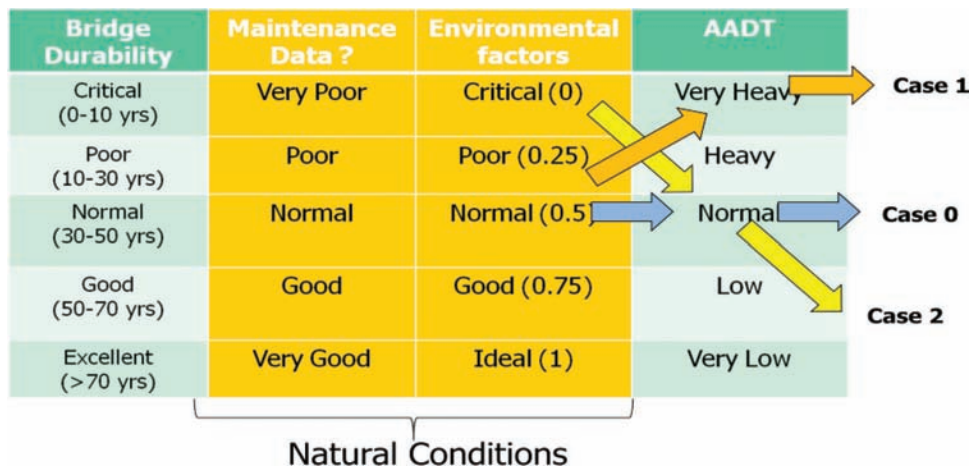


Figure 5.5 Depiction of scenarios used in different case studies.

average damage in all elements of superstructure reached 0.5. The validation for two different Δt was conducted comparing average values of results, maximum value and minimum value. Maximum damage resulted from analysis of 5-year Δt at 35 years was close to results of analysis of 2-year Δt . Average damage from analysis of 5-year Δt was thus chosen to be acceptable for realistic bridge analysis due to computational limitation of file size and running time.

Case 1 (increased truck traffic). In this case, an increased gross vehicle weight (GVW) of 535 kN (120 kips) was considered by scaling the regular truck load from Table 2.1 and in addition the values of AADT for the three overweight representative truck loadings (loading 3, 4 and 5) were doubled. This case would correspond to a hypothetical scenario of increased weight limits for regular trucks (which is actually under consideration currently) coupled with the initiation of heavy industries or a large infrastructure project in the vicinity of the bridge. The cumulative damage and condition rating plot for this case is shown in Figure 5.12 and it clearly demonstrates the reduction in life of both the concrete deck and the steel girders due to

increased truck traffic. Note that the contribution of $d_{Natural}$ to D_{Total} remains the same as the default case 0 and the additional damage in this case is caused only to increased $d_{Loading}$. It may also be noted that while most bridge designs are based on static load combinations with appropriate factors of safety, they seldom give consideration to durability of the bridge. Instead, the durability analysis in this case shows that if a bridge, that was likely to be subjected to heavy traffic loads, were designed with bigger structural members so that the resulting stresses under loading would be smaller, then that would also help in increasing the life of the bridge components.

Case 2 (critical environment condition). This case was used to simulate the effect of increased natural damage that may occur due to either the bridge being located in a highly corrosive environment or insufficient maintenance, or both. Values corresponding to “critical” conditions were chosen in Equations 5.3 and 5.4 for the steel superstructure and Equation 5.5 for the concrete deck and the resulting progression of damage index and condition rating is plotted in Figure 5.13. From the results of this case,

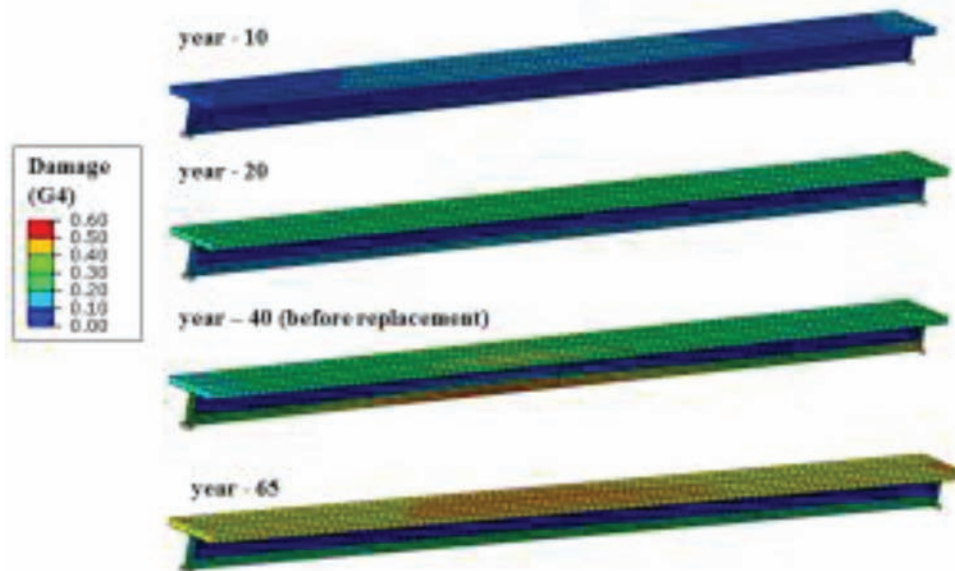


Figure 5.6 Damage propagation in steel superstructure obtained from durability model.



Figure 5.7 Photographs of the steel bridge superstructure in 2012.

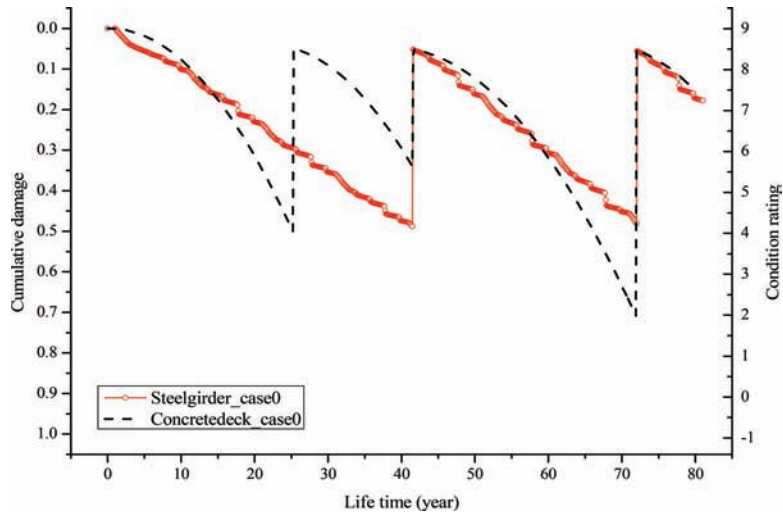


Figure 5.8 Evolution of condition rating of the representative steel bridge for case 0.

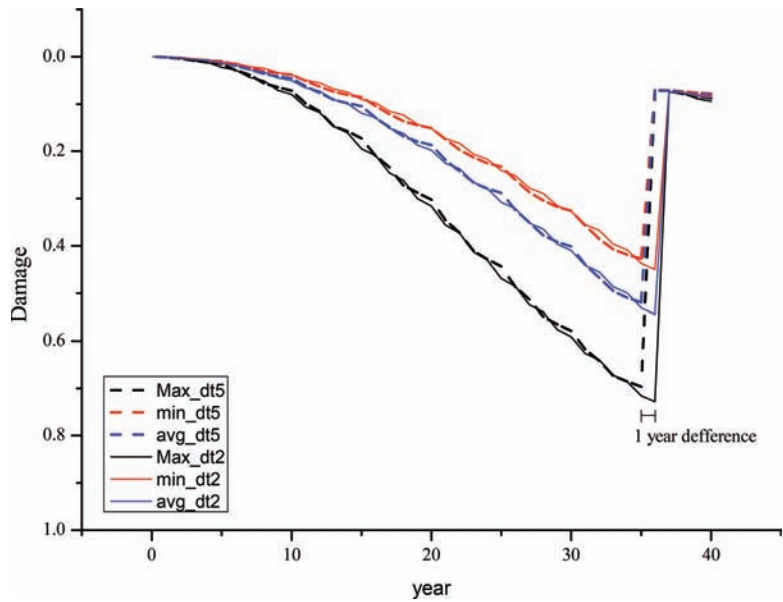


Figure 5.9 Comparison of computational increment year.

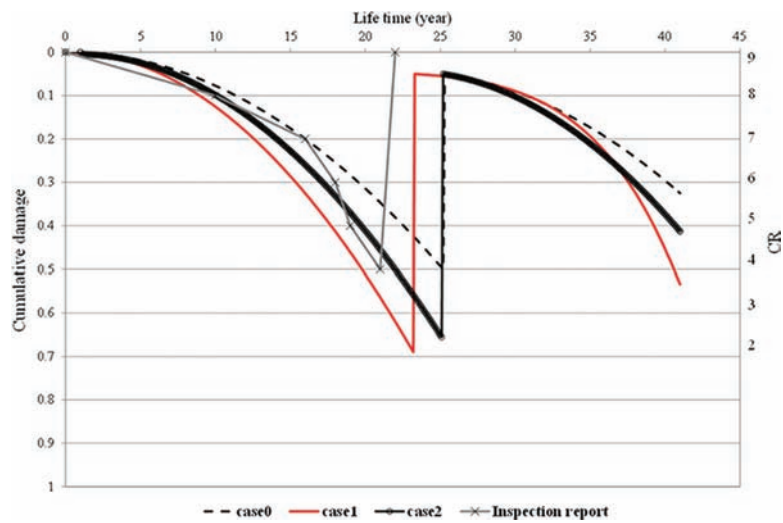


Figure 5.10 Comparison of deck condition rating for different cases.

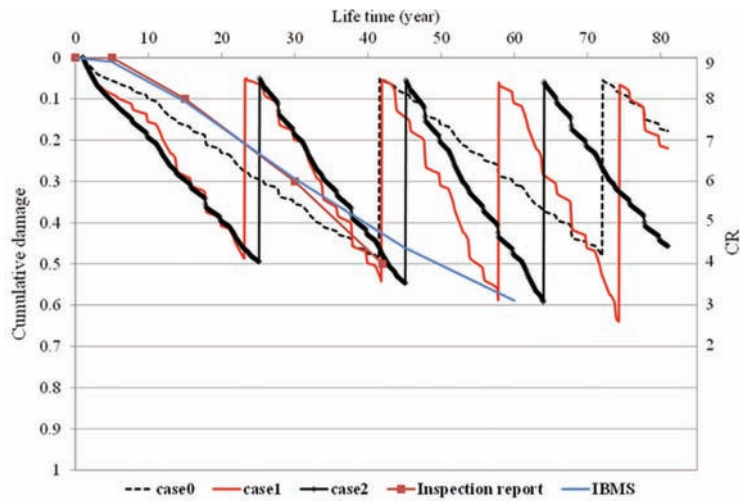


Figure 5.11 Comparison of condition rating of the steel superstructure under different cases.

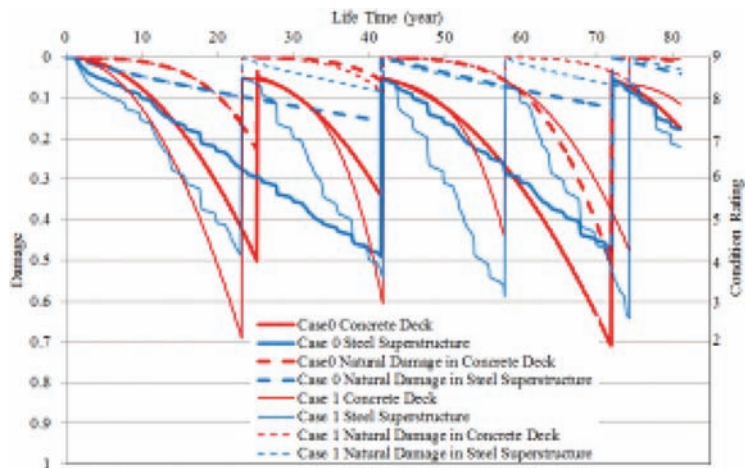


Figure 5.12 Detailed comparison of condition rating from cases 0 and 1.

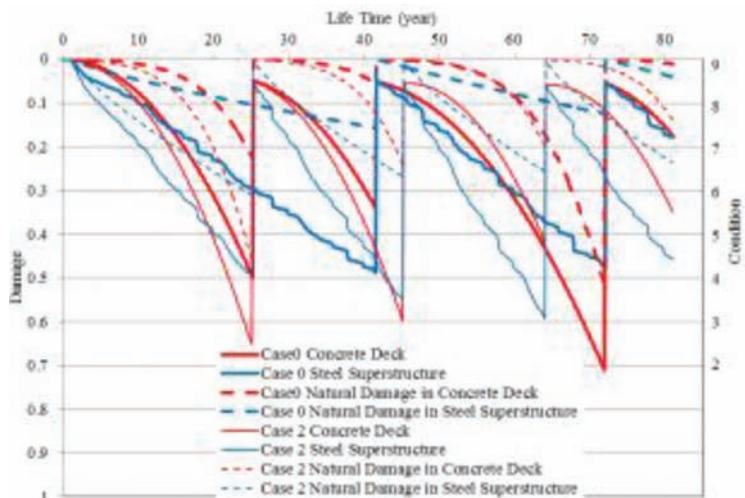


Figure 5.13 Detailed comparison of condition rating from cases 0 and 2.

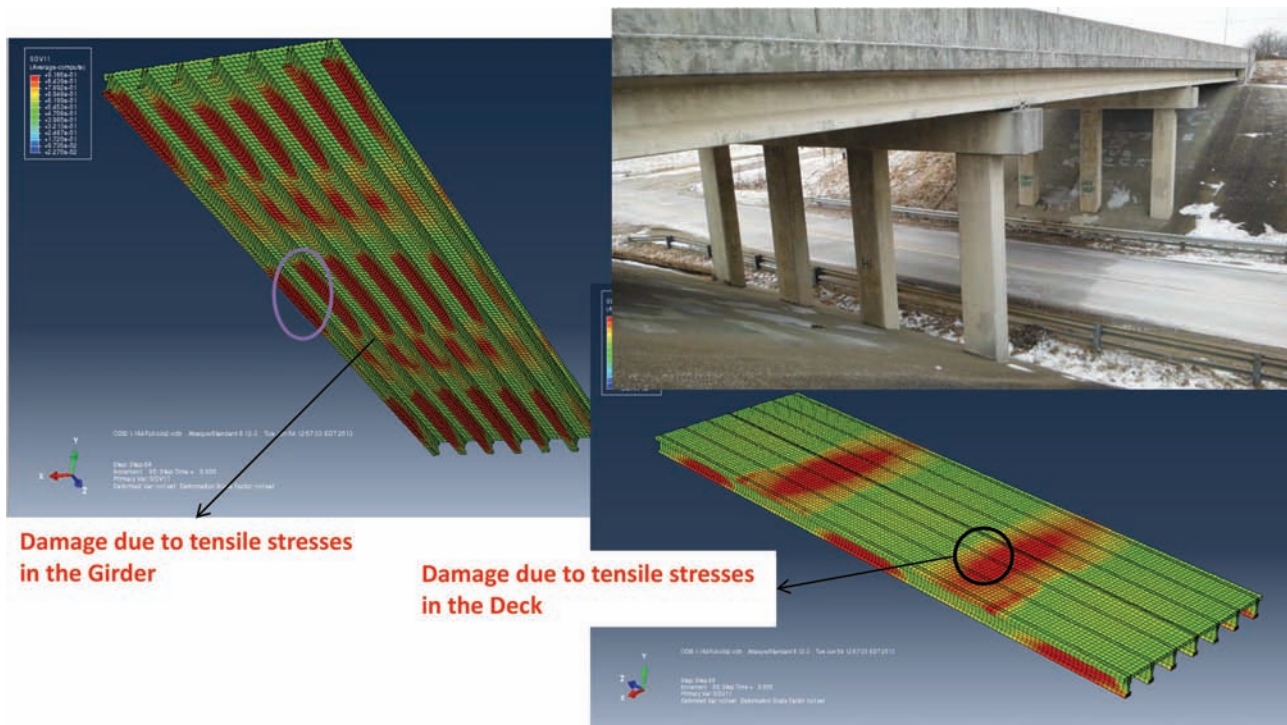


Figure 5.14 Typical damage profiles of the representative concrete bridge.

it is clear that “critical” environmental conditions also reduce the life of bridge components where the additional damage is primarily accounted for by $d_{Natural}$.

5.4.2 Simulation of Durability of the Representative Concrete Bridge

In this section (Figures 5.14, 5.15, 5.16, and 5.17) we apply the durability framework to the representative concrete bridge: I-164 bridge (NBI-70100).

5.4.3 Discussion and Limitations

One may note from Figure 5.10 that the real condition rating for the concrete deck obtained from

inspection reports deteriorates slightly faster than that predicted by the our model. Consequently, the concrete deck was replaced around 20 years, which is earlier than what is shown by our durability model. This difference occurs because the FE model used in this study does not account for all possible causes of damage to the deck. For instance, an important cause of damage to the deck results from snow-plows hitting the deck-joints, which causes concentrated zones of damage around the deck joints that propagate with time. The natural damage model used in this study assumes uniform natural damage at all points in the model and is not able to capture the damage due to snow-plows. This issue of damage in deck-joints is investigated further in the next chapter.

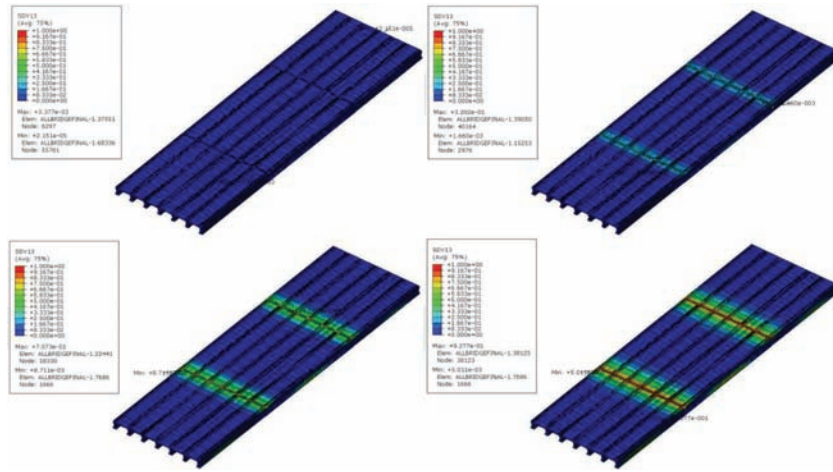


Figure 5.15 Depiction of typical damage evolution obtained from the durability model.

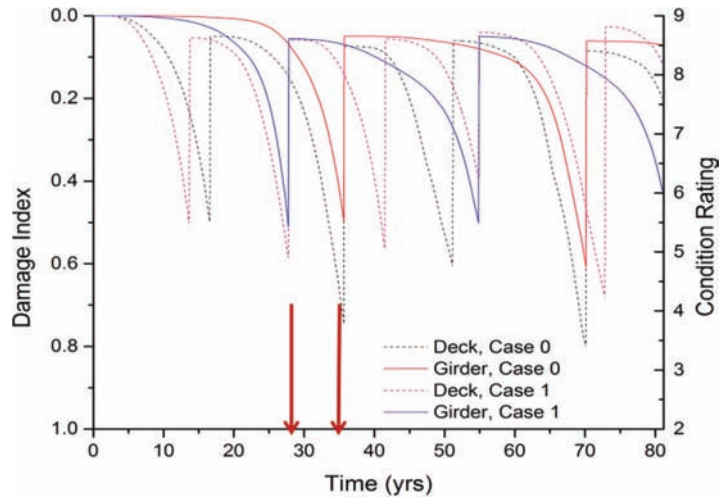


Figure 5.16 Comparison of condition rating for cases 0 and 1.

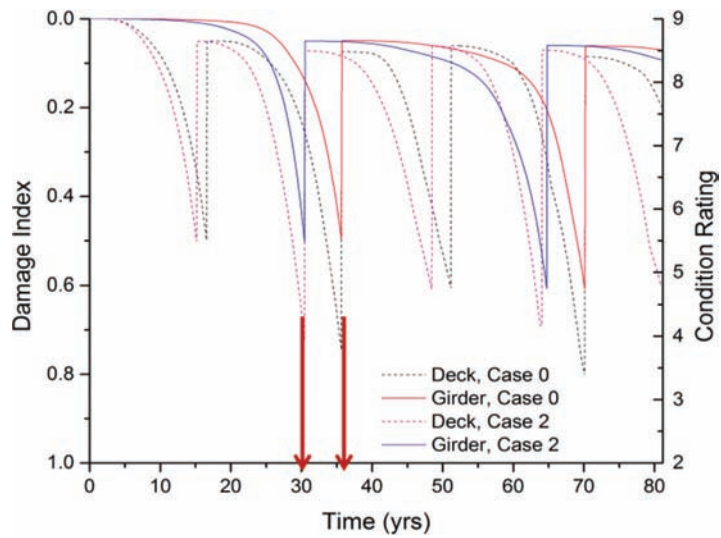


Figure 5.17 Comparison of condition ratings for cases 0 and 2.

6. DURABILITY OF DECK JOINTS SUBJECT TO REPETITIVE SINGLE AXLE LOADS

This study will address some of the major concerns associated with overweight trucks and their detrimental effects on the deck joints in a bridge in terms of damage and reduction in service-life of bridges. A report using Weigh-in-motion (WIM) (Green et al., 2002) indicated that the average daily traffic loads include approximately 3.3% overweight trucks over 200,000 pounds. Traffic volume and truck weights have been increasing with the growth and technical development of the freight industry. Overweight trucks are regular issues for state highway agencies to maintain bridges. The increased overweight trucks can cause greater damage and generate more micro-cracks in structural elements of bridges than typical vehicle classes of the Federal Highway Administration (FHWA). Eventually, cumulative damages resulting from overloads may cause more local damage on the deck joint region and affect the service life of the deck and of the bridge.

Currently, Indiana Department of transportation (INDOT) and other states' DOTs employ various simple empirical formulas to determine costs and use them to collect permit fees from regular and overweight trucks for the entire bridge without considering local damage. So, the formulas are not based on realistic durability analysis of bridges. Also, with increasing truck weight limits, a detailed study of the effects of single axle loads with dynamic amplification factors and condition rating to simulate realistic bridge has become necessary.

The study by Yanev (1997) indicated that deck joint did not significantly influence on estimation of overall condition rating of a bridge unlike girders and deck slab. But, deck joints have a role in accommodating necessarily structural movements of the bridge elements. If the bridge deck joint system becomes unable to accommodate the movement, the bridge elements experience over-stress that could eventually result in damage to bridge elements and/or the deck joints themselves (Chang & Lee, 2001).

6.1 Objective

Some of the main objectives of this research are:

- to investigate the effects of single axle loads of repetitive traffic on the cumulative damage in deck joint region
- to investigate the effects of interaction between overweight truck traffic and natural deterioration in deck joint region
- to evaluate the dynamic amplification effect for different wheel loads spanning the ends of deck subject to repetitive traffic or overweight trucks, and
- to assess the effects of timely repair on concrete deck compared to the inspection report data.

6.2 Background

A literature review examined studies related to expansion joints. Some examples related to advantages and disadvantages for deck joints are cited. Researchers at Purdue University (Chang & Lee, 2001) investigated deck joints for 5,300 bridges in Indiana. In the past, metal deck joints such as finger joint and sliding plate were largely used. Strip seal (S.S.) joint and compression seal (B.S.) joint have been used mainly since 2000 and these two types of deck joints are currently found in approximately 2,385 bridges in Indiana (See Figure 6.1).

It has been reported that B.S. joints and S.S. joints have good quality of the installation, in general, but B.S. joint and S.S. joints have issues with leakage and intrusion of water due to problems in their unsuitable installations. Moreover, Indiana Department of Transportation (INDOT) recommended that the use of B.S. joints be avoided due to more spalling causing salt deterioration along the leakage path and several maintenance issues (see Figure 6.2). It is known that traffic loads including overweight trucks accelerate deterioration on bearings and damaged joints. A study about B.S. joints and S.S. joints in NCHRP-synthesis 319, Bridge Deck Joint Performance by Purvis (2003) reported: "B.S. joints and S.S. joints are susceptible to tearing, puncturing, or detachment under traffic when

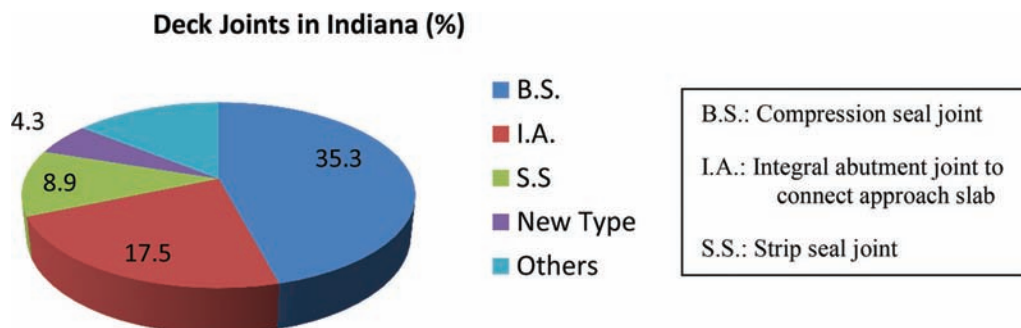


Figure 6.1 Deck joints in Indiana.

debris accumulation rates are high, and have issues with crushing in the block-out region.” Bolluyt et al. (2001) conducted a survey from 39 states in the United States and state that the main cause of failure of S.S. joint is wheel loads. Snow-plow blade often causes the failure of S.S. joint as well. States not related to the use of snow-plow blade reported on deck joint failures also. The Florida Department of Transportation (FLDOT) design manual (Florida DOT, 2011) states, “A number of joint problems and damage occur routinely on the bridge edge and surface. Edge damage is caused by crossing the deck with steel-wheeled rollers, steel-track equipment or routine traffic.” The Texas Department of Transportation states in “Bridge deck joint replacement practices” that spalling in deck joint is caused by poor installation, concrete material failure and concrete fatigue.

A study related to dynamic amplification factor for deck joints was conducted by Clauwaert (1986). The relationship between the vertical dynamic wheel load on an expansion joint and static wheel load was investigated. To evaluate the effect of axle loads on deck joints, dynamic vertical loads were calculated by multiplying static wheel loads by dynamic amplification factors ranging from 1.3 to 1.8 depending on vehicle speed, bump’s height and bump’s length. Also, it is reported that when truck travels deck joint with the height of over 1 inch positive bumps, dynamic amplification factors need to be considered.

In order to investigate cumulative damage using durability analysis, it was assumed that reduced capacity of bridge elements is in proportion to increased damage. The term “damage mechanics” was first introduced by Kachanov (1958) for creep-related problems and was applied to the description of progressive failure of metals and composites to represent the material behavior under the fatigue. Kachanov (1958) defined “damage” as a loss of stiffness or a reduction of the secant modulus.

In order to conduct analytical work with bridge deck joint, the information of various types of deck joints used in Indiana as shown in Figure 6.1 was used. In past, metal type deck joints were usually used. However, compression seal joint, strip seal joint and integral abutment joint are currently used in Indiana. This study indicates that most current deck joint are able to accommodate up to 4 in movement and current deck joints are designed for 10 years-service life by INDOT’s policy. The maintenance cycle of bridge deck joint is approximately every 2 years.

B.S. joint (35%) and S.S. joint (9%) have an advantage against water leakage. However, according to Indiana Bridge Inspector’s interview and survey, B.S. Joint has spalling on the joint’s back wall that causes leakage with salt deterioration. Also, traffic loadings can accelerate the deterioration of bearings and damaged joints. For SPR 3630 project, B.S. joints, which have the largest proportion in Indiana, are selected to be investigated in detail and simulated.

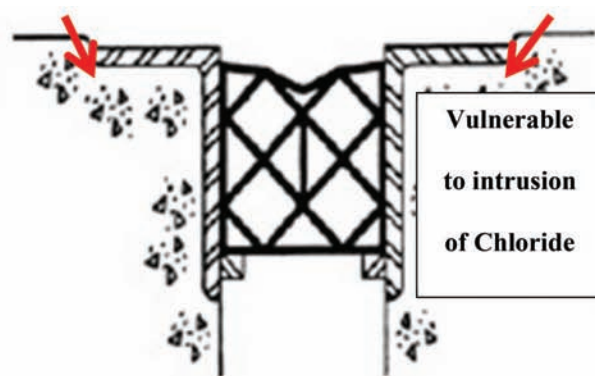
6.3 Research Approach and Scope

This study is focused on local damage analysis through a deck joint model separated from global bridge analysis. The deck joint model consisted of strip seal based on sealant property following ASTM D 5973, deck of concrete with 4 ksi of compressive strength, and concrete blockouts of both deck ends containing strip seals. This scope of this study is:

- i. Durability modeling consisted of accounting for the effect of cumulative damage on deck joint region due to repetitive loadings;
- ii. Damage of deck joint region was assumed to influence only concrete blockout along the width of deck end part;
- iii. Dynamic amplification factors was investigated based on numerical approach using ABAQUS version 6.12 IMPLICIT and,



A.1.1. Significant Spall



A.1.2. Armored B.S. Joint

Figure 6.2 Possible intrusion path of chloride ion.

- iv. Damage was presented by summation of environmental deterioration and cumulative damage due to loadings.

A schematic description of the computational procedure is shown in Figure 6.3. The analysis of deck joint model subject to 1,000 pounds axle load was conducted preliminary to deck joint analysis by cumulative damage resulted from applied realistic axle loads due to accessibility and effectiveness. Specifically, through results from preliminary FE analysis, different dynamic amplification factors were set to be applied to the surface of deck blockout. To evaluate effects of realistic traffic including overweight trucks, five representative axle load classes were selected considering configuration of FHWA vehicle classification and Michigan trailer trucks shown in Table 6.1. The load classes were applied by multiplying different amplification factors using DLOAD in ABAQUS user subroutine code.

The stress-time history was obtained when single axle loads with annual daily traffic (ADT) travel on deck blockout, and the stress-time history was used to determine cumulative damages using Miner’s rule (Miner, 1945) and S-N curve in concrete (Johansson, 2004). Miner’s rule is used to estimate the fatigue damage accumulation, and it is assumed that the damage of

each cycle in a stress time history is independent in Miner’s rule. Based on Miner’s rule, the total damage ($d_{loading}$) due to repetitive loads can be defined as a summation of the fatigue damage caused by each stress range, as given by:

$$d_{loading} = \sum \frac{n_i}{N_i} \quad (6.1)$$

where n_i is a number of cycles of the i -th stress range and N_i is the fatigue resistance.

Cumulative damages influenced by applied realistic traffic and natural deterioration attenuate stiffness of deck blockout, and total values of damage were used to estimate condition rating of blockout. The history of condition rating (CR) of realistic bridge was presented in the inspection report provided by INDOT, and the condition rating provided by INDOT was used to calibrate the condition rating resulted from FE analysis. For FE model, less four of condition rating for all bridge elements is usually required to be considered as replacement even depending on inspector’s judgment. In this study, it was assumed that 50% of cumulative damage meant 50% reduction of capacity for deck joint. Deck joint model was designed to be replaced when cumulative damage met 0.5.

TABLE 6.1
Applied single axle loads considering overweight (OW) trucks.

Vehicle Classification	GVW = Σ Axle Loads (kip)		Single Axles	Counts	Selected Load		
					Class	Counts	
FHWA Vehicle	2	CAR	4 = 2 + 2	2 kip	2	8 kip	3
	3	PU	12 = 6 + 6	6 kip	2	18 kip	11
	4	BUS	24 = 8 + 16	8 kip	3	20 kip	7
	5	2D	40 = 8 + 32	10 kip	1	27 kip	12
	6	SU 3	72 = 8 + 32 \times 2	12 kip	1	32 kip	16
	7	SU 4+	80 = 10 + 35 \times 2	15 kip	1		
	8	ST 4-	90 = 18 \times 5	16 kip	3		
	9	ST 5	126 = 18 + 27 \times 4	18 kip	11		
	10	ST 6+	126 = 18 + 27 \times 4	20 kip	7		
	11	MT 5-	126 = 18 + 27 \times 4	22 kip	5		
	12	MT 6	134 = 18 + 23.2 \times 5	25 kip	8		
	13	MT 7+	134 = 18 + 20 \times 6	27 kip	12		
	OW		138 kips of Michigan Trailer	138 = 12 + 16 \times 2 + 18 \times 5	30 kip	2	
				32 kip	16		
				35 kip	2		
			200 kip	15 + 25 \times 3 + 22 \times 5			
		496 kip	20 + 30 \times 2 + 32 \times 13				

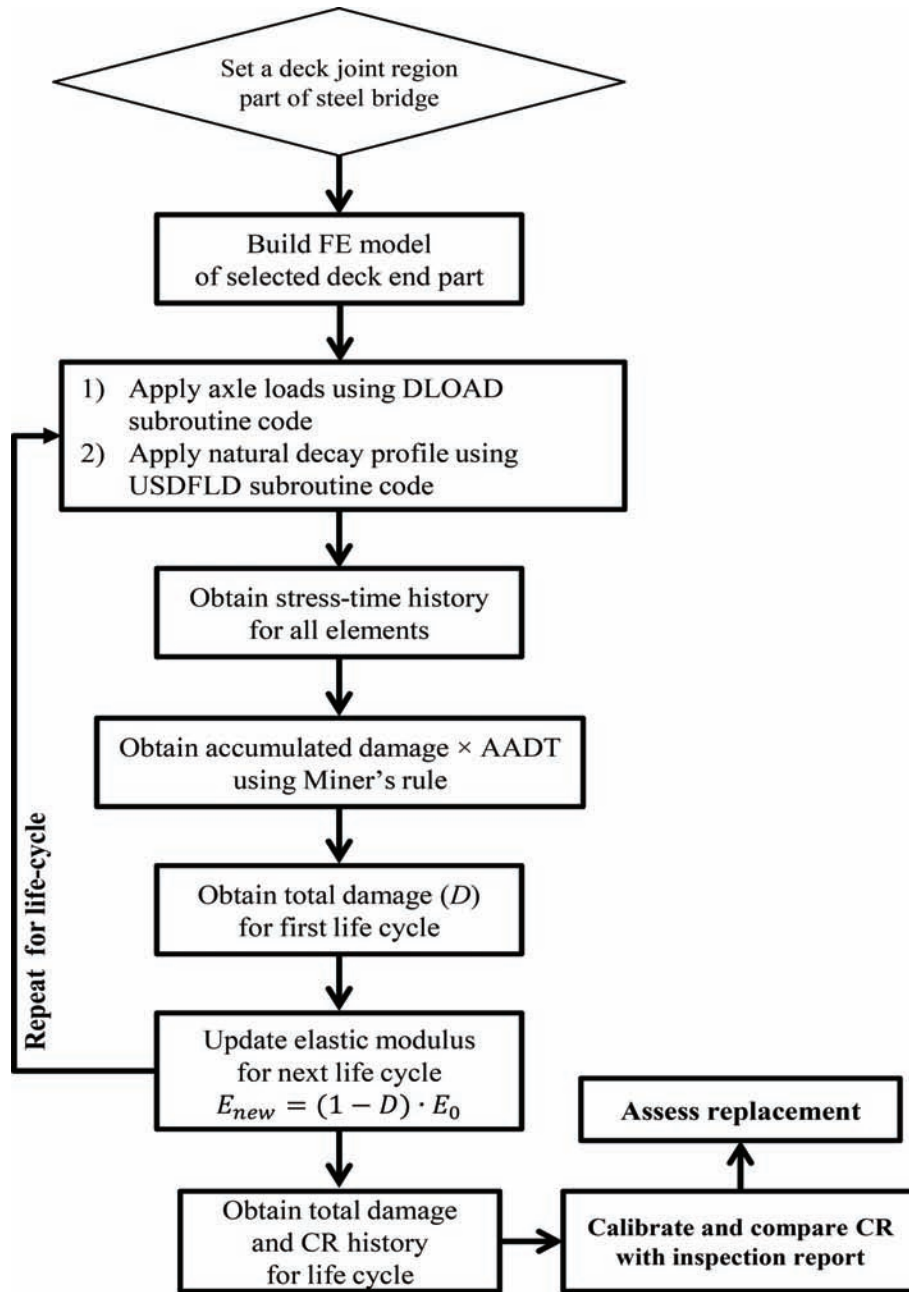


Figure 6.3 Procedure of deck joint FE model analysis.

For damage due to natural corrosion, it was assumed that the condition of bridge influenced on damages due to natural decay in reinforced concrete deck blockout follows the exponential curve in Equation 6.2, which shows damage due to natural deterioration correlates to the lifetime of the bridge:

$$d_{natural} = 1 - \exp(-t^2/n) \quad (6.2)$$

where t is age (year) of bridge and “ n ” is a constant depending on inspection report data.

Total damage in Equation 6.4 was used to update elastic modulus with reduction caused by cumulative damage for next cycle of durability model. Reduced elastic modulus was replaced for all elements in next life cycle. Damage model in this project considered total damage due to repetitive loadings and natural corrosion in concrete blockout as shown in Equation 6.3. Specifically, cumulative damage for concrete blockout due to repetitive loadings accounted for compressive stress and tensile stress using parameters of α_1 , α_2 , and α_3 calibrated by inspection report. In this study, α_1 , α_2 , and α_3 of 0.3, 0.5 and 0.2 were used, respectively. Modified elastic modulus (E_{new}) is expressed in Equation 6.4

by the concept of damage introduced by Kachanov (1958).

$$d_{total} = \sum_{i=1}^3 \alpha_i d_i = \alpha_1 d_{Natural} + \alpha_2 d_{L,tentile} + \alpha_3 d_{L,comp}. \quad (6.3)$$

$$E_{new} = (1 - d_{total}) E_o \quad (6.4)$$

The condition rating was calculated based on total damage (d_{total}) for every life cycle. A durability model including the effect of repair or replacement was developed based on a condition rating of under 3 or 5 over the lifetime of the bridge to estimate the life-cycle curve of the deck joint.

The condition rating was used to calibrate the results of durability analysis using finite element (FE) model calibrated using data from inspection reports. Inspection reports contain condition rating of deck joint of realistic bridge for bridge lifetime as shown in Figure 6.4. Inspection report indicated that life cycle of concrete deck including blockout and strip seal joint varies from 15 years to 25 years.

6.4 Description of Finite Element Model

To simulate realistic deck end part including expansion joint, realistic bridge data and FE modeling were required. Deck joint region was modeled with a part extracted from a bridge (NBI-19027) on US 52 as shown in Figure 6.5. The selected bridge on US 52 was used for the study “Life-Cycle of Steel Bridges: Effects of Local Damage due to Interaction between Truck Traffic and Natural Decay on Steel Superstructure” in

Chapter 2, and the bridge was analyzed by 3D full scale FE model calibrated with experimental data conducted by Canna and Bowman (2002). The US 52 bridge contains strip seal joint as shown in Figure 6.4, and condition rating from inspection report for the US 52 bridge is available to compare condition rating resulted from durability analysis of deck joint using FE modeling.

FE model of deck joint extracted from US 52 bridge (NBI-19027) was designed using four nodes shell (S4R) elements with six degrees of freedom (three translations and three rotations). The partial FE model consisted of a part of W30 × 230 steel girder with elastic modulus of 29,000 ksi and Poisson’s ratio of 0.27, and eight nodes solid (C3D8I) elements for 8-inch thick concrete slab and concrete blockout with compressive strength of 4 ksi and Poisson’s ratio of 0.2. The width of concrete

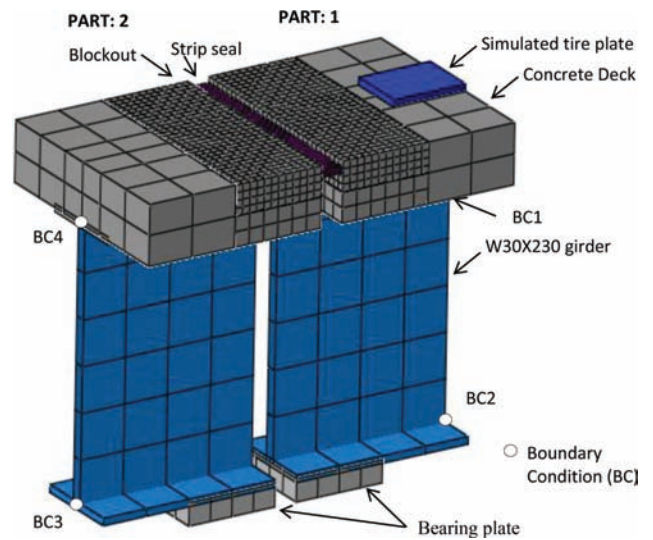


Figure 6.5 View of 3D deck joint model.

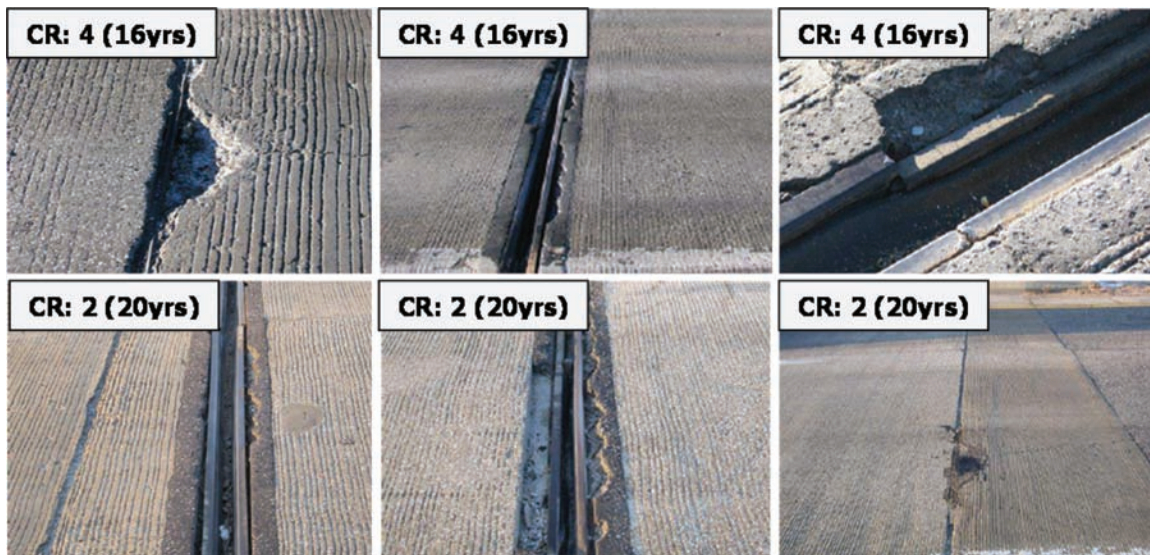


Figure 6.4 Condition rating for bridge ages and spalling on deck joint. (Source: INDOT inspection report (NBI-19027).)

deck was 30 inch (*i.e.*, $60 \text{ inch} \div 2 = 30 \text{ inch}$) based on the effective width in AISC specification; the smallest one among $\text{beamspan}/8$, $\text{beam-spacing}/2$ and distance to edge. For design of deck blockout, it was referred to NCHRP-synthesis 319: Bridge Deck Joint Performance by Purvis (2003). The survey conducted by Purvis (2003) indicates that accommodated movement of strip seal deck joint varies up to 4 inches, and blockout length varies between 12 and 24 inches. The initial gap between two decks for strip seal joint is 1.5 to 2.5 in. due to installation work. For this study, FE model of deck blockout with 30 in. \times 12 in. \times 8 in. was designed using 1,440 one-inch cubes as shown in Figure 6.5. A 3-inch-wide strip seal was designed with properties of neoprene; density of $3.47 \times 10^{-5} \text{ kip/in}^3$, tensile strength of 2 ksi, Poisson's ratio of 0.499 and Young's modulus of 11.8 psi according to the study of Guthrie (2005) FE modeling consisted of five parts; steel girder, bearing support, deck, strip seal and blockout in this study. The four parts were rigidly connected using "merge option" in ABAQUS version 6.12.

6.4.1 Analysis to Identify Different Dynamic Amplification Factor

The comparison of reaction forces between hand calculation and FE model results was conducted to ensure whether deck modeling properly works in the system. For bearing, the boundary conditions to restrict displacement in the x (transverse) and y (gravitational) direction were used. Also, four boundary conditions (BC1, BC2, BC3 and BC4) with constraint in the z (longitudinal) displacement were used at outside ends of FE model as shown in Figure 6.5. A frictionless plate with 20,000 pounds was applied to the top surface of concrete blockout by moving the plate along with the longitudinal direction for the analysis of reaction force and dynamic amplification factor. The weight of 20,000 pounds was selected as mean value of the majority of axle classes as shown in Table 6.1. In order to determine the size of reasonable tire, it was referred to the study by Salgado, R. (2002). The study indicates that the tire carrying 20,000 pounds yields the net contact area of 81.0 in². Thus, for this computational calibration analysis, the tire plate with 8 in. \times 10 in. was selected.

First, the tire plate model traveled on the top surface of deck and deck blockout for five seconds along with the longitudinal direction using ABAQUS IMPLICIT version 6.12. Specifically, a blockout element was based on one-inch cube. 8-inch-wide plate exactly passed on the top of eight one-inch cubes of blockout elements as shown in Figure 6.6. Eight one-inch cubes were set to a group from A to F. The reaction forces (RF) from bearing plate and a horizontal pin at BC1 were obtained from FE model analysis to compare hand-calculation as shown in Figure 6.7 and Figure 6.8. For FE model, the load of 20,000 pounds was uniformly distributed on the surface of plate. It was assumed that concentrated force of 20,000 pounds at point A at the center of plate was used for convenience in

hand-calculation. Figure 6.7 shows that reaction force history at BC1 by FE analysis followed result of hand-calculation (*i.e.*, $RF = 20 \text{ kip} \times (17 \text{ in.} - x) \div 36 \text{ in.}$). The reaction force history at bearing plate in part 1 shown in Figure 6.5 was obtained as shown in Figure 6.8 while the plate moved 6 in./sec from point A to the opposite blockout. The reaction force at bearing in part 1 as described in Figure 6.8 was constantly around 20 kip before plate moved to the opposite blockout. Figure 6.7 and Figure 6.8 indicated that local deck joint model represented behavior of realistic deck joint region. The assumed boundary conditions are in acceptable agreement.

Next, the analysis of moving plate on deck blockout was used to determine effects of different dynamic amplification factor on blockout. Stress-time histories in blockout were obtained as shown in Figure 6.9. Pressure values of eight elements in a column on the surface of blockout subject to moving plate with 0.25 ksi (*i.e.*, $20 \text{ kip} \div 80 \text{ in}^2 = 0.25 \text{ ksi}$) were averaged to obtain stress-time history. Pressure values from six representative groups consisting of eight elements as shown in Figure 6.6 were plotted as shown Figure 6.9 for 5 seconds while plate was traveling.

The obtained stress values were mostly 0.25 ksi due to applied pressure exclusive of values from group C and D. Ratios of averaged pressure values to 0.25 ksi are shown in Table 6.2. Figure 6.9, Figure 6.10 and Table 6.2 show that stresses resulted from the end of blockout were higher than other region in roadway of tire. This computational analysis results indicated that different dynamic amplification factors (DAF) need to be taken into account for durability analysis subject to repetitive loadings which may reduce the lifetime of a concrete deck.

6.4.2 Analysis of Durability Model of Deck Joint

To evaluate damage evolution in concrete blockout due to repetitive load with DAF, four different input parameters were set as shown in Figure 6.10. Group information from A to G was illustrated in Figure 6.6. Case 1 was set based on normal applied load effect with no DAF. Case 2, case 3 and case 4 were set with different dynamic amplification factors as shown in Figure 6.10 according to results from moving plate FE analysis. Stress-time history of deck joint region subject to repetitive axle load with AADT as shown in Table 6.3 was determined using ABAQUS DLOAD subroutine and ABAQUS IMPLICIT. Selected load classes

TABLE 6.2
Maximum pressure value for six groups.

Group	F	E	D	C	B	A
Max. pressure (ksi)	0.23	0.23	0.36	0.35	0.23	0.23
Ratio to 0.25 ksi	0.9	0.9	1.4	1.4	0.9	0.9

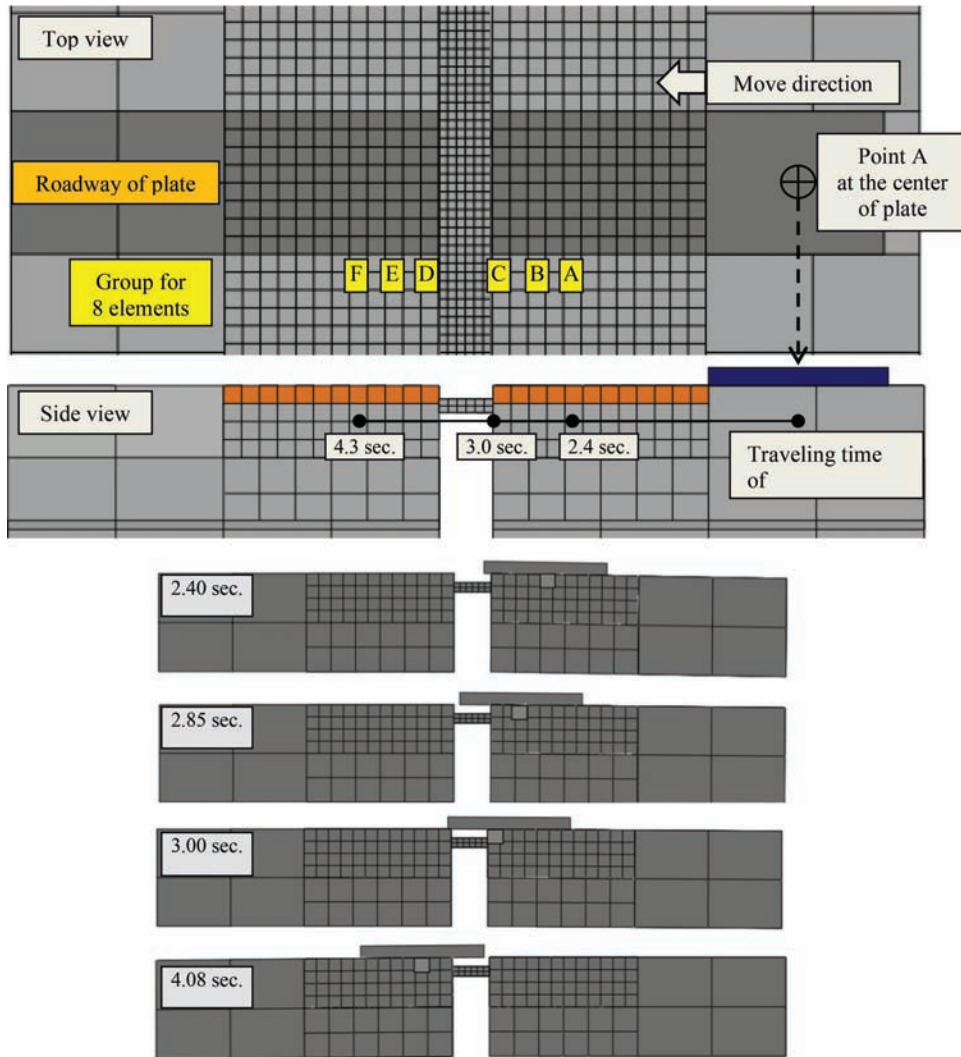


Figure 6.6 View of FE model for moving plate.

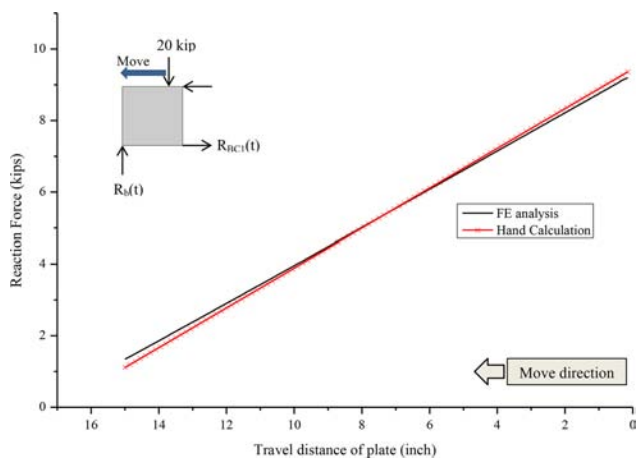


Figure 6.7 Reaction forces (RF) at BCI in PART 1 for validation of deck joint model.

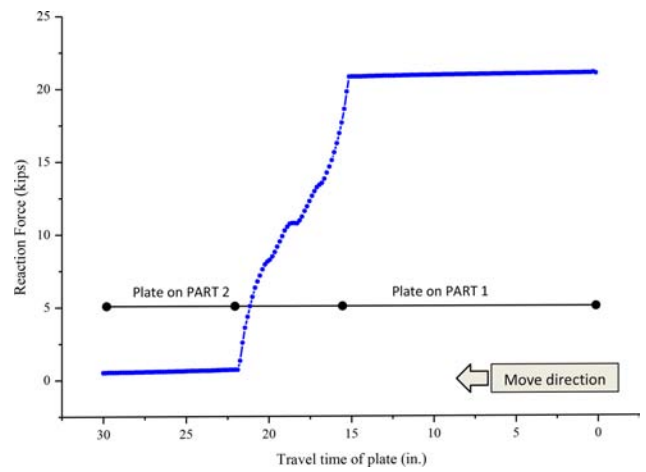


Figure 6.8 Reaction forces (RF) at bearing in PART 1 for validation of deck joint model.

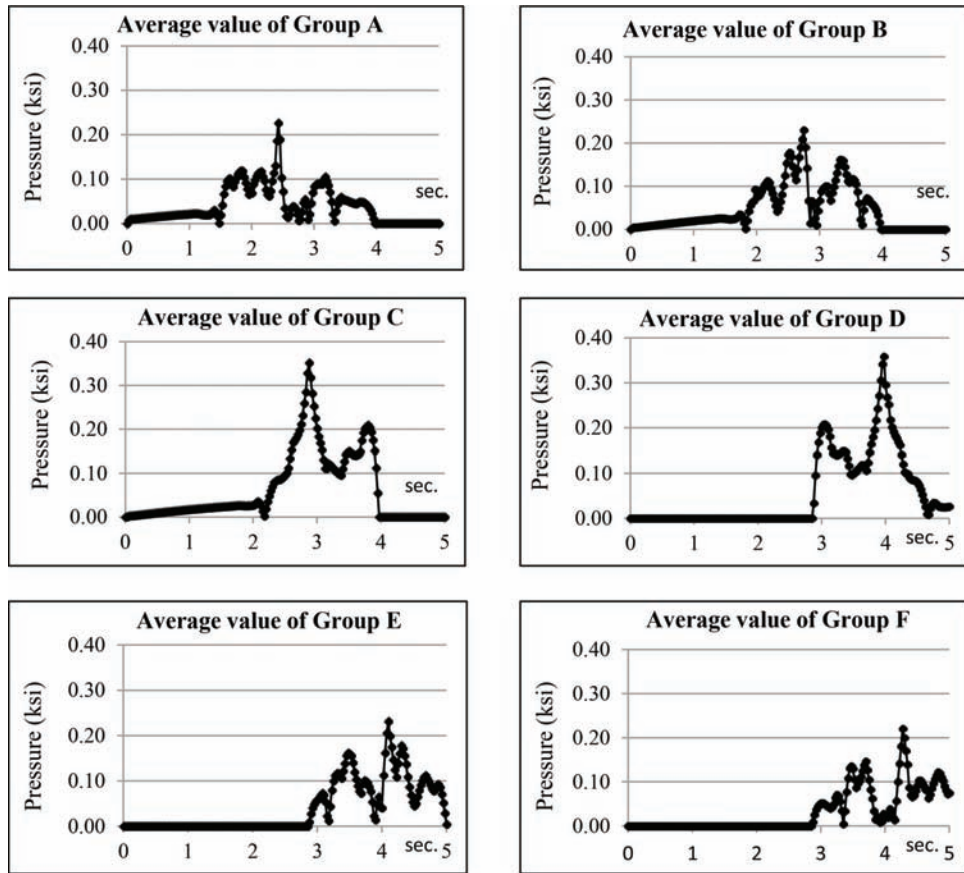


Figure 6.9 Pressure-time history for six groups of elements on the deck joint.

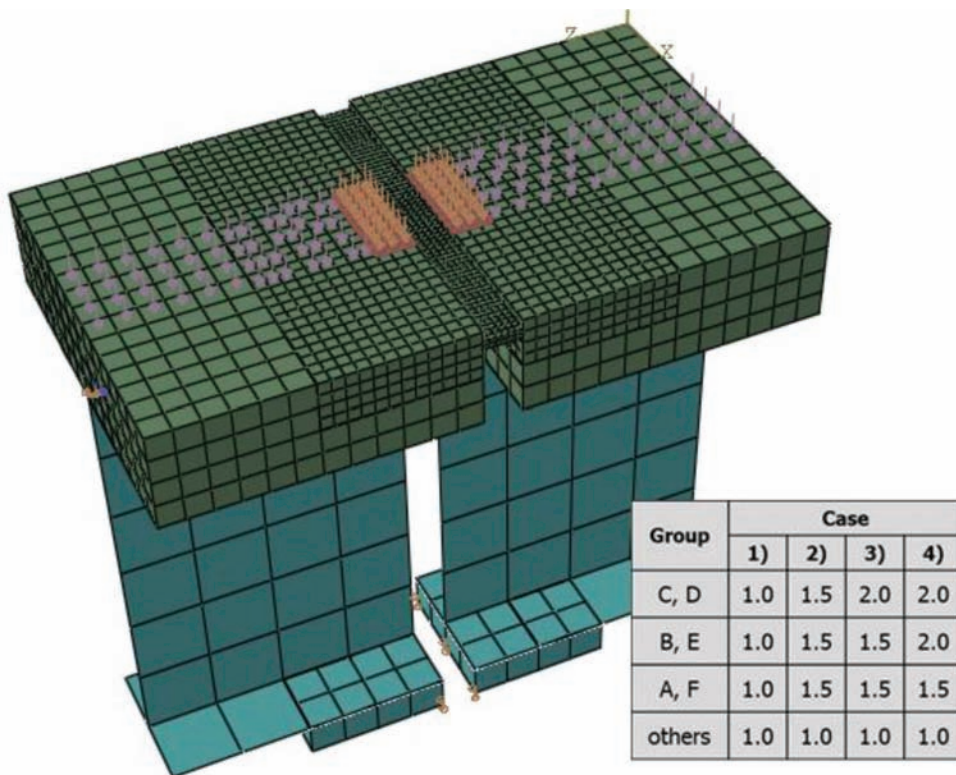


Figure 6.10 View of 3D FE modeling subject to different dynamic amplification factors (DAF) and potential cases.

were applied with very slow velocity of 25 in./sec to consider pressure by only different amplification factors in the vertical direction.

Figure 6.11 showed Von-Mises stress against lifetime of deck joint region. The stress values varied between 0.05 ksi and 0.35 ksi over the 35-year lifetime. Using Equation 6.3, accumulated damage in concrete block-out was plotted in Figure 6.12 with no repair or replacement stage. Figure 6.12 indicated that lifetime of concrete blockout was shortened as much as over 3 years due to dynamic amplification factors (DAF) compared to case 1 with no DAF effect when cumulative damage met 50% reduction in terms of modulus. Case 1 with no DAF was calibrated by inspection report, which provided 15 to 20 years as a lifetime of deck joint. When total damage of concrete blockout met 0.5 around 20 years, it was assumed that the capacity of blockout is 50% of undamaged elastic modulus. According to a study of the life cycle profile introduced by Sinha et al. (2009), deck joint region is required to be replaced around 15 years to 20 years.

Figure 6.13 based on Figure 6.12 showed cumulative damage by case 1 with replacement of deck blockout. Histograms of damage distribution at 14 years, 16 years and 18 years were illustrated on damage graph of case 1 to find out the range of damage before replacement. Damage with average value of 0.5 before replacement varied between 0.45 and 0.60.

In order to simulate realistic damage accumulation for deck joint region, replacement stage was considered in life cycle using 3 parameters; (i) Repair Damage (RD) provided by INDOT (ii) Future Increase Damage (FID), and (iii) New Damage (ND). Repair damage (RD) decided the time for replacement of concrete blockout to simulate spalling or fracture. 0.5 of RD was used to determine replacement point for first life cycle, which means 50% of reduction of capacity in terms of

modulus. When the average damage from all elements in damaged concrete blockout reached RD, reduced Young's modulus was replaced to damaged modulus multiplying by damage value subtracted 10% of RD from "1" (*non-damaged status*) as shown in Equation 6.5. The 10% of RD was defined as ND to differentiate from newly-built-bridge. Application of ND was required to increase RD for the next cycle. Equation 5.4 showed the relationship between RD for next cycle and FID using t_R of design life year.

$$RD(t) = RD + FID \times \frac{t}{t_R} \quad (6.5)$$

Cumulative damage against lifetime for case 1 with no DAF was plotted in using RD, FID and ND for concrete blockout. Figure 6.14 shows cumulative damage for all cases with replacement stage using RD and ND. The results from multiplying DAF by axle loads showed that more damage was caused by DAF. In order to compare condition rating of FE analysis results to inspection report information, condition rating based on damage results was plotted in Figure 6.15. Cumulative damages resulted from case 3 and case 4 were not different. That meant effect of group C and D was more effective than group B and E as shown in Figure 6.15. Thus, case 1 with no DAF and case 3 reflecting DAF effects were analyzed using ABAQUS 6.12 with 0.7 of RD to compare inspection report data. According to inspection report, deck joint including blockout is not primary element of bridge. Damaged blockout with spalling or torn S.S. deck joint is not immediately replaced or repaired. In this study, it was assumed that 70% reduction of capacity was appropriate for replacement. The results of case 1 and case 3 were compared to inspection report data as shown in Figure 6.16. Condition rating of realistic data in inspec-

TABLE 6.3
Applied traffic volumes of five loading classes using AADT of NBI-19027 bridge.

Vehicle Classification	GVW = Σ Axle Loads (kips)	Estimated AADT	Selected Load		Applied Traffic Counts
			Class		
2 CAR	4 = 2 + 2	7,000	8 kip		1,700 = 15 + 25 × 3 + 22 × 5
4 BUS	24 = 8 + 16	100	18 kip		9,470 = 3,000 + 120 + 250 + 100 + 5 × 1,200
5 2D	40 = 8 + 32	1,000	20 kip		680 = 6 × 100 + 80
FHWA 6 SU 3	72 = 8 + 32 × 2	600	27 kip		12,480 = 4 × 3,000 + 4 × 120
9 ST 5	126 = 18 + 27 × 4	3,000	32 kip		3,240 = 13 × 80 + 1,000 + 2 × 600
10 ST 6+	126 = 18 + 27 × 4	120			
12 MT 6	134 = 18 + 23.2 × 5	250			
13 MT 7+	134 = 18 + 20 × 6	100			
OW 138 kips of Michigan Trailer	138 = 12 + 16 × 2 + 18 × 5	1200			
200 kips	15 + 25 × 3 + 22 × 5	120			
496 kips	20 + 30 × 2 + 32 × 13	80			

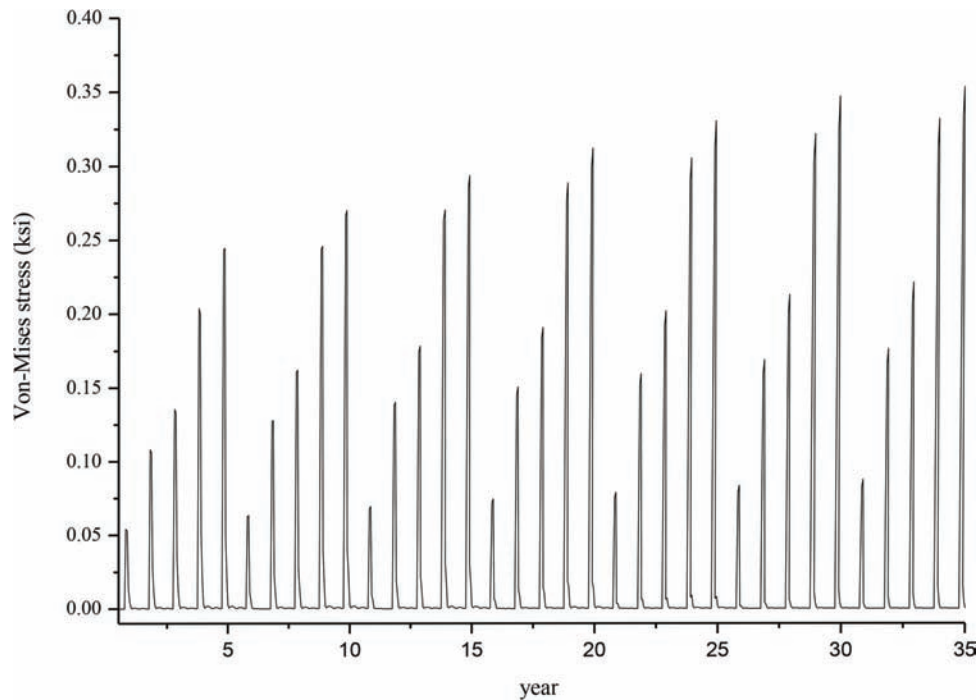


Figure 6.11 Von-Mises stress against lifetime due to 5 single axle load classes in concrete blockout obtained using DLOAD in ABAQUS 6.12.

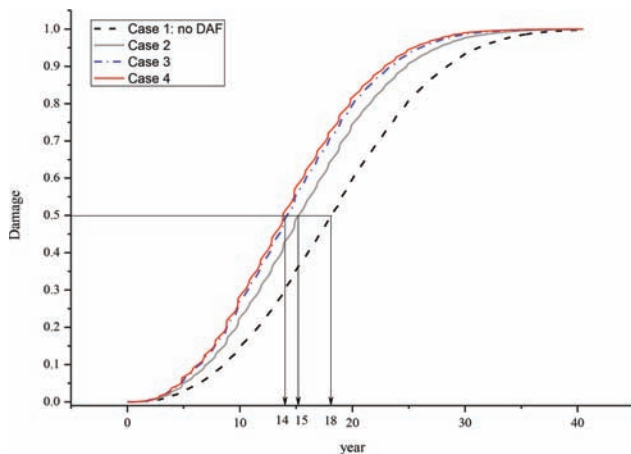


Figure 6.12 Comparison of averaged cumulative damage due to different dynamic amplification factors for four cases.

tion report was plotted for approximately 40 years. For first life cycle of deck joint, there was not enough data to compare. Figure 6.16 showed that condition rating resulted from FE analysis results represented inspection report data for the second life cycle of deck joint.

To investigate effect of overweight truck traffic on concrete blockout, 200% increased AADT of overweight trucks in Table 6.4 were applied using DLOAD ABAQUS 6.12. Specifically, AADT of NBI-19027 bridge located in West Lafayette, Indiana, was used for realistic data. According to traffic data for Tippecanoe county provided by INDOT (INDOT Traffic Data, <http://www.in.gov/indot/2469.htm>) and potential overweight

load of FHWA vehicle classification (Green et al., 2002), seven classifications considered as an overweight load as shown in Table 6.3 were increased as much as twice. Increased five single axle load classes were applied on the deck joint region model as shown in the column of applied traffic counts in Table 6.4. Figure 6.17 showed comparison of cumulative damage for case 3 to increased AADT of overweight trucks. The results of case 3 close to realistic condition rating curve was used for comparison to investigate effect of increased overweight Figure 6.17 indicated that increased AADT of overweight trucks caused more accumulation of damage. When cumulative damage met 70%, the results from case 3 was 18 years, and results based on increased overweight truck traffic was 13 years. It is evident that 200% increased overweight truck contributes to reduction of life of concrete blockout as well as the entire deck and the durability model is able to capture this reduction.

6.5 Summary

The results of simulated partial 3D bridge modeling for realistic deck joint region have been presented. This study presents durability model approach for concrete blockout, which is concrete parts newly-constructed to install expansion joint, using finite element analyses. Through the assumptions and methodologies adopted in the study, some conclusions can be obtained:

- An “accumulated damage” or quantitative estimate of deterioration of concrete blockout extracted from steel superstructure at different time periods using FE

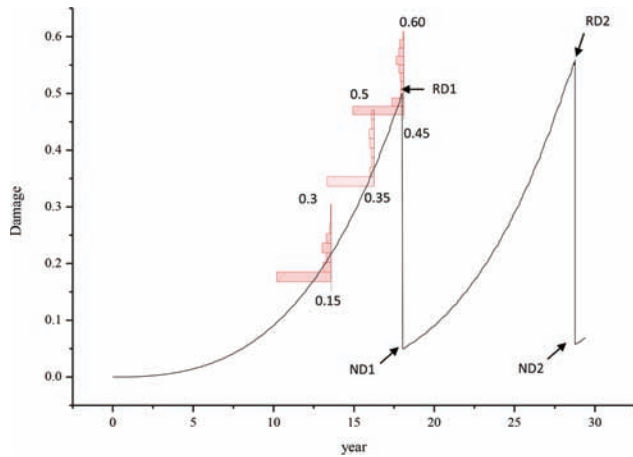


Figure 6.13 Average cumulative damage for case 1 with replacement stage.

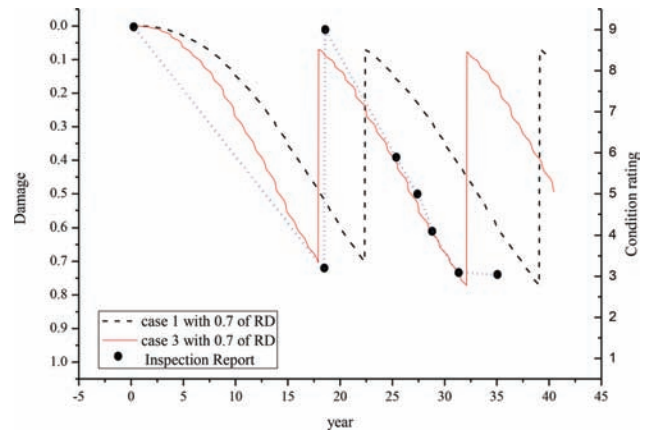


Figure 6.16 Comparison of condition rating based on FE

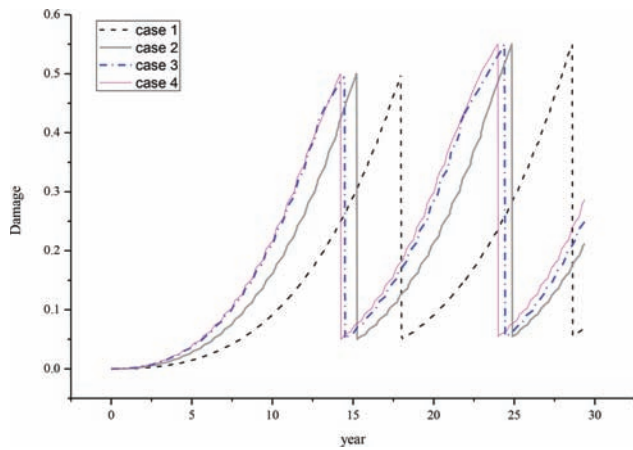


Figure 6.14 Average cumulative damage with repair stage by four cases.

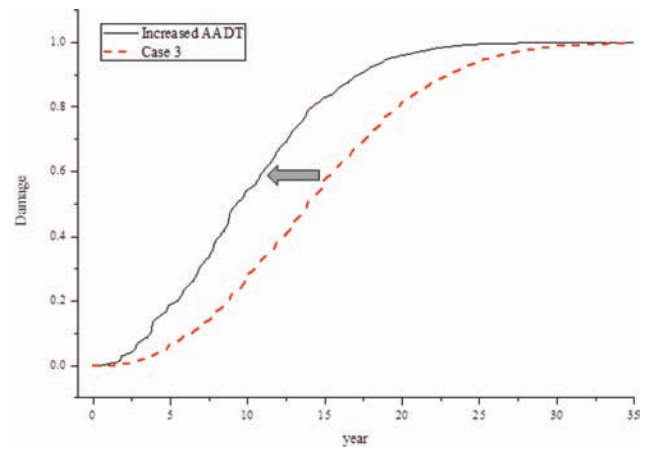


Figure 6.17 Comparison of accumulated damage by case 3 considering 200% increased AADT of overweight truck.

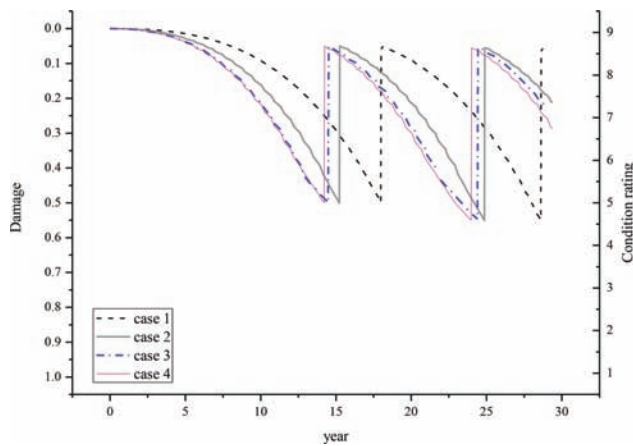


Figure 6.15 Condition rating based on cumulative damage for four cases.

model was obtained following illustrated procedure in Figure 6.3.

- The results predicted by the 3D FE model and calibrated dynamic amplification factors were in reasonably good agreement by calibrating the results using condition rating in the inspection report. FE analysis of moving plate using ABAQUS IMPLICIT provided reasonable dynamic amplification factors for durability analysis.
- Damage used in FE analysis was modeled as reduction of the Young's modulus. It was assumed that this reduction of elastic modulus includes deterioration due to repetitive loadings and natural corrosion using exponential curve with lifetime as shown in Equation 5.1.
- To simulate realistic cumulative damage in concrete blockout, replacement parameters such as Repair Damage (RD) and New Damage (ND) were introduced and used. Damage results based on replacement using 70% reduction of modulus for damaged blockout were in good agreement compared to inspection report information.

TABLE 6.4
 Applied traffic volumes considered 200% increased overweight trucks.

Vehicle Classification		GVW = Σ Axle loads (kips)	Estimated AADT	Selected Load Class	Applied Traffic Counts
FHWA	2 CAR	$4 = 2 + 2$	7,000	8 kip	$1,700 = 100 + 1,000 + 600$
	4 BUS	$24 = 8 + 16$	100	18 kip	$18,940 = 6,000 + 240 + 500 + 200 + 5 \times 2,400$
	5 2D	$40 = 8 + 32$	1,000	20 kip	$680 = 6 \times 200 + 160$
	6 SU 3	$72 = 8 + 32 \times 2$	600	27 kip	$24,960 = 4 \times 6,000 + 4 \times 240$
	9 ST 5	$126 = 18 + 27 \times 4$	6,000*	32 kip	$4,280 \text{ top} = 13 \times 160 + 1,000 + 2 \times 600$
	10 ST 6 +	$126 = 18 + 27 \times 4$	240*		
	12 MT 6	$134 = 18 + 23.2 \times 5$	500*		
	13 MT 7 +	$134 = 18 + 20 \times 6$	200*		
OW	138 kips of Michigan Trailer	$138 = 12 + 16 \times 2 + 18 \times 5$	2400*		
	200 kips	$15 + 25 \times 3 + 22 \times 5$	240*		
	496 kips	$20 + 30 \times 2 + 32 \times 13$	160*		

*200% increased counts of AADT.

7. CALIBRATION OF DURABILITY MODELS

In this chapter a parametric study is conducted based on real NBI data to calibrate the durability models developed. The NBI database was founded in 1982 and it contains a uniform format for every state for submitting bridge data to the FHWA. Usually this data has 110 items. In this study, bridges are classified according to two criteria corresponding to the loading and natural condition factors used in the durability models. Average Daily Traffic (ADT) is used to classify bridges into different load-related categories and location (latitude) is used to classify bridges for different natural conditions. Note that natural conditions encompass both, environment and local maintenance practices. However, in this study, the effect of maintenance practices could not be quantified. Further, the use of latitude as a proxy for natural condition is based on the assumption that the more northern latitudes suffer colder temperatures in general and some counties also receive substantial lake effect snow. While this is indeed an approximation, there are no other criteria in the NBI database that reflect natural conditions of a bridge and that would be amenable to the analysis conducted below.

7.1 Bridge Classification

The first step is to classify the bridges based on built material (reinforced concrete, pre-stressed concrete and steel), ADT (average daily traffic) and Latitude. Each of the parameters can be divided into five classes. In Figure 7.1, all RC bridges were first sorted according to their ADTs and a distribution of the number of bridges within a specific range of $\log(\text{ADT})$ was obtained (using natural logarithm). The same process was used to obtain classifications for Latitude. For both ADT and Latitude, the distribution of bridges was divided into 5 classes going from Very low, Low, Medium, High, to Very High. These classifications were used to categorize each bridge in terms of its loading classification (using ADT) and its natural condition (using Latitude). Ramp functions were used at the boundary of adjacent classes (shown with the dashed lines) to transition from one class to another. The loading and natural condition classifications of bridges were obtained for all INDOT owned RC bridges and for all Indiana RC bridges as well. The same process was utilized to classify PSC and Steel bridges owned by INDOT and within Indiana in general.

Note that while ADT and latitude are being used here to estimate and classify the loading and natural conditions of bridges, these parameters do not reflect the underlying load or natural condition well. In order to truly characterize the traffic loading on a bridge, it is essential to have data such as WIM that records not only the number of vehicles, but also their axle configurations and axle loads. ADT by itself is a very crude and insufficient measure of bridge loading. Similarly, latitude of a bridge by itself is not a good

indicator of the local natural conditions and maintenance practices. In order to obtain a realistic classification of natural conditions, local environmental quality and maintenance practices need to be quantified by the bridge inspectors or the owner.

Once the distribution of loading and natural conditions were obtained, the number of bridges in each of the categories going from Very Low to Very High were obtained as shown in Table 7.1 and Table 7.2 for INDOT owned and all Indiana bridges respectively. The deterioration rate for each bridge was then obtained by searching the evolution of structural condition ratings of the different components from historical NBI data as shown in Figure 7.2 where the top two plots show the evolution of condition rating of every RC bridge deck as a function of the age of the bridge, the second row of plots show distribution of deterioration rates (obtained by a least squares fit from the evolution of condition rating) for five classes of loading and natural condition, and the third row shows the average deterioration for each of these classes. Average deterioration rates for each of the 25 classes of bridges sorted by loading and natural condition were obtained and listed in Table 7.3 and Table 7.4 for RC bridge decks and in Table 7.5 and Table 7.6 for RC bridge girders. Figure 7.3 depicts similar data for RC bridge girders. Figure 7.4 plots the distribution of deterioration rates for all RC bridge decks and shows the average deterioration rate for all RC bridge decks for both INDOT owned and all Indiana bridges. Figure 7.5 plots a similar distribution of deterioration rates for all RC bridge girders. In a similar manner, average deterioration rates for each of the 25 classes of INDOT owned and all Indiana bridges were obtained for PSC and steel bridges, as shown in the following figures and tables.

7.1.1 Deterioration of RC Bridges

See Figures 7.1 through 7.5 and Tables 7.1 through 7.6.

7.1.2 Deterioration of PSC Bridges

See Figures 7.6 through 7.10 and Tables 7.7 through 7.12.

7.1.3 Deterioration of Steel Bridges

See Figures 7.11 through 7.19 and Tables 7.13 through 7.19.

A summary of the overall average deterioration rates decks and girders for all INDOT owned and all Indiana bridges is given in Table 7.19. Overall this data shows that deterioration rates for steel bridges were smaller than those of RC and PSC bridges for both decks and girders.

This data can be used to calibrate the overall deterioration rate for the durability models developed in the previous chapter. However, in order to determine the relative significance of the effect of loading and

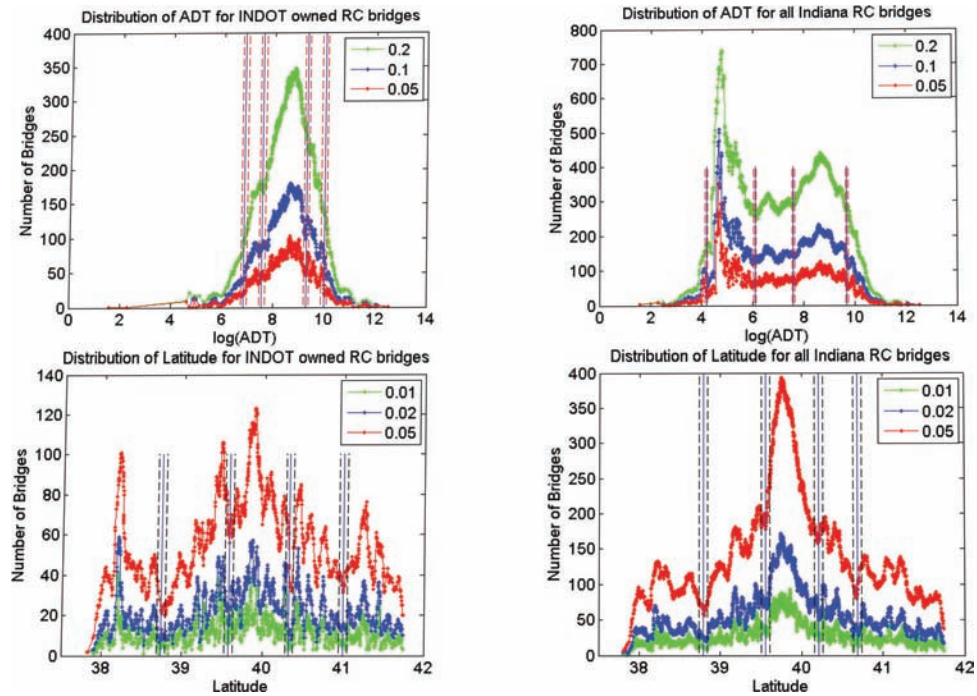


Figure 7.1 Classification of ADT and latitude for RC bridges (*left*, INDOT owned bridges; *right*, all Indiana bridges).

TABLE 7.1
Classification for INDOT owned RC bridges.

Weighted Number of Bridges		Average Daily Traffic (ADT)					Total
		1: Very Heavy	2: Heavy	3: Medium	4: Low	5: Very Low	
Environmental Condition	1: Critical	12.43	28.19	42.43	43.84	36.00	162.89
	2: Poor	37.36	58.57	64.53	67.53	41.56	269.54
	3: Normal	189.11	211.39	298.05	255.34	229.01	1182.89
	4: Good	63.29	48.56	111.36	67.22	47.92	338.34
	5: Excellent	38.31	6.03	78.09	14.00	21.91	158.33
Summary		340.51	352.73	594.45	447.92	376.39	2112.00

TABLE 7.2
Classification for all Indiana RC bridges.

Weighted Number of Bridges		Average Daily Traffic (ADT)					Total
		1: Very Heavy	2: Heavy	3: Medium	4: Low	5: Very Low	
Environmental Condition	1: Critical	39.77	27.46	69.79	34.79	44.93	216.74
	2: Poor	287.72	263.40	551.85	513.10	284.26	1900.33
	3: Normal	204.82	147.57	375.36	197.11	159.85	1084.71
	4: Good	463.05	254.08	561.55	327.72	297.37	1903.76
	5: Excellent	81.48	12.48	232.66	38.76	55.07	420.45
Summary		1076.83	704.99	1791.22	1111.48	841.49	5526.00

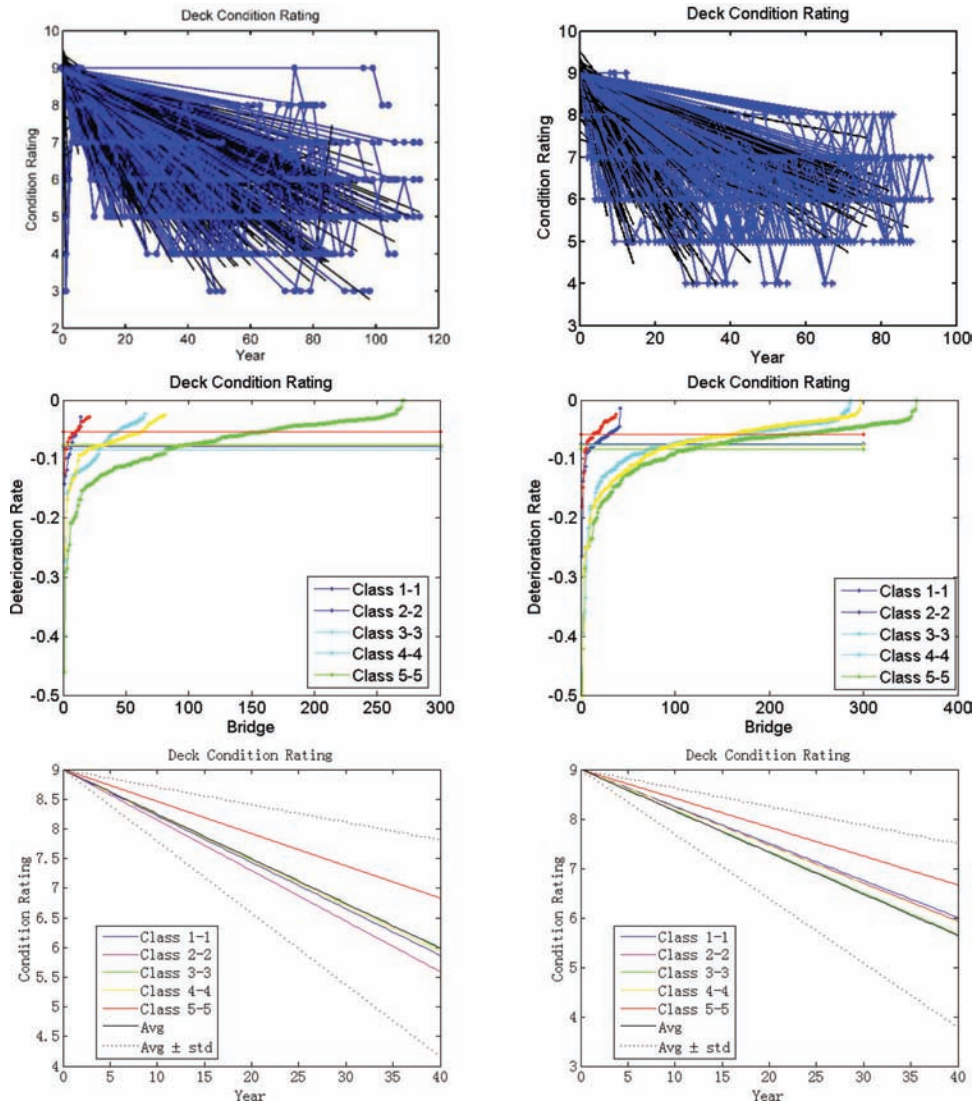


Figure 7.2 Deck condition rating for RC bridges (left, INDOT owned bridges; right, all Indiana bridges).

TABLE 7.3
INDOT RC decks.

	1: VH	2: H	3: M	4: L	5: VL
1: C	-0.078	-0.079	-0.096	-0.085	-0.084
2: P	-0.084	-0.085	-0.092	-0.098	-0.076
3: N	-0.086	-0.079	-0.075	-0.077	-0.061
4: G	-0.085	-0.061	-0.073	-0.077	-0.055
5: E	-0.087	-0.069	-0.061	-0.074	-0.054

natural condition on the deterioration rate, a linearly varying relationship was postulated:

$$r = r_{\min} + \frac{(\alpha_N N + \alpha_L L)}{(\alpha_N + \alpha_L)} (r_{\max} - r_{\min})$$

TABLE 7.4
All Indiana RC bridge decks.

	1: VH	2: H	3: M	4: L	5: VL
1: C	-0.075	-0.091	-0.075	-0.0692	-0.088
2: P	-0.088	-0.079	-0.078	-0.0689	-0.107
3: N	-0.092	-0.086	-0.113	-0.0847	-0.075
4: G	-0.106	-0.083	-0.090	-0.0772	-0.068
5: E	-0.082	-0.084	-0.067	-0.0764	-0.058

where r denotes the expected deterioration rate of a specific bridge, r_{\min} and r_{\max} denote the minimum and maximum expected deterioration rates for the specific type of bridge, L and N denote the loading and natural condition classification of the bridge, and α_N and α_L

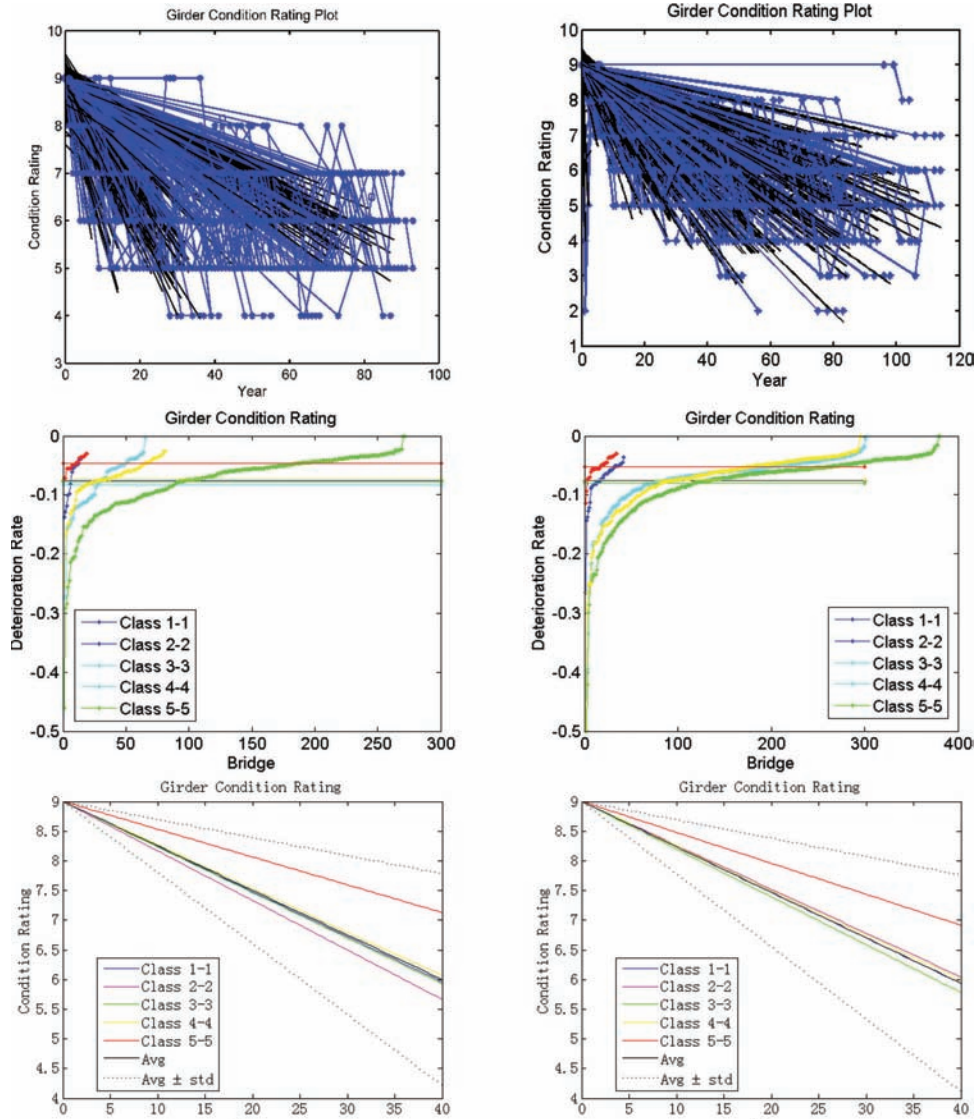


Figure 7.3 Girder condition rating for RC bridges (*left*, INDOT owned bridges; *right*, all Indiana bridges).

TABLE 7.5
INDOT RC girders.

	1: VH	2: H	3: M	4: L	5: VL
1: C	-0.076	-0.083	-0.084	-0.079	-0.083
2: P	-0.084	-0.083	-0.091	-0.088	-0.075
3: N	-0.083	-0.078	-0.077	-0.075	-0.060
4: G	-0.084	-0.064	-0.075	-0.073	-0.054
5: E	-0.071	-0.078	-0.065	-0.071	-0.047

TABLE 7.6
All Indiana RC girders.

	1: VH	2: H	3: M	4: L	5: VL
1: C	-0.077	-0.083	-0.074	-0.07376	-0.081
2: P	-0.088	-0.076	-0.075	-0.06919	-0.118
3: N	-0.091	-0.086	-0.113	-0.08128	-0.074
4: G	-0.114	-0.084	-0.090	-0.07506	-0.067
5: E	-0.077	-0.089	-0.066	-0.07584	-0.052

denote the relative weighting of load-related and natural condition-related deterioration. Figure 7.16 depicts the anticipated variation of deterioration rates as modeled by this equation showing that one would expect bridges with very low loading (approximately characterized by ADT) and with excellent natural

conditions (approximately characterized by latitude), would have the lowest deterioration rate and bridges with high loading and poor natural condition would have the highest deterioration rate. For instance, the variation of deterioration rates for RC bridge decks

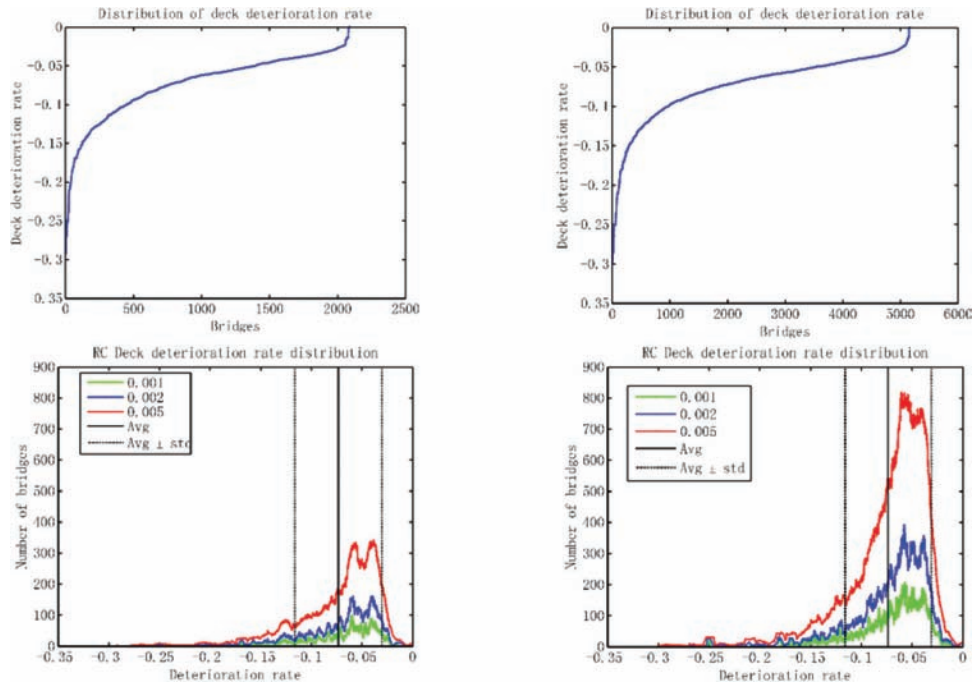


Figure 7.4 Distribution of deterioration rate for RC bridge decks (left, INDOT owned bridges; right, all Indiana bridges).

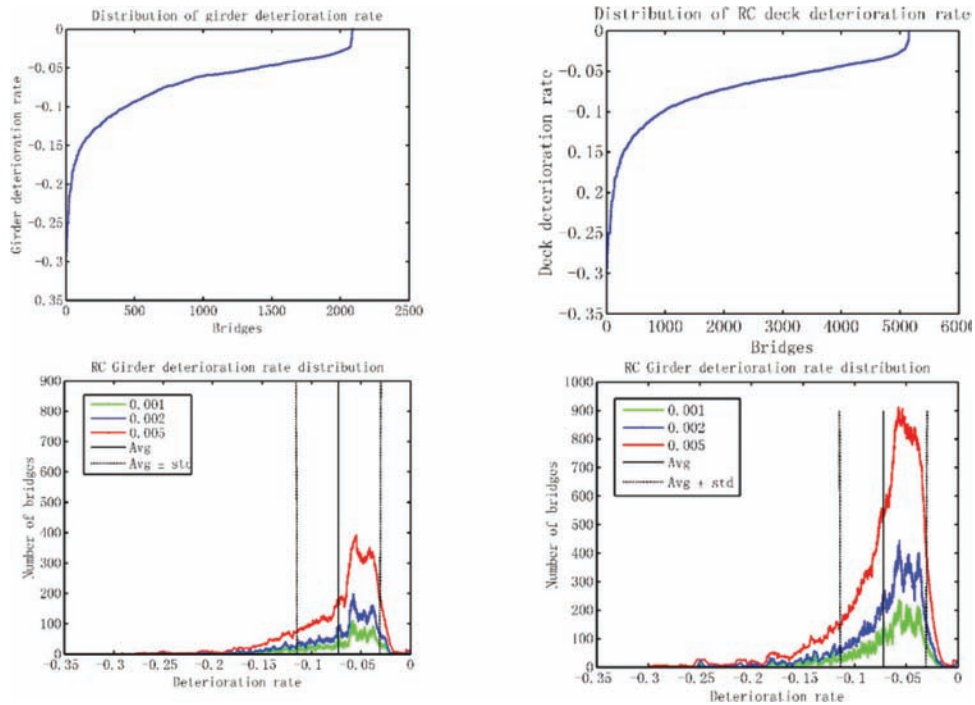


Figure 7.5 Distribution of deterioration rate for RC bridge girders (left, INDOT owned bridges; right, all Indiana bridges).

listed in Table 7.3 and Table 7.4 and for RC bridge girders listed in Table 7.5 and Table 7.6 may be expected to follow the trend shown in Figure 7.16. The minimum and maximum deterioration rates above may be taken as the maximum and minimum values from these tables or they may be taken as the average

standard deviation of the deterioration rates mentioned in Table 7.19.

The variation of actual deterioration rates obtained from the above analysis are shown in Figure 7.17, Figure 7.18, and Figure 7.19 for RC, PSC and Steel bridges respectively. For RC bridges, a rough trend of

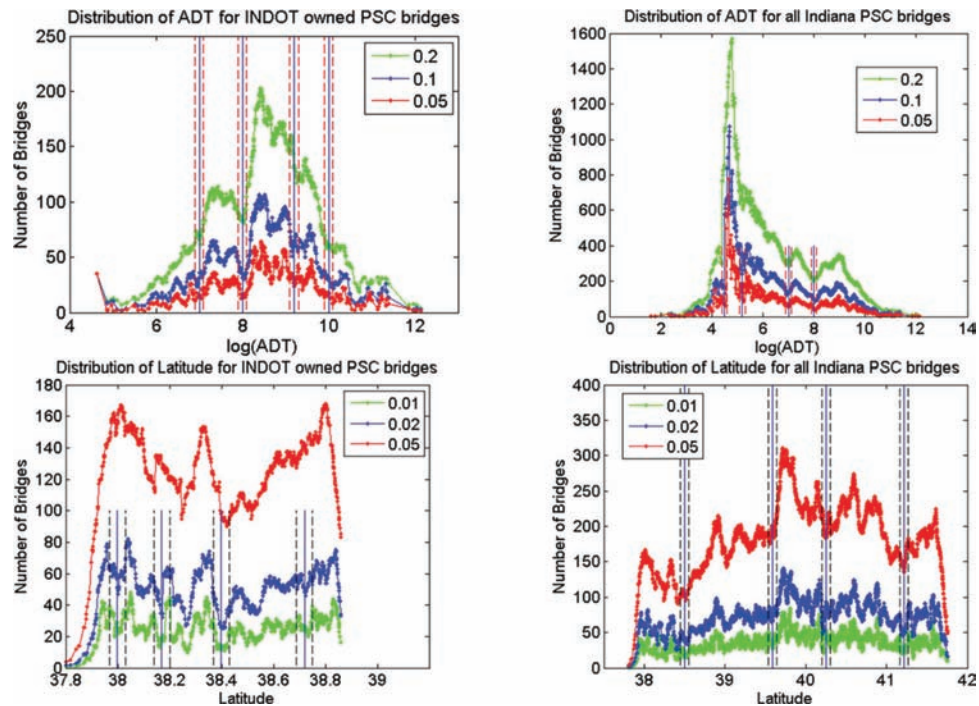


Figure 7.6 Classification of ADT and latitude for PSC bridges (*left*, INDOT owned bridges; *right*, all Indiana bridges).

TABLE 7.7
Classification for INDOT owned PSC bridges.

Weighted Number of Bridges		Average Daily Traffic (ADT)					Total
		1: Very Heavy	2: Heavy	3: Medium	4: Low	5: Very Low	
Environmental Condition	1: Very poor	34.81	97.01	94.96	54.23	6	287.01
	2: Poor	54.32	67.51	81.48	62.19	65.59	331.09
	3: Normal	85.64	82.12	101.47	123.51	76.38	469.12
	4: Good	52.5	127.01	84.1	44.05	24.69	332.35
	5: Excellent	47.41	95.21	40.34	76.58	7.89	267.43
Summary		274.68	468.86	402.35	360.56	180.55	1687

TABLE 7.8
Classification for all Indiana PSC bridges.

Weighted Number of Bridges		Average Daily Traffic (ADT)					Total
		1: Very Heavy	2: Heavy	3: Medium	4: Low	5: Very Low	
Environmental Condition	1: Very poor	53.92	303.51	246.15	245.1	10.8	859.48
	2: Poor	356.43	745.28	542.12	489.52	8.82	2142.17
	3: Normal	436.57	777.79	610.39	471.62	106.93	2403.3
	4: Good	172.34	226.59	165.93	166.05	193.15	924.06
	5: Excellent	120.75	280.99	236.06	657.52	462.67	1757.99
Summary		1140.01	2334.16	1800.65	2029.81	782.37	8087

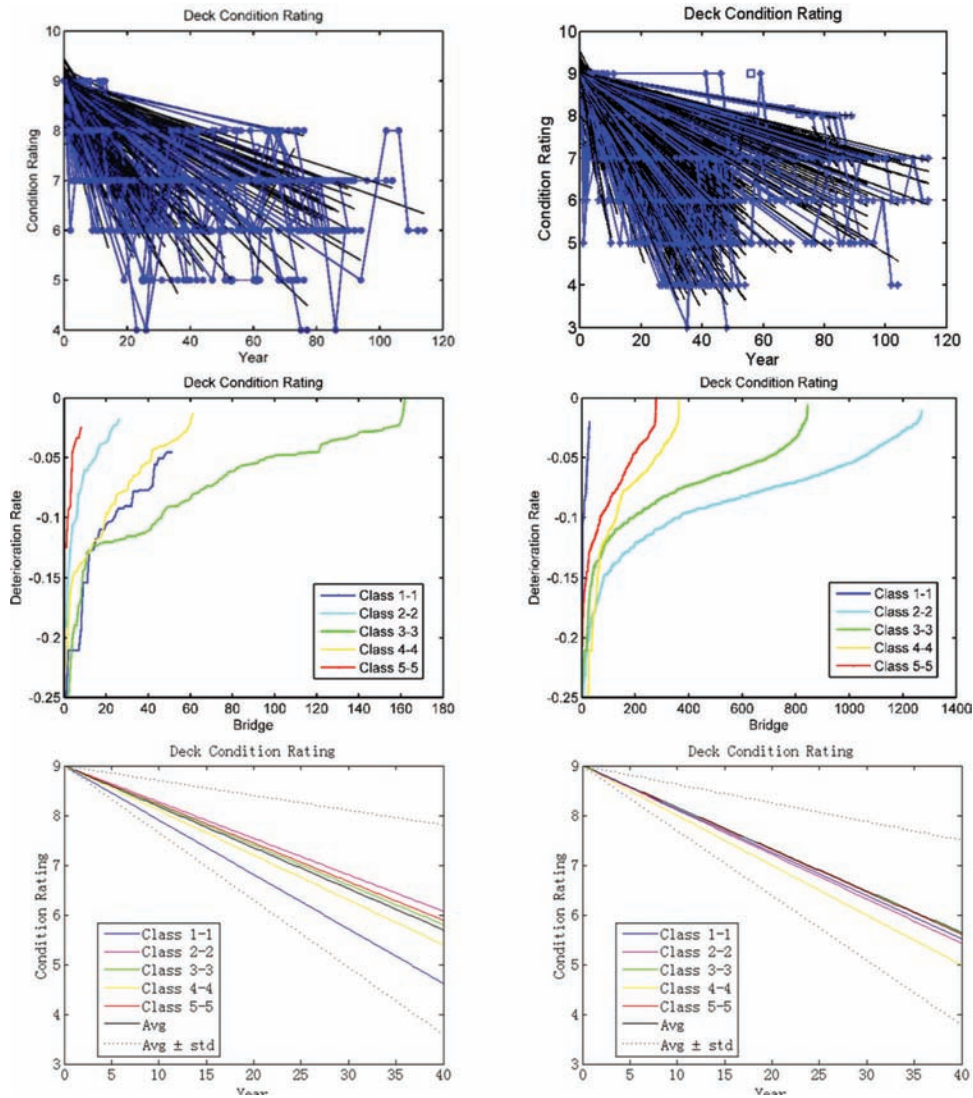


Figure 7.7 Deck condition rating deterioration (*left*, INDOT owned bridges; *right*, all Indiana bridges).

TABLE 7.9
INDOT PSC concrete decks.

	1: VH	2: H	3: M	4: L	5: VL
1: C	-0.110	-0.083	-0.062	-0.073	-0.095
2: P	-0.225	-0.073	-0.069	-0.083	-0.095
3: N	-0.215	-0.096	-0.080	-0.081	-0.081
4: G	-0.183	-0.086	-0.100	-0.090	-0.079
5: E	-0.311	-0.104	-0.124	-0.111	-0.078

low deterioration rates at the bottom-left of the plot and high deterioration rates at the top-right of the plot are visible, suggesting that $\alpha_N = \alpha_L = 0.5$ may be an appropriate choice for RC bridges.

For PSC bridges, trends within the INDOT inventory and all Indiana bridges are very different. This discrepancy may be due to a design or construction

TABLE 7.10
All Indiana PSC bridge decks.

	1: VH	2: H	3: M	4: L	5: VL
1: C	-0.087	-0.087	-0.097	-0.090	-0.089
2: P	-0.091	-0.091	-0.087	-0.092	-0.102
3: N	-0.086	-0.084	-0.084	-0.089	-0.070
4: G	-0.094	-0.096	-0.080	-0.100	-0.073
5: E	-0.111	-0.093	-0.097	-0.198	-0.085

issue leading to high deterioration of a certain class of PSC bridges. For INDOT PSC bridges, the data seems to suggest that there is minimal effect of environmental condition and only ADT seems to govern deterioration. Thus one may adopt values of α_N between 0 and 0.25 and α_L between 0.75 and 1 for INDOT PSC bridges.

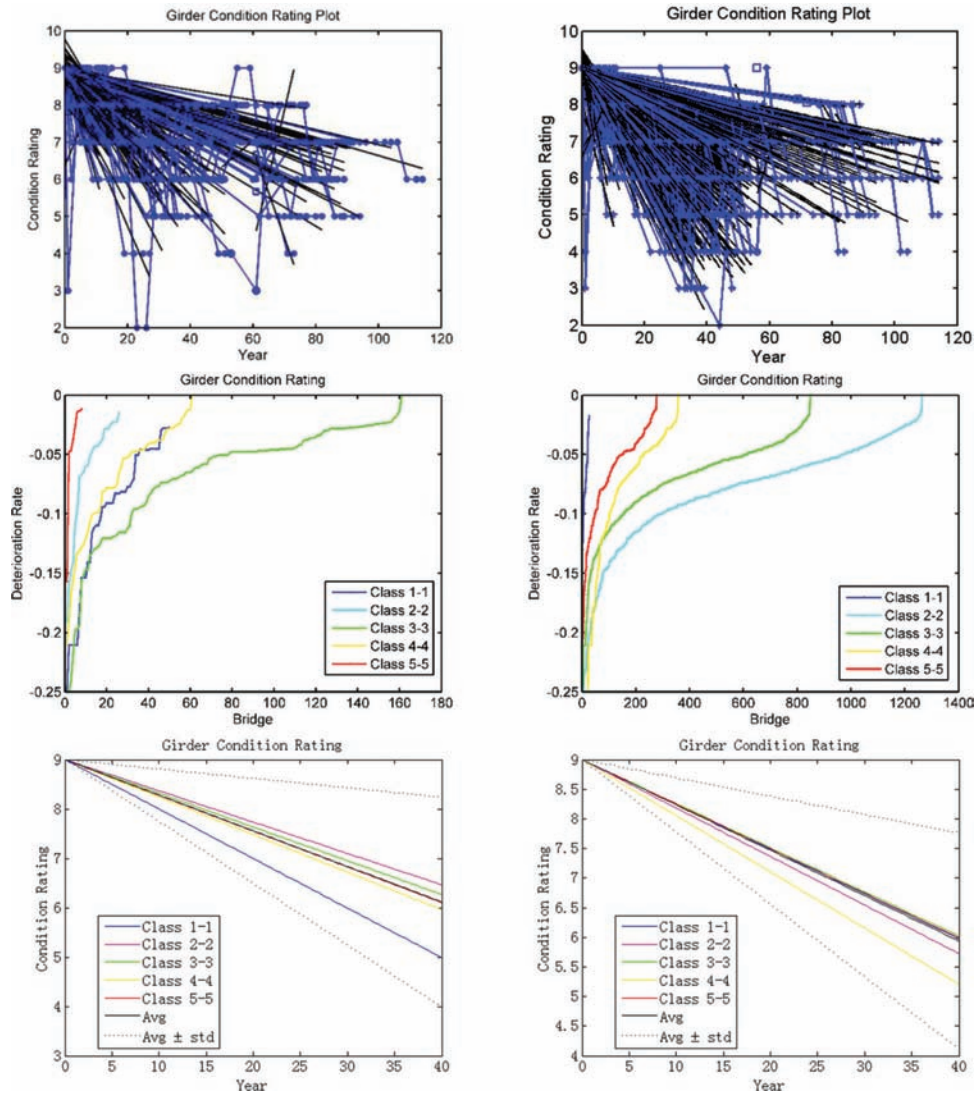


Figure 7.8 Girder condition rating deterioration (left, INDOT owned bridges; right, all Indiana bridges).

TABLE 7.11
INDOT PSC bridge girders.

	1: VH	2: H	3: M	4: L	5: VL
1: C	-0.100	-0.076	-0.062	-0.075	-0.104
2: P	-0.223	-0.063	-0.063	-0.065	-0.061
3: N	-0.221	-0.092	-0.068	-0.067	-0.067
4: G	-0.198	-0.088	-0.104	-0.076	-0.064
5: E	-0.301	-0.093	-0.118	-0.104	-0.073

TABLE 7.12
All Indiana PSC bridge girders.

	1: VH	2: H	3: M	4: L	5: VL
1: C	-0.076	-0.081	-0.090	-0.087	-0.082
2: P	-0.085	-0.084	-0.081	-0.086	-0.106
3: N	-0.085	-0.077	-0.075	-0.081	-0.066
4: G	0.079	-0.083	-0.073	-0.099	-0.061
5: E	-0.093	-0.076	-0.084	-0.188	-0.075

Trends in the deterioration rates of INDOT owned steel bridges were not conclusive. However, for all Indiana steel bridges, it seems that environmental condition was the

governing factor for deterioration while loading had minimal effect. One may chose α_N between 0.75 and 1 and α_L between 0 and 0.25 for such situations.

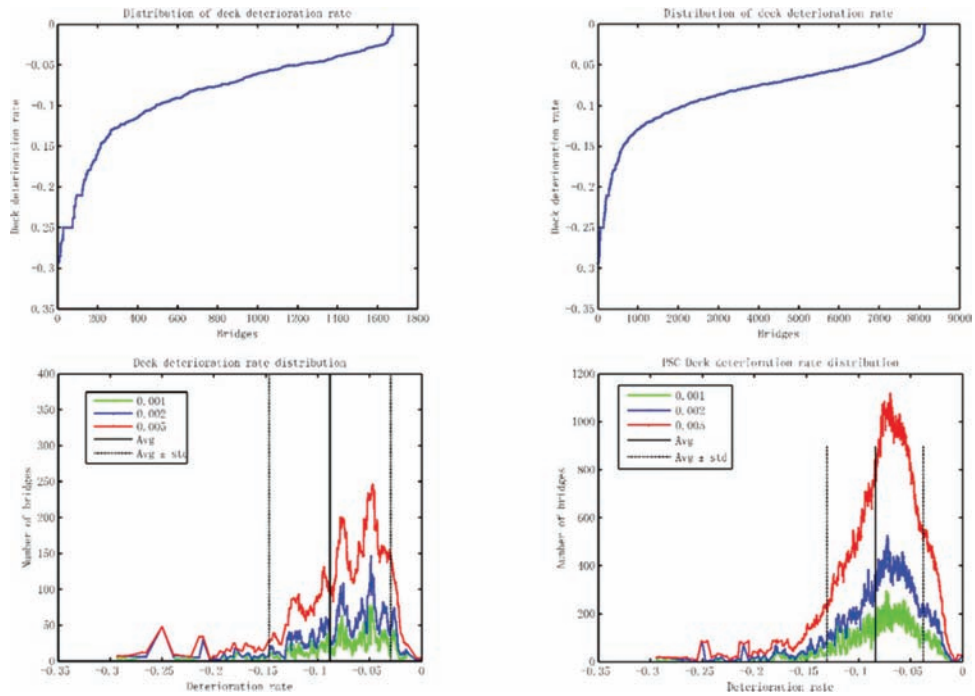


Figure 7.9 Distribution of deterioration rate for PSC bridge decks (*left*, INDOT owned bridges; *right*, all Indiana bridges).

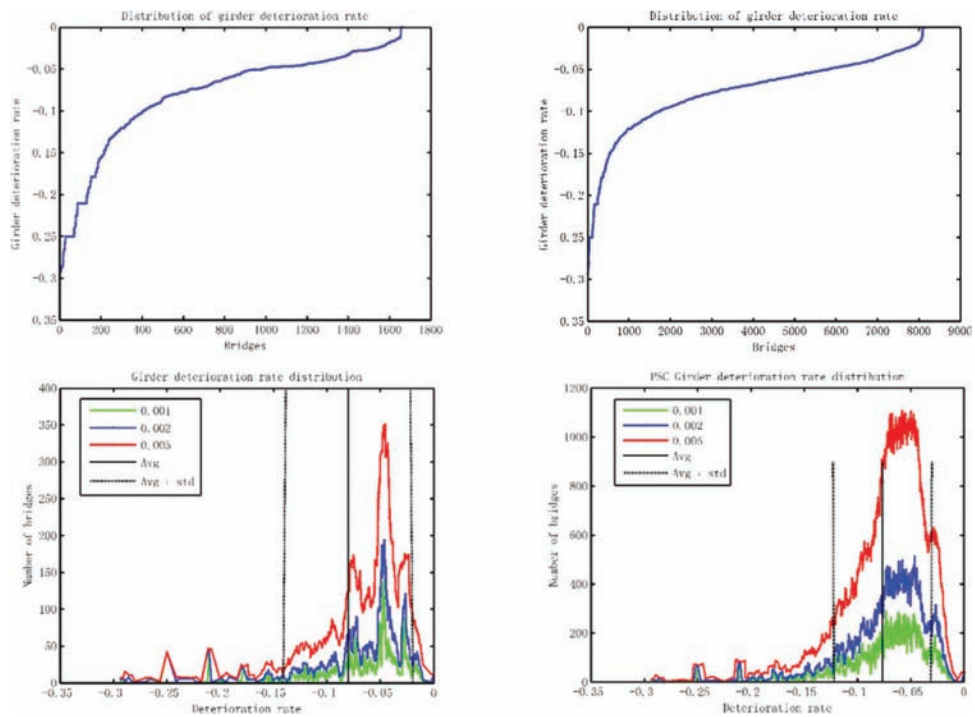


Figure 7.10 Distribution of deterioration rate for PSC bridge girders (*left*, INDOT owned bridges; *right*, all Indiana bridges).

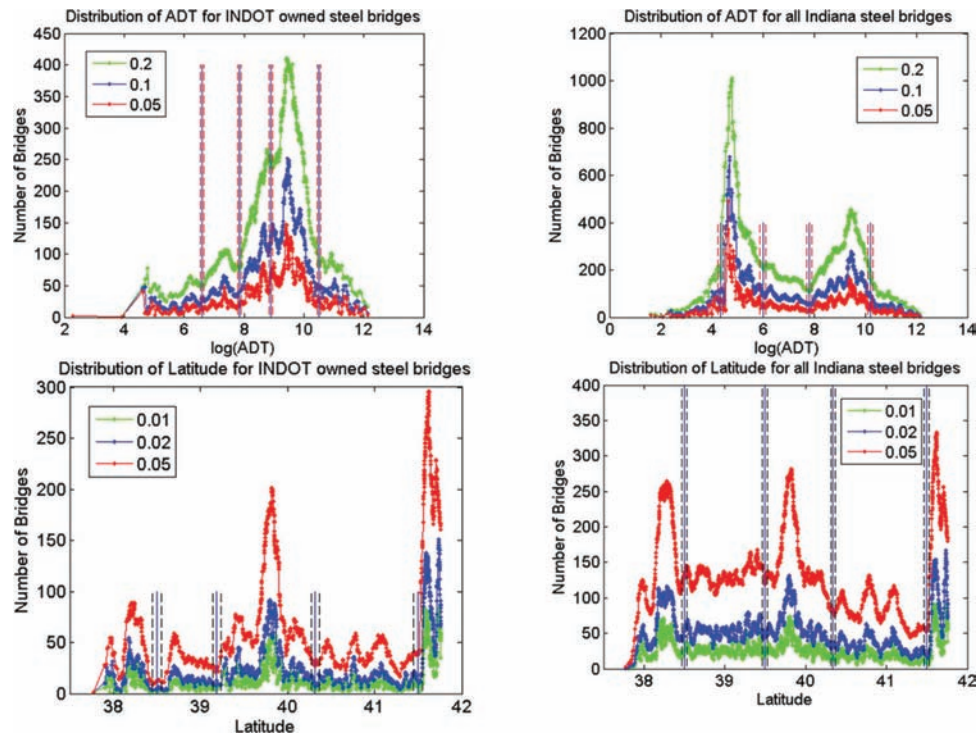


Figure 7.11 Classification of ADT and latitude for steel bridges (left, INDOT owned bridges; right, all Indiana bridges).

TABLE 7.13
Classification for INDOT owned steel bridges.

Weighted Number of Bridges		Average Daily Traffic (ADT)					Total
		1: Very Heavy	2: Heavy	3: Medium	4: Low	5: Very Low	
Environmental Condition	1: Very poor	72.44	51.68	63.88	19.70	37.79	245.50
	2: Poor	43.83	54.77	87.07	40.48	25.39	251.55
	3: Normal	52.24	139.16	138.61	62.32	73.33	465.67
	4: Good	323.48	183.04	344.89	87.81	111.51	1050.73
	5: Excellent	39.44	8.06	185.98	2.08	24.00	259.56
Summary		531.43	436.72	820.44	212.38	272.02	2273.00

TABLE 7.14
Classification for all Indiana steel bridges.

Weighted Number of Bridges		Average Daily Traffic (ADT)					Total
		1: Very Heavy	2: Heavy	3: Medium	4: Low	5: Very Low	
Environmental Condition	1: Very poor	4.58	74.62	52.64	109.38	107.14	348.36
	2: Poor	63.23	343.09	330.72	668.74	481.98	1887.76
	3: Normal	85.56	154.62	211.61	159.37	101.83	712.99
	4: Good	316.78	268.52	352.69	279.61	194.55	1412.15
	5: Excellent	58.69	20.42	195.02	13.98	38.63	326.74
Summary		528.84	861.27	1142.68	1231.08	924.13	4688

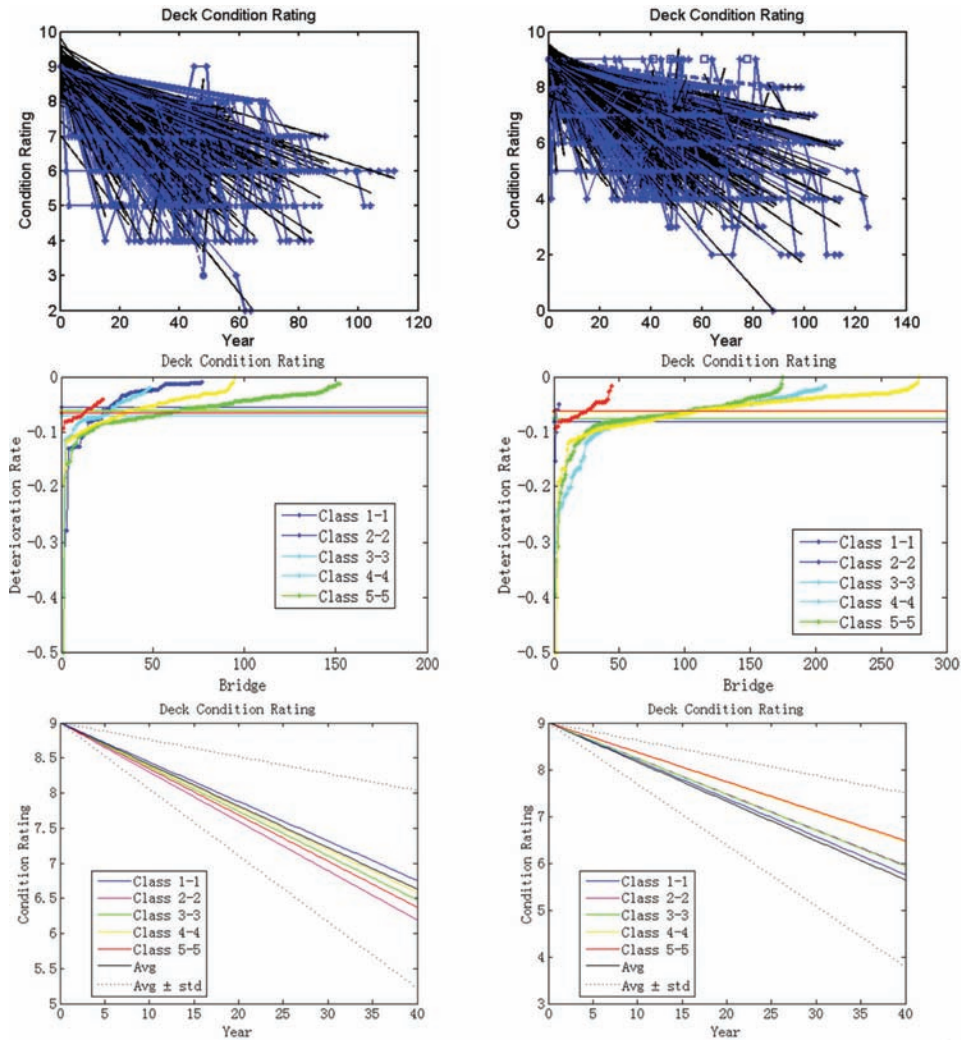


Figure 7.12 Deck condition rating deterioration rate (*left*, INDOT owned bridges; *right*, all Indiana bridges).

TABLE 7.15
INDOT steel bridge decks.

	1: VH	2: H	3: M	4: L	5: VL
1: C	-0.056	-0.073	-0.062	-0.065	-0.052
2: P	-0.071	-0.070	-0.063	-0.065	-0.051
3: N	-0.090	-0.071	-0.063	-0.054	-0.057
4: G	-0.070	-0.063	-0.065	-0.060	-0.065
5: E	-0.125	-0.036	-0.056	-0.097	-0.066

TABLE 7.16
All Indiana steel bridge decks.

	1: VH	2: H	3: M	4: L	5: VL
1: C	-0.081	-0.099	-0.102	-0.078	-0.088
2: P	-0.067	-0.082	-0.093	-0.113	-0.079
3: N	-0.062	-0.070	-0.079	-0.081	-0.067
4: G	-0.074	-0.067	-0.067	-0.064	-0.071
5: E	-0.123	-0.042	-0.061	-0.094	-0.063

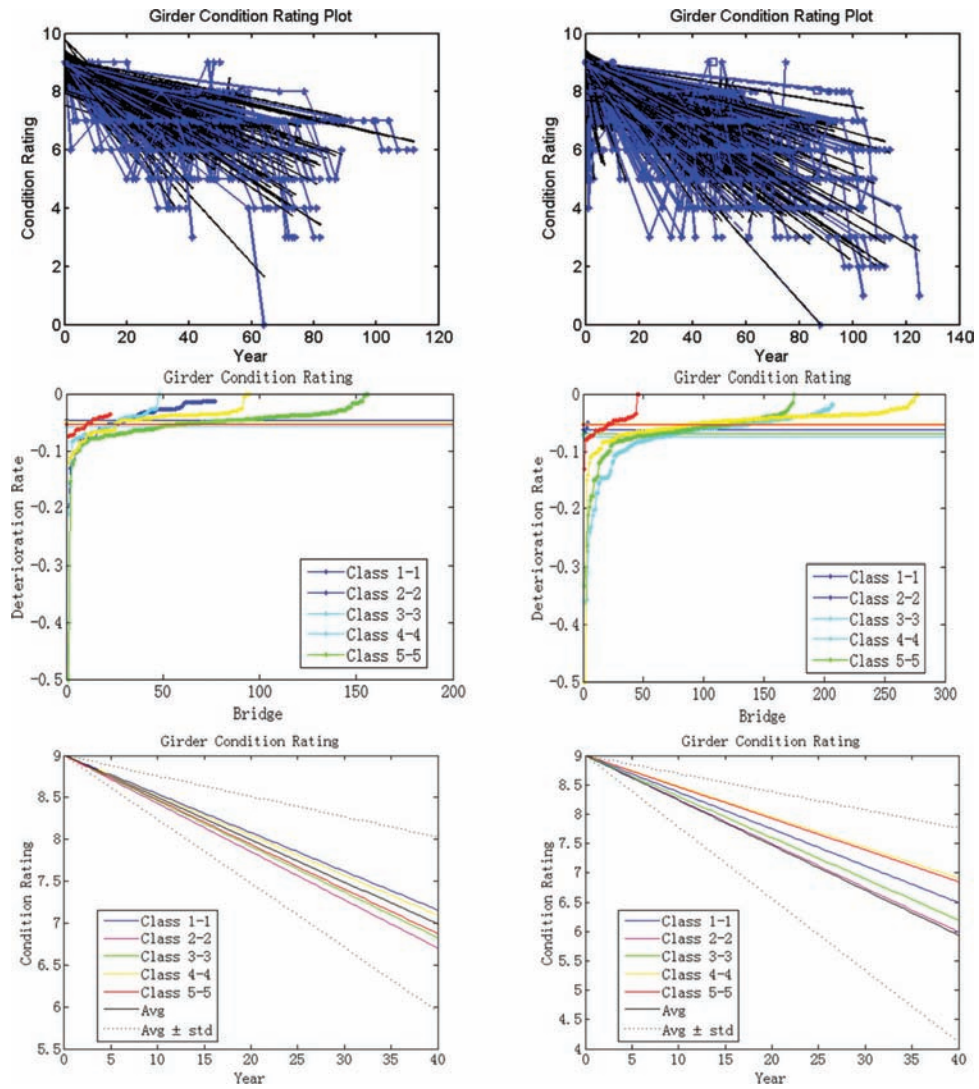


Figure 7.13 Girder condition rating deterioration rate (left, INDOT owned bridges; right, all Indiana bridges).

TABLE 7.17
INDOT steel girders.

	1: VH	2: H	3: M	4: L	5: VL
1: C	-0.046	-0.056	-0.055	-0.060	-0.050
2: P	-0.066	-0.057	-0.055	-0.052	-0.050
3: N	-0.079	-0.057	-0.054	-0.045	-0.051
4: G	-0.059	-0.053	-0.054	-0.048	-0.053
5: E	-0.095	-0.028	-0.052	-0.072	-0.053

TABLE 7.18
All Indiana steel bridge girders.

	1: VH	2: H	3: M	4: L	5: VL
1: C	-0.063	-0.103	-0.099	-0.100	-0.103
2: P	-0.050	-0.088	-0.088	-0.116	-0.084
3: N	-0.060	-0.063	-0.073	-0.079	-0.069
4: G	-0.063	-0.055	-0.058	-0.052	-0.061
5: E	-0.089	-0.034	-0.055	-0.079	-0.054

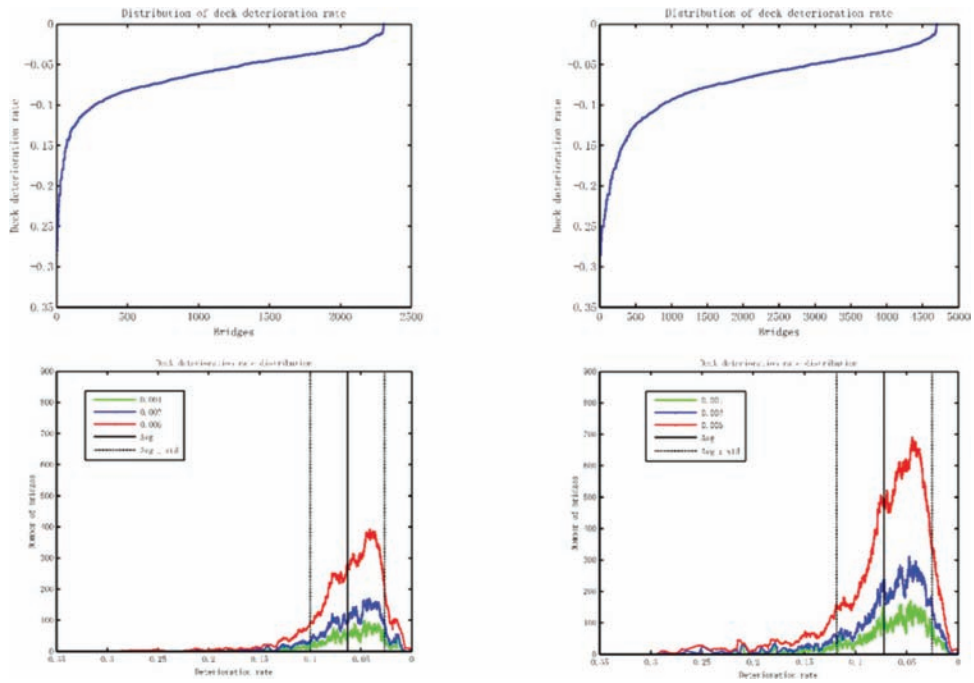


Figure 7.14 Distribution of deterioration rate for steel bridge decks (*left*, INDOT owned bridges; *right*, all Indiana bridges).

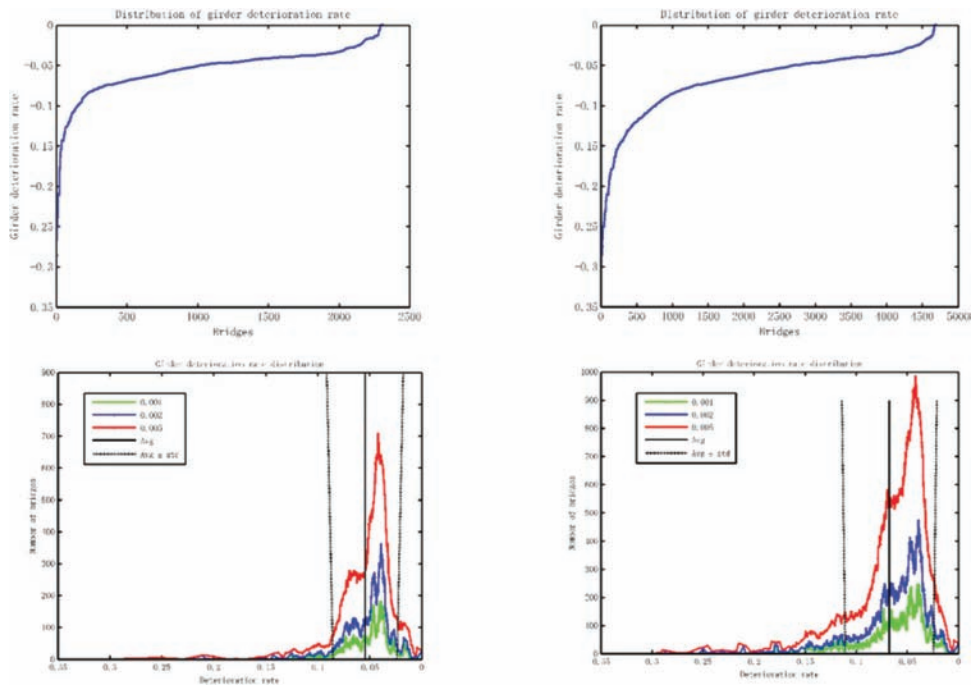


Figure 7.15 Distribution of deterioration rate for steel bridge girders (*left*, INDOT owned bridges; *right*, all Indiana bridges).

TABLE 7.19
Summary of deterioration rates: average \pm standard deviation.

Parameter Group	Deck		Girder	
	INDOT	INDIANA	INDOT	INDIANA
Reinforced Concrete	-0.0732 ± 0.0428	-0.0735 ± 0.0425	-0.0728 ± 0.0418	-0.0723 ± 0.0415
Pre-stressed concrete	-0.0882 ± 0.0584	-0.0840 ± 0.0465	-0.0802 ± 0.0607	-0.0766 ± 0.0456
Steel	-0.0663 ± 0.0368	-0.0719 ± 0.0465	-0.0546 ± 0.0308	-0.0676 ± 0.0431

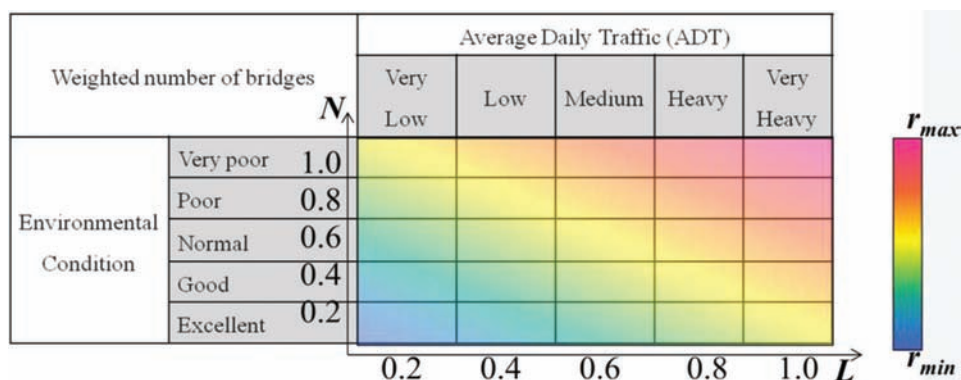


Figure 7.16 Modeling the variation of deterioration rate with loading and natural condition.

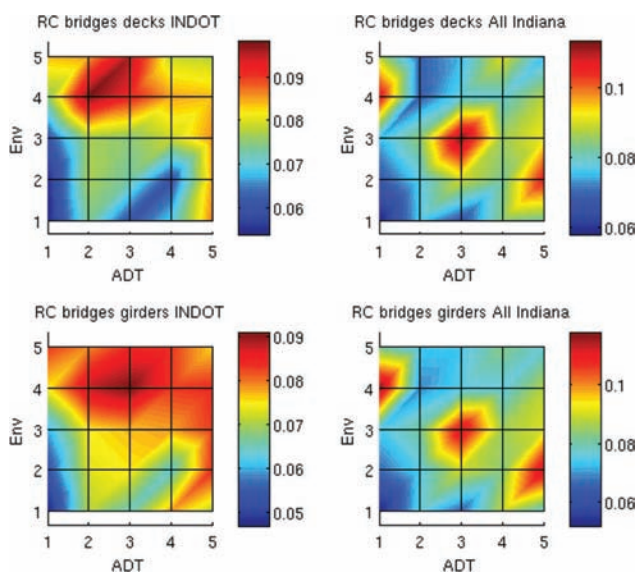


Figure 7.17 Variation of deterioration rates for RC bridge decks and girders (left, INDOT owned bridges; right, all Indiana bridges).

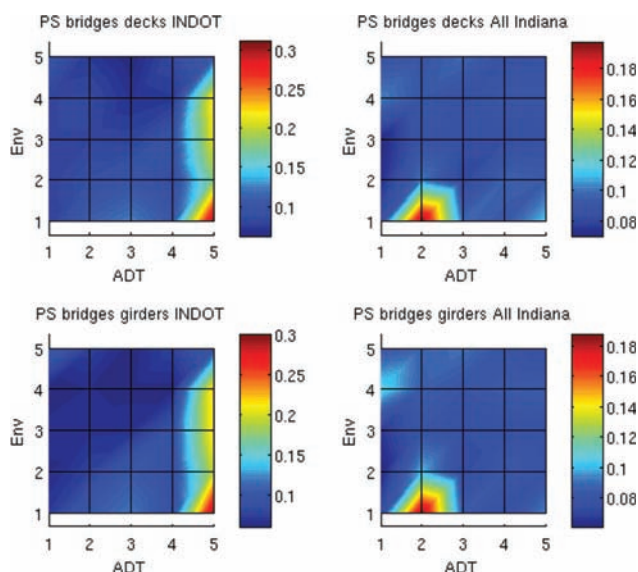


Figure 7.18 Variation of deterioration rates for PSC bridge decks and girders (left, INDOT owned bridges; right, all Indiana bridges).

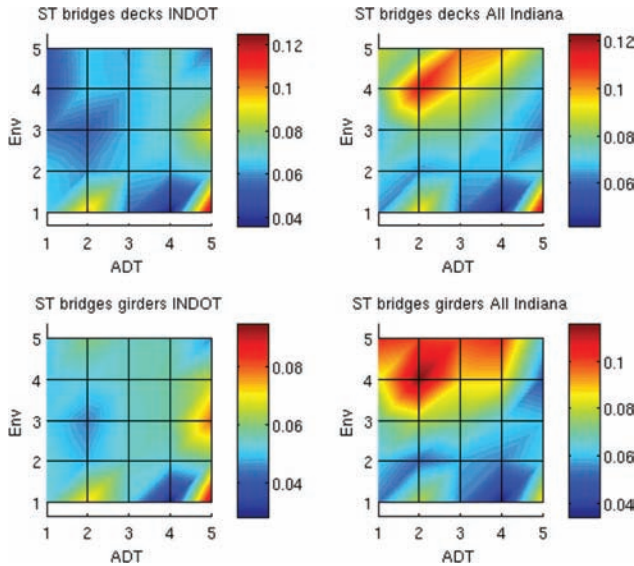


Figure 7.19 Variation of deterioration rates for steel bridge decks and girders (*left*, INDOT owned bridges; *right*, all Indiana bridges).

8. SUMMARY AND CONCLUSIONS

In this research, an approach for conducting durability analysis of bridges based on the technique for FE model updation was developed to simulate the progression of damage in the various components of a steel bridge. The numerical analysis approach presented in this study is able to model the damage progression in different components of a steel bridge by representing total cumulative damage as a sum of damage due to repetitive traffic loading and due to natural conditions. A novel aspect of the durability analysis approach is that it can capture the state of damage in *all* the elements of the bridge by updating the FE model with decreased Young’s modulus corresponding to the level of accumulated damage at various times during the lifetime of the bridge. Results of the time-dependent damage obtained from 3D full scale bridge modeling were compared to data from historical inspection reports, showing that the model works well for capturing the salient features of how damage progresses in steel bridge components.

In particular, the durability analysis (under normal conditions, case 0) was able to reproduce the state of damage of the steel superstructure well in comparison to the inspection reports. However, the state of damage in the concrete deck was under-predicted by the model because of the inability of the current model to represent localized damage near the deck joints. Further, this approach for durability analysis was also used to conduct an investigation of the rate of damage progression under different hypothetical scenarios. It was shown that the effect of increased AADT including overweight truck traffic was to increase cumulative damage in the steel superstructures as well as the concrete bridge decks. In addition, it was shown that deteriorating natural conditions, either due to poor environment or

due to poor maintenance, also lead to a faster deterioration of bridge components.

Lastly, it is postulated that this approach can be used to investigate different hypothetical scenarios and answer important questions such as “How would increasing truck weight limits affect lifecycle of steel bridges?” We envision that a user may be able to adapt the durability analysis framework to their particular scenario (in a way similar to what was shown in case 1 of the numerical case studies), by modifying the number and weight limits of the load classes and the AADTs associated with each class as needed. This approach may also be used in conjunction with a structural health monitoring program and help highway agencies in making important decisions regarding their bridge infrastructure.

8.1 Implementation and Recommendations

A possible implementation item from this research is evaluation of permit fees processes for overweight trucks. Using the durability models developed and along with the equation for calculating the deterioration rate for a given bridge:

$$r = r_{\min} + \frac{(\alpha_N N + \alpha_L L)}{(\alpha_N + \alpha_L)} (r_{\max} - r_{\min})$$

where the terms in the model are defined in the previous chapter, it is possible to quantify the damage resulting from individual classes of vehicles and to ensure that the permit fee reflects the cost of the incremental damage caused by a given truck.

Example: As an example, consider an RC bridge in INDOT’s inventory that is similar in configuration to the representative RC bridge modeled in Chapter 4: “Finite-Element Modeling of Reinforced and Prestressed Concrete Bridges.” Assuming r_{\min} and r_{\max} values of 0.116 and 0.03 respectively for both concrete decks and concrete girders, based on Table 7.19, and further adopting $\alpha_N = \alpha_L = 0.5$, consistent with the conclusion drawn from the previous chapter, one can determine the expected deterioration rate r , for different loading and natural conditions L and N . For instance, a bridge under “normal” natural conditions ($N = 0.6$) will undergo, on average, deterioration rate ranging between $r = 0.03 + 0.5 * (0.6 + 0.2) * (0.116 - 0.03) = 0.06$ per year for very low traffic loading, and $r = 0.03 + 0.6 + 1.0) * (0.116 - 0.03) = 0.1$ per year for very high traffic loading, implying a single point drop in condition rating in 16 years and 10 years respectively under the two cases with “normal” maintenance being conducted on the bridges. Note that these estimates are still limited by the assumptions underlying the model and its calibration as presented in the previous chapters. In order to obtain better estimates of the deterioration rates, and explore the variation of these deterioration rates with varying conditions, reliable historical data on how the loading conditions, environmental

conditions, and maintenance practices evolved for all the representative bridges would be needed to recalibrate the models.

Another possible implementation of the results of this research is on the management of INDOT's bridge inventory based on expected deterioration rates for different classes of bridges. Knowing the expected deterioration rates and how they may change with changing traffic patterns, maintenance policies and natural conditions may allow better planning of resource allocation to different bridge operations. However, before this implementation item can be realized, significant additional research would be needed to first ensure that the durability models can be effectively calibrated with real data from inspection reports and that other factors affecting deterioration (such as design or construction issues that may cause premature deterioration) are properly accounted for in the durability model.

REFERENCES

- AASHTO (2012). *LRFD bridge design specifications* (6th ed.). Washington, DC: American Association of State Highway and Transportation Officials.
- ABAQUS. (2011). ABAQUS/standard version 6.11 user's manuals. Providence, RI: DS SIMULIA Corp. Retrieved from <http://www.3ds.com/products-services/simulia/portfolio/abaqus/overview/>
- Ahmad, S. (2003). Reinforcement corrosion in concrete structures, its monitoring and service life prediction—A review. *Cem. Concr. Compos.*, 25(4), 459–471.
- Ahmed, A., Agbelie, B. R. D. K., Lavrenz, S., Keefer, M., Labi, S., & Sinha, K. C. (2013). *Costs and revenues associated with overweight trucks in Indiana* (Joint Transportation Research Program Publication No. FHWA/IN/JTRP-2013/01). West Lafayette, IN: Purdue University. <http://dx.doi.org/10.5703/1288284314987>
- Albrecht, P., & Naeemi, A. H. (1984). *Performance of weathering steel in bridges* (National Cooperative Highway Research Program (NCHRP) Report 272). Washington, DC: Transportation Research Board. Retrieved from http://onlinepubs.trb.org/Onlinepubs/nchrp/nchrp_rpt_272.pdf
- Bazant, Z. P. (1979). Physical model for steel corrosion in concrete sea structures—theory. *Journal of the Structural Division*, 105(6), 1137–1153.
- Beddoe, R. E., Schmidt, K., Alexander, M. G., & Bertron, A. (2009). Effect of concrete composition on resistance of concrete to acid attack. In *Concrete aggressive aqueous environments, Vol. I: Performance, testing and modeling* (RILEM proceedings 63), pp. 187–195.
- Bolluyt, J. E., Kau, V. B., & Greimann, L. F. (2001). *Performance of strip seals in Iowa bridges: Pilot study* (Iowa Highway Research Board Project TR-437). Ames, IA: Iowa State University.
- Boufiza, M., Sakai, K., Banthia, N., & Yoshida, H. (2003). Prediction of chloride ions ingress in uncracked and cracked concrete. *ACI Materials Journal*, 100(1), 38–48.
- Canna, T. L., & Bowman, M. D. (2002). *Fatigue behavior of beam diaphragm connections with intermittent fillet welds, Part I, Vol. 1, Field evaluation* (Joint Transportation Research Program Publication No. FHWA/IN/JTRP-2001/10-I-1). West Lafayette, IN: Purdue University, <http://dx.doi.org/10.5703/1288284313222>
- Chang, L., & Lee, Y. (2001). *Evaluation and policy for bridge deck expansion joints* (Joint Transportation Research Program Publication No. FHWA/IN/JTRP-2000/1). West Lafayette, IN: Purdue University. <http://dx.doi.org/10.5703/1288284313206>
- Clauwaert, C. (1986). A study of expansion joints and buried joints for bridges in Belgium. In *Proceedings of the Second World Congress on Joint Sealing and Bearing Systems for Concrete Structures* (pp. 613–642; ACI Publication SP-94). Farmington Hills, MI: American Concrete Institute.
- Crank, J. (1979). *The mathematics of diffusion*. Oxford, UK: Oxford University Press.
- Cusson, D., Lounis, Z., & Daigle, L. (2011). Durability monitoring for improved service life predictions of concrete bridge decks in corrosive environments. *Computer-Aided Civil and Infrastructure Engineering*, 26(7), 524–541.
- De Schutter, G. (1999). Quantification of the influence of cracks in concrete structures on carbonation and chloride penetration. *Magazine of Concrete Research*, 51(6), 427–435.
- Downing, S. D., & Socie, D. F. (1982). Simple rainflow counting algorithms. *International Journal of Fatigue*, 4(1), 31–40.
- Fehlmann, P., & Vogel, T. (2009). Experimental investigations on the fatigue behavior of concrete bridges. In *IABSE Symposium Report*, 96(5), 45–54.
- Fisher, J. W., Kulak, G. L., & Smith, I. F. C. (1998). *A fatigue primer for structural engineers*. Chicago, IL: American Institute of Steel Construction.
- Florida DOT. (2011). *Bridge maintenance & repair handbook*. Retrieved from http://www.dot.state.fl.us/statmaintenance/office/STR/IN/Maintenance_and_Repair_Handbook_08-13-11.pdf
- Francois, R., & Arliguie, G. (1999). Effect of microcracking and cracking on the development of corrosion in reinforced concrete members. *Magazine of Concrete Research*, 51(2), 143–150.
- Gérard, B., & Marchand, J. (2000). Influence of cracking on the diffusion properties of cement-based materials: Part I: Influence of continuous cracks on the steady-state regime. *Cement and Concrete Research*, 30(1), 37–43.
- Guo, T., Frangopol, D. M., & Chen, Y. (2012). Fatigue reliability assessment of steel bridge details integrating weigh-in-motion data and probabilistic finite element analysis. *Computers & Structures*, 245–257.
- Green, J. G., Nichols, A. P., Allen Ed., Nuber, L., Thomaz, J. E., & Bullock, D. (2002). Virtual weigh station (Joint Transportation Research Program Publication No. FHWA/IN/JTRP-2001/09). West Lafayette, IN: Purdue University. <http://dx.doi.org/10.5703/1288284313348>
- Gylltoft, K. (1983). *Fracture mechanics models for fatigue in concrete structures* (Doctoral thesis). Lulea University of Technology, Lulea, Sweden.
- Hjelmstad, K. D., Lange, D. A., Parsons, I. D., & Lawrence, F. V. (1998). Framework for modeling durability cost of structural systems. *J. Infrastruct. Syst.*, 4(3), 126–133.
- Hu, N., Haider, S. W., & Burgueno, R. (2013). *Development and validation of deterioration models for concrete bridge decks, Phase 2: Mechanics-based degradation models* (Final Report, No. RC-1587b). East Lansing, MI: Michigan Department of Transportation and Michigan State University.
- INDOT. (2010) *Indiana bridge inspection manual*. Retrieved from http://www.in.gov/dot/div/contracts/standards/bridge/inspector_manual/INDIANA%20BRIDGE%20INSPECTION%20MANUAL.pdf

- Johansson, U. (2004). *Fatigue tests and analysis of reinforced concrete bridge deck models* (Licentiate thesis). Institutionen för byggetenskap, Kungl, Tekniska högskolan, Stockholm.
- Kachanov, L. (1958). Time of the rupture process under creep conditions. *Isv. Akad. Nauk*, 8, 26–31.
- Kachanov, L. M. (1986). Introduction to continuum damage mechanics [SpringerLink edition]. Retrieved from <http://link.springer.com/book/10.1007%2F978-94-017-1957-5>
- Kayser, J. R., & Nowak, A. S. (1989). Reliability of corroded steel girder bridges. *Structural Safety*, 6(1989), 53–63.
- Komp, M. E. (1987). Atmospheric corrosion ratings of weathering steels—Calculations and significance. *Mater. Perform.*, 26(7), 42–44.
- Krykowsky, T., & Zybura, A. (2009). Fem modeling of concrete cover degradation caused by rebars corrosion in reinforced concrete. *Archit. Civ. Eng. Environ. J.*, 2(4), 71–80.
- Marchand, J., Pigeon, M., & Setzer, M. J. (eds.). (1996). *Freeze-thaw durability of concrete* (RILEM Proceedings 30). New York, NY: E & FN Spon.
- McIlrath, D. S., Frank, K. H., Wood, S. L., & Yura, J. A. (2000). *Improving bridge rating and truck permitting procedures through finite element analysis* (Research Report 1746-2). Austin, TX: Texas Department of Transportation.
- Menéndez, E., Matschei, T., & Glasser, F. P. (2013). Sulfate attack of concrete. In *Performance of cement-based materials in aggressive aqueous environments* (pp. 7–74) [SpringerLink edition]. Retrieved from <http://link.springer.com/book/10.1007%2F978-94-007-5413-3>
- Miner, M. A. (1945). Cumulative damage in fatigue. *Transactions of the American Society of Mechanical Engineers*, 67, A159–164.
- Morinaga, S. (1990). Prediction of service lives of reinforced concrete buildings based on the corrosion rate of reinforcing steel. In *Proceedings of the fifth international conference on durability of building materials and components* (pp. 5–13).
- National Bridge Inventory Database. (2011). [Database search] <http://nationalbridges.com/>
- Olsson, K., & Pettersson, J. (2010). *Fatigue assessment methods for reinforced concrete bridges in eurocode: Comparative study of design methods for railway bridges*. Retrieved from <http://publications.lib.chalmers.se/records/fulltext/132147.pdf>
- Pascual, F. G., & Meeker, W. Q. (1999). Estimating fatigue curves with the random fatigue-limit model. *Technometrics*, 41(4), 277–302.
- Purvis, R. (2003). *Bridge deck joint performance: A synthesis of highway practice* (NCHRP Synthesis 319). Washington, DC: Transportation Research Board.
- Rodriguez, O. G., & Hooton, R. D. (2003). Influence of cracks on chloride ingress into concrete. *ACI Materials Journal*, 100(2), 120–126.
- Saydam, D., & Frangopol, D. M. (2011). Time-dependent performance indicators of damaged bridge superstructures. *Engineering Structures*, 33(9), 2458–2471. <http://dx.doi.org/10.1016/j.engstruct.2011.04.019>
- Shi, X., Xie, N., Fortune, K., & Gong, J. (2012). Durability of steel reinforced concrete in chloride environments: An overview. *Constr. Build. Mater.*, 30, 125–138.
- Sinha, K. C., Labi, S., McCullouch, B., Bhargava, A., & Bai, Q. (2009). *Updating and enhancing the Indiana bridge management system (IBMS)* (Joint Transportation Research Program Publication No. FHWA/IN/JTRP-2008/30). West Lafayette, IN: Purdue University. <http://dx.doi.org/10.5703/1288284314306>
- Sinha, K. C., Zang, Y., Kepaptsoglou, K., & Woods, R. E. (2000). *An operational manual for the Indiana bridge management system*. West Lafayette, IN: Purdue University.
- Stark, J. (2011). Recent advances in the field of cement hydration and microstructure analysis. *Cem. Concr. Res.*, 41(7), 666–678.
- Transportation Research Board. (1990). *Truck weight limits: Issues and options* (Committee for the Truck Weight Study, Special Report 225), Washington, DC: Transportation Research Board.
- Van de Lindt, J. W., & Ahlborn, T. M. (2005). *Development of steel beam end deterioration guidelines* (Research Report RC-1454). Lansing, MI: Michigan Department of Transportation. Retrieved from https://www.michigan.gov/documents/mdot-RC-1454_116318_7.pdf
- Wardhana, K., & Hadipriono, F. C. (2003). Analysis of recent bridge failures in the United States. *Journal of Performance of Constructed Facilities*, 17:3(144), 144–150.
- Wood, S., Akinci, N., Liu, J., & Bowman, M. D. (2007). *Long-term effects of super heavy-weight vehicles on bridges* (Joint Transportation Research Program Publication No. FHWA/IN/JTRP-2007/10). West Lafayette, IN: Purdue University. <http://dx.doi.org/10.5703/1288284313355>
- Yanev, B. (1997). Life-cycle performance of bridge components in New York City. In *Recent advances in bridge engineering* (pp. 385–392). Dubendorf, Switzerland: EMPA.
- Yang, Z., Weiss, W. J., & Olek, J. (2004). *Interaction between micro-cracking, cracking, and reduced durability of concrete: Developing methods for considering cumulative damage in life-cycle modeling* (Joint Transportation Research Program Publication No. FHWA/IN/JTRP-2004/10). West Lafayette, IN: Purdue University. <http://dx.doi.org/10.5703/1288284313255>

APPENDICES

APPENDIX A: STATISTICAL SAMPLING OF REPRESENTATIVE BRIDGES

TABLE A.1
Bridges based on different materials and length.

	Structure No.	Material	Length	Type
1	5000104	Pre-stressed concrete	15.2	Box Beam or Girders – Multiple
2	0001530	Pre-stressed concrete	23.8	Box Beam or Girders – Multiple
3	6300118	Pre-stressed concrete	16.2	Box Beam or Girders – Single
4	8300079	Reinforced concrete	17.5	Arch – Deck
5	7000128	Reinforced concrete	18.6	Arch – Deck
6	8800039	Reinforced concrete	19.5	Arch – Deck
7	8200007	Steel	92.7	Truss – Deck
8	1500079	Steel	91.1	Through Truss
9	5300061	Steel	21.9	Through Truss
10	6500163	Steel	18.3	Through Truss

TABLE A.2
Bridges on routes with high AADT.

	Structure No.	Route	County	Length (m)	AADT
1	049650	I-65	Clark	66.4	42578
2	034616	I-65	Clark	211.5	44150
3	050280	I-69	Marion	61.5	50280
4	050240	I-69	Marion	62.9	57725
5	042750	I-70	Marion	33.4	31813
6	042810	I-70		54	31486
7	044500	I-74	Marion	79.6	28605
8	044520	I-74	Marion	66.4	28605

TABLE A.3
Bridges on highways in the corridor with WIM stations.

	Highway	WIM Site	City	NBI No.	Distance from WIM Site	Type	Length (ft)	Breadth (ft)
1	I-65	1100	Lafayette	037720	0.2 mile	Steel, Girder	1286	38
2	I-65	1100	Lafayette	037640	2.4 mile	Steel, Girder	394	38
3	I-65	4100	Rensselaer	038120	4.0 mile	Concrete, Slab	72	21.9
4	I-65	4200	Merrillville	038590	1.1 mile	Steel, Girder	153	61
5	I-65	5500	Clarksville	034720	1.4 mile	P-S* Concrete, Tee Beam	303	83
6	I-65	5500	Clarksville	034700	0.9 mile	P-S* Concrete, Tee Beam	124	82
7	I-80/90	7300	Chesterton	047020	0.3 mile	Steel(S**), Girder	136	42
8	I-80/90	7340	South Bend	047670	1.6 mile	Steel(S**), Girder	215	42
9	I-80/90	7340	South Bend	047690	1.8 mile	Steel, Girder	492	42
10	I-64	5400	New Albany	034360	0.6 mile	Concrete, Slab	120	42
11	I-64	6200	Dale	033800	0.4 mile	Concrete, Slab	80	40
12	I-70	3600	Greenfield	042910	1.1 mile	Concrete, Slab	79	38
13	I-70	3700	Richmond	043670	0.9 mile	Steel(S**), Girder	141	39
14	I-70	3700	Richmond	043750	0.5 mile	Steel, Girder	266	39

*P-S: Pre-stressed concrete.

**S: Single-span bridge.

TABLE A.4
Bridges in the extra heavy duty highway corridor.

	Place	Structure Name	Length (m)	Type
1	Michigan City	076834	27.6	Concrete, Slab
2	Michigan City	028800	53	Steel, Frame
3	Michigan City	076836	27.6	Concrete, Slab

TABLE A.5
Structurally deficient bridges.

	Region	Structure No.	Length (m)	Type
1	NW Indiana	6400134	62.6	Pre-stressed Concrete
2	East Indiana	8900226	26.1	Reinforced Concrete
3	West Indiana	0400073	26	Steel
4	NW Indiana	4500132	60.3	Steel
5	Central Indiana	0300133	71	Steel

TABLE A.6
Bridges-based sufficiency rating.

	Sufficiency Rating	NBI No.	Material	Length (m)	Design
1	80.8	049190	Steel continuous	79.9	Stringer/Multi-beam or Girder
2	70.3	041060	Steel continuous	56.1	Stringer/Multi-beam or Girder
3	60.7	013460	Concrete continuous	21.9	Slab
4	50.6	015380	Pre-stressed concrete	40.2	Slab
5	41.2	050950	Concrete	67.9	Stringer/Multi-beam or Girder

TABLE A.7
Bridges on Interstate routes.

	Route	NBI No.	Material	Length (m)	Design
1	I-64	034440	Pre-stressed concrete	65.5	Stringer/Multi-beam or Girder
2	I-80	076760	Pre-stressed concrete	34.1	Tee Beam
3	I-90	046050	Steel	46.9	Stringer/Multi-beam or Girder
4	I-94	049280	Pre-stressed concrete	34.7	Stringer/Multi-beam or Girder
5	I-164	070270	Steel	92.4	Stringer/Multi-beam or Girder
6	I-265	070580	Pre-stressed concrete	56.4	Stringer/Multi-beam or Girder
7	I-275	049675	Steel continuous	66.4	Stringer/Multi-beam or Girder
8	I-465	050770	Steel continuous	85.7	Stringer/Multi-beam or Girder
9	I-469	076400	Pre-stressed concrete	79.2	Tee Beam
10	I-865	051310	Steel continuous	91.5	Stringer/Multi-beam or Girder

TABLE A.8
Bridges on state routes.

	Route	NBI No.	Material	Length (m)	Design
1	SR 5	001600	Steel continuous	17.7	Girder and Floorbeam System
2	SR 38	012880	Pre-stressed concrete	15.7	Box Beam or Girders – Single or Spread
3	SR 75	024835	Pre-stressed concrete	40.8	Stringer/Multi-beam or Girder
4	SR 236	029880	Concrete continuous	31.7	Slab
5	SR 827	048840	Steel continuous	43.0	Stringer/Multi-beam or Girder

TABLE A.9
Bridges on US routes.

	Route	NBI No.	Material	Length (m)	Design
1	US 6	001770	Pre-stressed concrete	11.6	Stringer/Multi-beam or Girder
2	US 12	003220	Pre-stressed concrete	13.1	Box Beam or Girders – Multi
3	US 20	075101	Pre-stressed concrete	73.8	Stringer/Multi-beam or Girder
4	US 24	011265	Steel continuous	55.8	Stringer/Multi-beam or Girder
5	US 27	007370	Pre-stressed concrete	49.1	Box Beam or Girders – Single or Spread
6	US 30	008310	Pre-stressed concrete	50.3	Stringer/Multi-beam or Girder
7	US 31	009970	Pre-stressed concrete	88.1	Stringer/Multi-beam or Girder
8	US 33	010970	Concrete continuous	61.3	Slab
9	US 35	001070	Steel continuous	48.6	Stringer/Multi-beam or Girder
10	US 36	011654	Pre-stressed concrete	51.2	Stringer/Multi-beam or Girder
11	US 40	013560	Concrete continuous	40.5	Slab
12	US 41	015580	Steel continuous	79.2	Stringer/Multi-beam or Girder
13	US 50	018570	Pre-stressed concrete	209.4	Tee Beam
14	US 52	019270	Concrete continuous	57.2	Slab
15	US 136	026900	Pre-stressed concrete	39.6	Stringer/Multi-beam or Girder
16	US 150	027600	Concrete continuous	36.3	Slab
17	US 224	029130	Pre-stressed concrete	72.2	Box Beam or Girders – Multi
18	US 231	076676	Pre-stressed concrete	79.9	Tee Beam
19	US 421	032160	Pre-stressed concrete	64.6	Box Beam or Girders – Single or Spread

APPENDIX B: ABAQUS SUBROUTINE FOR DURABILITY MODEL

Two types of subroutine code in ABAQUS 6.12 were used:

(i) DLOAD to simulate moving loads along with longitudinal direction, and

(ii) USDFLD to simulate reduced elastic modulus in every computational increment year (Δt) depending increasing damage.

Subroutine code based on FORTRAN program for ABAQUS modeling is following.

```
C*****C
C      This code was provided for simple bridge modeling
C      DLOAD: user defined load subroutine
C      1st Edition by Gnana Teja Pudipeddi on 2013.03.20
C      2nd Edition by Hun Cha on 4.06, 2013

SUBROUTINE
DLOAD(F,KSTEP,KINC,TIME,NOEL,NPT,LAYER,KSPT,COORDS,DLTYP,SNAME)

INCLUDE 'ABA_PARAM.INC'
      DIMENSION TIME(2), COORDS (3)
      CHARACTER*80 SNAME
      REAL(8):: TravelTime, VehicleLength,Length1,F, WLD1F, WLD1M1
      REAL(8):: FI1F, ST1F,ST1M1,ST1M2,FIM1,FI1M2, WLD1M2
C      ROAD LENGTH (unit: inch)
      RDL=480.
C      TIRE LENGTH (unit: inch)
      TYL=10.
C      TRAVEL TIME (STEP TIME):
      TravelTime=1.0D0

C      Apply load configuration
      IF(MOD(KSTEP,3).EQ.2)THEN
C      20k -----> 10k+10k
C      (10 k / (2tires x tire area)
      WLD1F=0.108
      WLD1M1=0.108
      WLSP1=72.0D0

      ELSEIF(MOD(KSTEP,3).EQ.0)THEN
C      50k = 10k + 20k + 20k
      WLD1F=0.083
      WLD1M1=0.167
      WLD1M2=0.167

      WLSP1=72
      WLSP2=120

      ELSEIF(MOD(KSTEP,3).EQ.1)THEN
```

```

C-----GROUP D (125 kips) -----> 2 rows x 62.5k = 12.5k + 25k+ 25k
      WLD1F=0.104
      WLD1M1=0.208
      WLD1M2=0.208

      WLS1=72
      WLS2=120
      ENDIF

C   VEHICLE LENGTH
      Length1=WLS1+WLS2
      VehicleLength=Length1+TYL

C   WHEEL POSITIONS
      IF(TIME(1).LE.TravelTime)THEN
      F1IF=0.+(TIME(1)/TravelTime)*(RDL+VehicleLength)
      ST1F=(TIME(1)/TravelTime)*(RDL+VehicleLength)-TYL
      ST1M1=ST1F-WLS1
      F1M1=F1IF-WLS1
      ST1M2=ST1M1-WLS2
      F1M2=F1M1-WLS2

      ENDIF

      F=0.

C   VEHICLE 1 FRONT WHEEL load
      IF(COORDS(3).GE.ST1F.AND.COORDS(3).LE.F1IF) THEN
C
C   FOR UNIFORM LOADING over the loaded region
      F=WLD1F
C   VEHICLE 1 MIDDLE WHEEL 1 load
      ELSEIF(COORDS(3).GE.ST1M1.AND.COORDS(3).LE.F1M1)THEN
      F=WLD1M1
C   VEHICLE 1 MIDDLE WHEEL 2 load
      ELSEIF(COORDS(3).GE.ST1M2.AND.COORDS(3).LE.F1M2)THEN
      F=WLD1M2
      ENDIF
C
      RETURN
      END

```

```

C*****C
C-- USDFLD: user defined field subroutine
C-- 1st Edition by Gnana Teja Pudipeddi on 2013.03.20
C-- 2nd Edition by Hun Cha on 2013.04.20

```

C-- 3rd Edition by Boyuan Liu on 2013.10.26
 C-- 4th Edition by Boyuan Liu on 2013.11.05
 C-- 5th Edition by Hun Cha on 2014.01.03

C*****Updating Info*****C

C In the 3rd edition, the rain-flow cycle counting method has been changed
 C in to the ASTM standrad rainflow cycle counting method.
 C This algorithm could be found in the following website
 C http://enterprise.astm.org/filtrexx40.cgi?+REDLINE_PAGES/E1049.htm

C***** (Parameters Lists) *****C

C STATEV(1,2,3,4) Using for calculate the damage
 C STATEV(5) Cycle Damage
 C STATEV(6) Time(1).
 C STATEV(7) Not-assigned
 C STATEV(9) Elastic Modulus

C*****

```

SUBROUTINE USDFLD(FIELD,STATEV,PNEWDT,DIRECT,T,CELENT,
1 TIME,DTIME,CMNAME,ORNAME,NFIELD,NSTATV,NOEL,NPT,LAYER,
2 KSPT,KSTEP,KINC,NDI,NSHR,COORD,JMAC,JMATYP,MATLAYO,
3 LACCFLA)

```

C

```

INCLUDE 'ABA_PARAM.INC'

```

C

```

CHARACTER*80 CMNAME,ORNAME
CHARACTER*3 FLGRAY(15)
DIMENSION FIELD(NFIELD),STATEV(NSTATV),DIRECT(3,3)

```

C

```

Time(2) is total time
DIMENSION T(3,3),TIME(2), ARRAY(15),JARRAY(15)
DIMENSION COORD(*)
DIMENSION JMAC(*)
DIMENSION JMATYP(*)

```

C

All parameters assigned below could not be used for this simple bridge model because this subroutine code was shared with 3D full scale bridge.

C

```

Using for material Properties
REAL(KIND=16):: SigmaCr, SigmaComp, Stress, Envd,Cmod0, Ccon0
REAL(KIND=16):: SigmaCon, SigmaCont

```

C

```

Using for S-N
REAL(KIND=16):: ampl, CNum, mid, NS(400), AADTT(5)
REAL(KIND=16):: A1, A2, A3, A4, StrInc, Power, Ntemp,SN
INTEGER:: ii,jj,kk,xx, MAX100, MIN100

```

C

```

Using for Time
REAL(KIND=16):: SubNum,ADF,ADF1,sumaadT,TravelTime, StepCheck
INTEGER:: Sumflag, StartStep,dt,Numloadclass
INTEGER:: NumDeck, NumBeam,TRSTEP1,TRSTEP2,NumElement1,NumElement2

```

```

C      For user
      Real(16):: Alpha,StrRatio1,Envcoeff,totald,MAX1,CumulD2,CumulD3
C      For Repair
      INTEGER:: RDcount1,RDcount2
      Real(16):: SumDamage1, SumDamage2, Refreshflag1, Refreshflag2,stepflag
      Real(16):: RD1,RD2,FID,ND,TR1,TR2,Svar8,alphaN,alpha2,alpha3

      Common /coeff/ Sumdamage1, Sumdamage2, Refreshflag1,Refreshflag2
      Common /coeff/ TR1,TR2,TRSTEP1,TRSTEP2,stepflag1,stepflag2

C-----Initalization-----
      TravelTime = 2.0D0
      Numloadclass = 3
C---life cycle, year
      dt=5.0D0
      Envcoeff=0.0000405
C---Concrete durability model coefficients
      alphaN = 0.3
      alpha2 = 0.5
      alpha3 = 0.2

C---Number of elements for deck (NumDeck), corroded steel girder (NumBeam)
C---Find number in inp
      NumDeck = 240.0D0
      NumBeam = 740.0D0

      SubNum = 200.0D0

C      E of steel (ksi)
      Cmod0 = 2.9D4
C      E of concrete (ksi)
      Ccon0 = 3605.0D0

C      SigmaCr,Comp = steel yield strength (ksi)
      SigmaCr = 36.0D0
      SigmaComp = 36.0D0
      SigmaCon = 4.0D0
C      7.5*sqrt(4000)/1000 (ksi)
      SigmaCont = 0.5D0
C** On the step beginning computing fatigue
      StartStep = 1.0D0
      Sumflag = 0.0D0
      ampl = 0.0D0
      CNum = 0.0D0
      mid = 0.0D0

```

```

C---Parameters
C---RepairDamage(RD), Future Increase Damage(FID), NewDamage(ND)
  RD1=0.5D0
  RD2=0.5D0
  FID=0.1D0
  ND=0.1D0
  stepflag1 = 0
  stepflag2 = 0
  STATEV(6) = TIME(1)
C apply modulus
  IF(KSTEP.LE.1)THEN
  MAX100 = -100.0D0
  MIN100 = 100.0D0
  TR1=0
  TR2=0
  TRSTEP1 = 0
  TRSTEP2 = 0
  SumDamage1 = 0
  SumDamage2 = 0

  IF(CMNAME(1:8).EQ.'CONCRETE')THEN
  STATEV(9) = Ccon0
  FIELD(1)= STATEV(9)
  ELSE
  STATEV(9) = Cmod0
  FIELD(1)= STATEV(9)
  ENDIF

  ELSE
  FIELD(1)= STATEV(9)
  ENDIF

C   AADT based on INDOT traffic zone (2012) of NBI-19027 Bridge
  AADTT(1) = 3500.0D0
  AADTT(2) = 1200.0D0
  AADTT(3) = 100.0D0

  IF(MOD(KSTEP,3).EQ.2)THEN
  ADF1=AADTT(1)*365
  ELSEIF(MOD(KSTEP,3).EQ.0)THEN
  ADF1 = AADTT(2)*365
  ELSEIF(MOD(KSTEP,3).EQ.1)THEN
  ADF1=AADTT(3)*365
  ENDIF
C   START Damage Model
  IF(KSTEP.GT.1)THEN

```



```

IF(KSTEP.EQ.TRSTEP1)THEN
  IF(CMNAME(1:8).EQ.'DMSTCORR')THEN
    SumDamage1 = RD1*ND
    STATEV(5) = RD1*ND
    STATEV(9) = Cmod0*(1-SumDamage1)
    FIELD(1)= STATEV(9)
    RDcount1 = RDcount1 + 1.0D0
    RD1=RD1+FID*RDcount1
    Refreshflag1 = 0
  ELSEIF(CMNAME(1:8).EQ.'DMGSTEEL')THEN
    SumDamage1 = RD1*ND
    STATEV(5) = RD1*ND
    STATEV(9) = Cmod0
    FIELD(1)= STATEV(9)
    RDcount1 = RDcount1 + 1.0D0
    RD1=RD1+FID*RDcount1
    Refreshflag1 = 0
  ENDIF
ENDIF
IF(KSTEP.EQ.TRSTEP2)THEN
  IF(CMNAME(1:8).EQ.'CONCRETE')THEN
    SumDamage2 = ND*(RD2)
    totald = ND*(RD2)
    STATEV(9) = Ccon0*(1-SumDamage2)
    FIELD(1)= STATEV(9)
    RDcount2 = RDcount2 + 1.0D0
    RD2=RD2+FID*RDcount2*0.5
    TR2 = TIME(2)
    Refreshflag2 = 0
    stepflag2 = 1
  ENDIF
ENDIF
FIELD(1)= STATEV(9)

C-----1% inflation of AADT per year
ADF=ADF1*(1+(TIME(2)-1)/(TravelTime*Numloadclass)*dt*0.01)

C-----DURABILITY MODEL for STEEL
IF(CMNAME(1:8).EQ.'DMGSTEEL')THEN
C   Sub routine begin
C   Get Stress
CALL GETVRM('S',ARRAY,JARRAY,FLGRAY,JRCD,JMAC,JMATYP,MATLAYO
1 ,LACCFLA)
S11 = ARRAY(1)
S22 = ARRAY(2)
S33 = ARRAY(3)

```

```
S12 = ARRAY(4)
S13 = ARRAY(5)
S23 = ARRAY(6)
```

```
IF(ABS(STATEV(6)-TravelTime/SubNum).LE.1e-6)THEN
STATEV(1) = 200.
STATEV(2) = 200.
STATEV(3) = 200.
STATEV(5) = 0.
STATEV(7) = 0.
ENDIF
```

```
IF(ABS(S11).GT.ABS(S22))THEN
STATEV(4)=S11
ELSEIF(ABS(S22).GE.ABS(S11))THEN
STATEV(4)=S22
ENDIF
```

```
C see the maximum minimum stress
IF(STATEV(4).GT.MAX100)THEN
MAX100 = STATEV(4)
ENDIF
IF(STATEV(4).LT.MIN100)THEN
MIN100 = STATEV(4)
ENDIF
```

C calculation begin in one step.

```
A1 = STATEV(1)
A2 = STATEV(2)
A3 = STATEV(3)
A4 = STATEV(4)
```

```
IF(KSTEP.LT.StartStep)THEN
Sumflag = 0
ELSEIF(ABS(A3-200.).LE.1e-6)THEN
Sumflag = 0
ELSEIF(ABS(A2-200.).LE.1e-6)THEN
Sumflag = 0
ELSEIF(ABS(A1-200.).LE.1e-6)THEN
Sumflag = 0
ELSE
Sumflag = 1
ENDIF
IF(Sumflag)THEN
IF(ABS(A3-300.).LE.1e-6)THEN
STATEV(3) = STATEV(4)
```

```

ELSEIF(((A2.GT.A3).AND.(A4.GT.A2).AND.(A3.GT.A1)).OR.((A2.LT.A3).AND.(A4.LT.A2).
AND.(A3.LT.A1)))THEN
    ampl = 0.5*ABS(A2-A3)
    CNum = CNum + 1.
    mid = 0.5*(A2+A3)
    STATEV(2) = STATEV(4)
    STATEV(3) = 300.
C    STATEV(4) = 300.

ELSE
    ampl = 0.5*ABS(A1-A2)
    CNum = CNum + 0.5
    mid = 0.5*(A1+A2)
    STATEV(1) = STATEV(2)
    STATEV(2) = STATEV(3)
    STATEV(3) = STATEV(4)
ENDIF

ELSEIF(KSTEP.GE.StartStep)THEN
    STATEV(1) = STATEV(2)
    STATEV(2) = STATEV(3)
    STATEV(3) = STATEV(4)
ENDIF

C    S-N Curve based on AISC code
    IF(ABS(STATEV(4)).LT.5)THEN
        Power = 9.4*ABS(exp(abs(STATEV(4))*(-0.052)))
    ELSEIF(ABS(STATEV(4)).GE.5.AND.ABS(STATEV(4)).LT.36.)THEN
        Power = 7.7346*abs(exp(abs(STATEV(4))*(-0.013)))
    ENDIF
    NTemp = INT(10**(Power))

C Env. damage
    EnvD = 0.
C    'StrRatio1' DEFINITION
    StrRatio1 = ABS(STATEV(4)/SigmaCr)
    Alpha = MAX(0.001,MIN(StrRatio1,1.0D0))
C    DEFINING ALPHA
C    cycle damage parameter
    STATEV(5) = STATEV(5) + (1+Alpha)*CNum*ADF*dt/NTemp + EnvD
C    total damage
    totald = STATEV(5)
C    number of 3 means to controll if damage reaches "1", STATEV(7) needs to vary between
    "1" and "2".
    STATEV(7) = ABS(1-exp(-3.0D0*totald*totald))

```

```

C      Update modulus
      STATEV(9) = Cmod0*(1-abs(STATEV(7)))

C      Durability model for corroded steel
      ELSEIF(CMNAME(1:8).EQ.'DMSTCORR')THEN
C      Sub routine begin
C      Get Stress
      CALL GETVRM('S',ARRAY,JARRAY,FLGRAY,JRCD,JMAC,JMATYP,MATLAYO
1 ,LACCFLA)
      S11 = ARRAY(1)
      S22 = ARRAY(2)
      S33 = ARRAY(3)
      S12 = ARRAY(4)
      S13 = ARRAY(5)
      S23 = ARRAY(6)

      IF(ABS(STATEV(6)-TravelTime/SubNum).LE.1e-6)THEN
      STATEV(1) = 200.
      STATEV(2) = 200.
      STATEV(3) = 200.
      STATEV(5) = 0.
      STATEV(7) = 0.
      ENDIF

      IF(ABS(S11).GT.ABS(S22))THEN
      STATEV(4)=S11
      ELSEIF(ABS(S22).GE.ABS(S11))THEN
      STATEV(4)=S22
      ENDIF

C      see the maximum minimum stress
      IF(STATEV(4).GT.MAX100)THEN
      MAX100 = STATEV(4)
      ENDIF
      IF(STATEV(4).LT.MIN100)THEN
      MIN100 = STATEV(4)
      ENDIF

C      calculation begin in one step.
      A1 = STATEV(1)
      A2 = STATEV(2)
      A3 = STATEV(3)
      A4 = STATEV(4)
      IF(KSTEP.LT.StartStep)THEN
      Sumflag = 0

```

```

ELSEIF(ABS(A3-200.).LE.1e-6)THEN
Sumflag = 0
ELSEIF(ABS(A2-200.).LE.1e-6)THEN
Sumflag = 0
ELSEIF(ABS(A1-200.).LE.1e-6)THEN
Sumflag = 0.0D0
ELSE
Sumflag = 1.0D0
ENDIF
IF(Sumflag)THEN
IF(ABS(A3-300.).LE.1e-6)THEN
STATEV(3) = STATEV(4)
ELSEIF(((A2.GT.A3).AND.(A4.GT.A2).AND.(A3.GT.A1)).OR.((A2.LT.A3).AND.(A4.
LT.A2).AND.(A3.LT.A1)))THEN
ampl = 0.5*ABS(A2-A3)
CNum = CNum + 1.
mid = 0.5*(A2+A3)
STATEV(2) = STATEV(4)
STATEV(3) = 300.

ELSE
ampl = 0.5*ABS(A1-A2)
CNum = CNum + 0.5
mid = 0.5*(A1+A2)
STATEV(1) = STATEV(2)
STATEV(2) = STATEV(3)
STATEV(3) = STATEV(4)
ENDIF

ELSEIF(KSTEP.GE.StartStep)THEN
STATEV(1) = STATEV(2)
STATEV(2) = STATEV(3)
STATEV(3) = STATEV(4)
ENDIF

C S-N Curve based on AISC code
IF(ABS(STATEV(4)).LT.5.0D0)THEN
Power = 9.4*ABS(exp(abs(STATEV(4))*(-0.052)))
ELSEIF(ABS(STATEV(4)).GE.5.0D0.AND.ABS(STATEV(4)).LT.36.0D0)THEN
Power = 7.7346*abs(exp(abs(STATEV(4))*(-0.013)))
ENDIF

NTemp = INT(10**(Power))

C Environmental damage (Envd) due to steel corrosion
StepCheck=(TIME(2)-1)/(TravelTime*Numloadclass)*dt

```

```

IF(TR1.GT.0)THEN
StepCheck=(TIME(2)-TR1)/(TravelTime*Numloadclass)*dt
ENDIF

Envd = ABS(0.0066*StepCheck**0.591)

C   DEFINING ALPHA
C   'StrRatio1' DEFINITION
StrRatio1 = ABS(STATEV(4)/SigmaCr)
Alpha = MAX(0.0001,MIN(StrRatio1,1.0))

C   Cycle damage parameter
STATEV(5) = ABS(STATEV(5)) + ABS((1+Alpha)*CNum*ADF*dt/NTemp)
C   Total damage
totald = (STATEV(5)*(alpha2+alpha3)+ Env d*alphaN)
STATEV(7) = ABS(1-exp(-3.0D0*totald*totald))

C   Repair
IF(SumDamage1.GE.RD1)THEN
Refreshflag1 = 1.0D0
TR1 = TIME(2)
TRSTEP1 = KSTEP
ELSEIF(NOEL.LE.740.AND.NOEL.GE.1)THEN
Count1=Count1 + 1
SumDamage1 = SumDamage1+STATEV(7)/(4)
ENDIF
STATEV(9) = Cmod0*(1-abs(STATEV(7)))

C   Durability model for Deck
ELSEIF(CMNAME(1:8).EQ.'CONCRETE')THEN

C   Sub routine begin
C   Get Stress
CALL GETVRM('S',ARRAY,JARRAY,FLGRAY,JRCD,JMAC,JMATYP,
MATLAYO,LACCFLA)
S11 = ARRAY(1)
S22 = ARRAY(2)
S33 = ARRAY(3)
S12 = ARRAY(4)
S13 = ARRAY(5)
S23 = ARRAY(6)

IF(ABS(STATEV(9)-TravelTime/SubNum).LE.1e-6)THEN
STATEV(1) = 200.
STATEV(2) = 200.
STATEV(3) = 200.

```

```
STATEV(7) = 0.  
STATEV(6) = 0.  
STATEV(5) = 0.
```

```
ENDIF
```

```
MAX1 = MAX(ABS(S22),ABS(S33),ABS(S12),ABS(S13),ABS(S23))
```

```
IF(MAX1.EQ.ABS(S22))THEN  
STATEV(4)=S22  
ELSEIF(MAX1.EQ.ABS(S33))THEN  
STATEV(4)=S33  
ELSEIF(MAX1.EQ.ABS(S12))THEN  
STATEV(4)=S12  
ELSEIF(MAX1.EQ.ABS(S13))THEN  
STATEV(4)=S13  
ELSEIF(MAX1.EQ.ABS(S23))THEN  
STATEV(4)=S23  
ENDIF
```

```
C See the maximum minimum stress  
IF(STATEV(4).GT.MAX100)THEN  
MAX100 = STATEV(4)  
ENDIF
```

```
IF(STATEV(4).LT.MIN100)THEN  
MIN100 = STATEV(4)  
ENDIF
```

```
C Calculation begin in one step.  
A1 = STATEV(1)  
A2 = STATEV(2)  
A3 = STATEV(3)  
A4 = STATEV(4)
```

```
IF(KSTEP.LT.StartStep)THEN  
Sumflag = 0  
ELSEIF(ABS(A3-200.).LE.1e-6)THEN  
Sumflag = 0  
ELSEIF(ABS(A2-200.).LE.1e-6)THEN  
Sumflag = 0  
ELSEIF(ABS(A1-200.).LE.1e-6)THEN  
Sumflag = 0  
ELSE  
Sumflag = 1  
ENDIF
```

```

IF(Sumflag)THEN
IF(ABS(A3-300.).LE.1e-6)THEN
STATEV(3) = STATEV(4)
ELSEIF(((A2.GT.A3).AND.(A4.GT.A2).AND.(A3.GT.A1)).OR.((A2.LT.A3).AND.(A4.
LT.A2).AND.(A3.LT.A1)))THEN
ampl = 0.5*ABS(A2-A3)
CNum = CNum + 1.
mid = 0.5*(A2+A3)
STATEV(2) = STATEV(4)
STATEV(3) = 300.
ELSE
ampl = 0.5*ABS(A1-A2)
CNum = CNum + 0.5
mid = 0.5*(A1+A2)
STATEV(1) = STATEV(2)
STATEV(2) = STATEV(3)
STATEV(3) = STATEV(4)
ENDIF

```

```

ELSEIF(KSTEP.GE.StartStep)THEN
STATEV(1) = STATEV(2)
STATEV(2) = STATEV(3)
STATEV(3) = STATEV(4)
ENDIF

```

```

C S-N curve
IF(STATEV(4).GT.0)THEN
C In tension
Power = 10*(1 - ABS(STATEV(4)/SigmaCont))
NTemp = ABS(10**(Power))
ELSE
C In Compression, use fatigue strength of 3.08ksi
Power = 10*(1 - ABS(STATEV(4)/3.08))
NTemp = ABS(10**(Power))
ENDIF

```

SN = ADF*dt/NTemp

```

C This area of code corrects the overflow number of the cycle,
IF(ABS(CNum).GT.1)THEN
CNum = 0.5
ENDIF
C Environmental damage
IF(TR2.GT.0)THEN
StepCheck=ABS((TIME(2)-TR2)/(TravelTime*Numloadclass)*dt)
ELSE

```



```

StepCheck=(TIME(2)-1)/(TravelTime*Numloadclass)*dt
ENDIF
Envd = ABS(1-exp(-Envcoeff*StepCheck*StepCheck))
C   damage parameters due to loadings,STATEV(5) for just identify damage due to loadings
STATEV(5) = STATEV(5) + abs(CNum*SN)
C   total damage
totald = abs(totald) + abs(CNum*SN)*(alpha2+alpha3) + alphaN*Envd
STATEV(7) = ABS(1-exp(-3.0D0*totald*totald)) + RD2*ND*stepflag2
C   Repair
IF(SumDamage2.GE.RD2)THEN
Refreshflag2 = 1.0D0
TR2 = TIME(2)
TRSTEP2 = KSTEP
ELSEIF(NOEL.LE.240.AND.NOEL.GE.1)THEN
Count2 = Count2+1
SumDamage2 = (SumDamage2 + STATEV(7))/(240*8)
ENDIF
STATEV(9) = Ccon0*(1-abs(STATEV(7)))
ENDIF
ENDIF
RETURN
END

```

About the Joint Transportation Research Program (JTRP)

On March 11, 1937, the Indiana Legislature passed an act which authorized the Indiana State Highway Commission to cooperate with and assist Purdue University in developing the best methods of improving and maintaining the highways of the state and the respective counties thereof. That collaborative effort was called the Joint Highway Research Project (JHRP). In 1997 the collaborative venture was renamed as the Joint Transportation Research Program (JTRP) to reflect the state and national efforts to integrate the management and operation of various transportation modes.

The first studies of JHRP were concerned with Test Road No. 1—evaluation of the weathering characteristics of stabilized materials. After World War II, the JHRP program grew substantially and was regularly producing technical reports. Over 1,500 technical reports are now available, published as part of the JHRP and subsequently JTRP collaborative venture between Purdue University and what is now the Indiana Department of Transportation.

Free online access to all reports is provided through a unique collaboration between JTRP and Purdue Libraries. These are available at: <http://docs.lib.purdue.edu/jtrp>

Further information about JTRP and its current research program is available at: <http://www.purdue.edu/jtrp>

About This Report

An open access version of this publication is available online. This can be most easily located using the Digital Object Identifier (doi) listed below. Pre-2011 publications that include color illustrations are available online in color but are printed only in grayscale.

The recommended citation for this publication is:

Cha, H., Liu, B., Prakash, A., & Varma, A. H. (2016). *Efficient load rating and quantification of life-cycle damage of Indiana bridges due to overweight loads* (Joint Transportation Research Program Publication No. FHWA/IN/JTRP-2016/06). West Lafayette, IN: Purdue University. <http://dx.doi.org/10.5703/1288284316329>